

FEEDBACK CONTROL OF MULTI-STORY STRUCTURES UNDER SEISMIC EXCITATIONS

Yang Dai

Dissertation submitted to the Faculty of the
Virginia Polytechnic Institute and State University
in partial fulfillment of the requirements for the degree of

Doctor of Philosophy
in
Engineering Mechanics

Dr. Leonard Meirovitch, Chair

Dr. Daniel J. Inman

Dr. Liviu Librescu

Dr. Yilu Liu

Dr. Mahendra P. Singh

April 4, 2002
Blacksburg, Virginia

Keywords: Active control, Vibration, Seismic excitation, Hierarchical finite element method

Copyright 2002, Yang Dai

FEEDBACK CONTROL OF MULTI-STORY STRUCTURES UNDER SEISMIC EXCITATIONS

Yang Dai

(ABSTRACT)

This dissertation studies the feedback control of the dynamic response of multi-story structures to seismic excitations. The seismic excitations are represented by arbitrary unknown stochastic disturbances. The research consists of modeling of the structure with a control system and a control design in the state space. A combination of the extended Hamilton's principle and the Hierarchical Finite Element Method (HFEM) was used to derive the discrete differential equations of motion. This method exhibits superior accuracy with fewer degrees of freedom (DOF). The discrete equation were realized in the state space, where the Multiple Channel Control (MCC) model, the Single Channel Control (SCC) model and the Special Single Channel Control (SSCC) model were proposed. The MCC model is a general multiple input/multiple output (MIMO) dynamic system; the SSCC model is a single input/multiple output (SIMO) dynamic system; which requires only one actuator acting on the base; the SCC model has duality. On one hand, the system can be classified as MIMO when control actuators are regarded as the input. On the other hand, it can be regarded as a SIMO system when control signal as the input.

Moreover, three different types of control methodologies, the Linear Quadratic Gaussian (LQG) control, the Disturbance Accommodating Control (DAC), and the hybrid LQG/DAC approaches, were successfully developed to actively mitigate the vibration of the multi-story

structures subjected to the seismic disturbance. In addition, the Kalman filter was used as an optimal observer to estimate the state of the system in the LQG and the LQG/DAC design.

Finally a numerical simulation of a four-story structure was carried out under nine cases. The cases covered various combinations of the three models and the three control designs to verify the effectiveness of control technique developed in this study. The simulation results found were quite encouraging. The results show each combination has its preponderance corresponding to special priority. In general, the hybrid LQG/DAC control in conjunction with the SSCC model is the best choice.

To my wife Claire, and my daughters Sylvia and Rini.

ACKNOWLEDGEMENT

First and foremost I would like to thank my adviser Professor Leonard Meirovitch, for his support and guidance of both my research and career.

I also want to express my gratitude to my committee members Professors Daniel J. Inman, Liviu Librescu, Yilu Liu and Mahendra P. Singh, for guiding my research and for reviewing my dissertation.

And, I am grateful to Professors Larry D. Mitchell and Hugh F. VanLandingham, for the part they played in furthering my education as former committee members.

Special thanks to Marc Hanchak and Abhay Bhivare for editing my dissertation.

My deepest gratitude goes to my wife, Claire, and daughters Sylvia and Rini. Without their support and patience, I couldn't have completed my dissertation. They have helped me write and rewrite it, edit and read. I am so thankful to have such a family, words can never express how much.

Finally, I am very appreciative of the love from my parents Luwu Dai and Peisheng Ding. They have given me life and a wonderful environment to grow up in. Their never-ending encouragement, support, and kind words helped me through the rough times.

Table of Contents

Chapter 1	Introduction-----	1-1
1.1	Literature Review-----	1-3
1.2	Dissertation Outline -----	1-14
Chapter 2	Fundamental Modeling Theory -----	2-1
2.1	The Extended Hamilton's Principle-----	2-2
2.2	The Hierarchical Finite Element Method (HFEM) -----	2-4
Chapter 3	The Equations of Motion-----	3-1
3.1	Basic Assumption-----	3-2
3.2	Analysis of Disjoint Substructures-----	3-3
3.3	The Kinetic Energy of the System-----	3-8
3.4	The Potential Energy of the System -----	3-15
3.5	Virtual Work of the Nonconservative Forces-----	3-22
3.6	Derivation of Discrete Equations of Motion -----	3-26
3.7	Model Reduction-----	3-27
Chapter 4	State Space Realization of Dynamic System-----	4-1
4.1	Introduction -----	4-2
4.2	Differential Equation of Motion-----	4-3
4.3	Multiple Control Channel (MCC) Model-----	4-7
4.4	Single Control Channel (SCC) Model-----	4-10
4.5	Special Single Control Channel (SSCC) Model-----	4-13
Chapter 5	Control System Design -----	5-1
5.1	Introduction to Optimum Feedback Control Theory-----	5-2

5.2	Disturbance Rejection Problem -----	5-6
5.3	Linear Quadratic Regulator (LQR) Problem-----	5-9
5.4	Linear Quadratic Estimator (LQE) Problem-----	5-12
5.5	Steady State LQG Problem-----	5-14
5.6	Disturbance Accommodation Control (DAC)-----	5-17
5.7	The Hybrid LQG/DAC Approach-----	5-20
Chapter 6 System Identification Problem-----		6-1
Chapter 7 Numerical Example-----		7-1
7.1	Basic Description and Assumption-----	7-2
7.2	Modeling of the System by Using the HFEM Technique-----	7-5
7.3	The State Space Implementation of the Control Models -----	7-6
7.4	Control Simulation-----	7-7
7.5	Simulation Results and Discussion-----	7-9
7.5.1	<i>The MCC Model with the LQG Control</i> -----	7-10
7.5.2	<i>The MCC Model with the DAC Control</i> -----	7-13
7.5.3	<i>The MCC Model with the LQG/DAC Control</i> -----	7-18
7.5.4	<i>The SCC Model with the LQG Control</i> -----	7-23
7.5.5	<i>The SCC Model with the DAC Control</i> -----	7-28
7.5.6	<i>The SCC Model with the LQG /DAC Control</i> -----	7-32
7.5.7	<i>The SSCC Model with the LQG Control</i> -----	7-35
7.5.8	<i>The SSCC Model with the DAC Control</i> -----	7-41
7.5.9	<i>The SSCC Model with the LQG/DAC Control</i> -----	7-45
7.6	Summary-----	7-50
Conclusions -----		8-1
Bibliography -----		9-1
Vita		

LIST OF FIGURES

Figure 3-1	<i>Model of building structure with a base subjected to ground motion</i> -----	3-2
Figure 3-2	<i>Model of the ith substructure</i> -----	3-4
Figure 4-1	<i>Block diagram of the system</i> -----	4-8
Figure 4-2	<i>Block diagram of the MCC model</i> -----	4-9
Figure 4-3	<i>Block diagram of the system in the SCC model</i> -----	4-11
Figure 5-1	<i>Schematic of a typical dynamic system with a regulator</i> -----	5-3
Figure 5-2	<i>Block diagram of the Kalman estimator</i> -----	5-4
Figure 5-3	<i>Block diagram of LQG regulator</i> -----	5-5
Figure 5-4	<i>Block diagram of the system in the disturbance rejection problem</i> -----	5-8
Figure 5-5	<i>Block diagram of the system in the form of the LQR problem with noise</i> -----	5-9
Figure 5-6	<i>Block diagram of the LQE</i> -----	5-15
Figure 5-7	<i>Block diagram of the LQG control system</i> -----	5-16
Figure 5-8	<i>Block diagram of the Hybrid LQG/DAC system</i> -----	5-22
Figure 7-1	<i>Model of a four-storey building system subjected to ground motion</i> -----	7-2
Figure 7-2	<i>The mean and 4 random samples of the motion of ground</i> -----	7-4
Figure 7-3	<i>Simulation block diagram of the LQG control and the LQG/DAC control</i> -----	7-8
Figure 7-4	<i>Simulation block diagram of the DAC design</i> -----	7-9
Figure 7-5	<i>Relative displacements of the top floor, (MCC model, LQG control)</i> -----	7-12
Figure 7-6	<i>Relative velocities of the top floor, (MCC model, LQG control)</i> -----	7-12
Figure 7-7	<i>Control force applied on the base, (MCC model, LQG control)</i> -----	7-14
Figure 7-8	<i>Control forces applied on the building, (MCC model, LQG control)</i> -----	7-14
Figure 7-9	<i>Displacements of the base, (MCC model, DAC control)</i> -----	7-16
Figure 7-10	<i>Relative displacement of the top floor, (MCC model, DAC control)</i> -----	7-16
Figure 7-11	<i>Control force applied on the base, (MCC model, DAC control)</i> -----	7-17

Figure 7-12	<i>Control forces applied on the building, (MCC model, DAC control)</i>	7-17
Figure 7-13	<i>Relative displacements of the top floor, (MCC model, LQG/DAC control)</i>	7-20
Figure 7-14	<i>Displacements of the base, (MCC model, LQG/DAC control)</i>	7-20
Figure 7-15	<i>Relative velocities on the top floor, (MCC model, LQG/DAC control)</i>	7-21
Figure 7-16	<i>Control forces applied on the building, (MCC model, LQG/DAC control)</i>	7-21
Figure 7-17	<i>Relative displacements of the top floor, (SCC model, LQG control)</i>	7-25
Figure 7-18	<i>Relative velocities of the top floor, (SCC model, LQG control)</i>	7-25
Figure 7-19	<i>Relative accelerations of the top floor, (SCC model, LQG control)</i>	7-26
Figure 7-20	<i>Control forces applied on the building, (SCC model, LQG control)</i>	7-26
Figure 7-21	<i>Relative displacements of the top floor, (SCC model, DAC control)</i>	7-30
Figure 7-22	<i>Displacements of the base, (SCC model, DAC control)</i>	7-30
Figure 7-23	<i>Relative velocities on the top floor, (SCC model, DAC control)</i>	7-31
Figure 7-24	<i>Control forces applied on the building, (SCC model, DAC control)</i>	7-31
Figure 7-25	<i>Relative displacements of the top floor, (SCC model, LQG/DAC control)</i>	7-34
Figure 7-26	<i>Relative velocities of the top floor, (SCC model, LQG/DAC control)</i>	7-34
Figure 7-27	<i>Relative accelerations of the top floor, (SCC model, LQG/DAC control)</i>	7-36
Figure 7-28	<i>Control forces applied on the building, (SCC model, LQG/DAC control)</i>	7-36
Figure 7-29	<i>Relative displacements of the top floor, (SSCC model, LQG control)</i>	7-38
Figure 7-30	<i>Displacements of the base, (SSCC model, LQG control)</i>	7-38
Figure 7-31	<i>Relative accelerations of the top floor, (SSCC model, LQG control)</i>	7-39
Figure 7-32	<i>Control forces applied on the base, (SSCC model, LQG control)</i>	7-39
Figure 7-33	<i>Relative displacements of the top floor, (SSCC model, DAC control)</i>	7-43
Figure 7-34	<i>Displacements of the base, (SSCC model, DAC control)</i>	7-43
Figure 7-35	<i>Relative velocities of the top floor, (SSCC model, DAC control)</i>	7-44
Figure 7-36	<i>Velocities of the base, (SSCC model, DAC control)</i>	7-44
Figure 7-37	<i>Relative displacements of the top floor, (SSCC model, LQG/DAC control)</i>	7-47
Figure 7-38	<i>Displacements of the base, (SSCC model, LQG/DAC control)</i>	7-47

Figure 7-39 *Relative velocities on the top floor, (SSCC model, LQG/DAC control)* -----7-48

Figure 7-40 *Velocities on the base, (SSCC model, LQG/DAC control)*-----7-48

LIST OF TABLES

Table 2-1	<i>Coefficients a_i, b_i, c_i and d_i</i>	2-8
Table 7-1	<i>The structural parameters used in the example</i>	7-3
Table 7-2	<i>Parameters used in the random motion of ground</i>	7-4
Table 7-3	<i>The variance of white noise</i>	7-5
Table 7-4	<i>Comparison of natural frequencies using HFEM and NASTRAN</i>	7-6
Table 7-5	<i>Simulation results of the MCC model with the LQG control</i>	7-11
Table 7-6	<i>The closed-loop eigenvalues for the MCC model with the LQG control</i>	7-13
Table 7-7	<i>Simulation results of the MCC model with the DAC control</i>	7-15
Table 7-8	<i>Simulation results of the MCC model with the LQG/DAC control</i>	7-19
Table 7-9	<i>Simulation results of the SCC model with the LQG control</i>	7-24
Table 7-10	<i>The closed-loop eigenvalues for the SCC model with the LQG control</i>	7-27
Table 7-11	<i>Simulation results of the SCC model with the DAC control</i>	7-29
Table 7-12	<i>Simulation results of the SCC model with the LQG/DAC control</i>	7-33
Table 7-13	<i>Simulation results of the SSCC model with the LQG control</i>	7-37
Table 7-14	<i>The closed-loop eigenvalues for the SCC model with the LQG control</i>	7-40
Table 7-15	<i>Simulation results of the SSCC model with the DAC control</i>	7-42
Table 7-16	<i>Simulation results of the SSCC model with the LQG/DAC control</i>	7-46

CHAPTER ONE

INTRODUCTION

Over the past three decades, active vibration control has received considerable attention from researchers [15, 19, 23, 27, 30, 32, 43-45, 61, 81, 89]. Extensive efforts have been devoted to the theoretical and practical development of active vibration control of building structures subject to the seismic excitation [2-3, 5, 24, 39, 49, 54, 66, 76, 82].

In general, vibration control is classified into two categories: passive and active control. No matter what control system is adopted, the action fits into one of following five functions or their combination: i.) to isolate the path of power flow into the structure; ii.) to add damping to the structure; iii.) to avoid structural resonance; iv.) to transfer the vibration energy from the main structure to an auxiliary oscillator; v.) to provide the structure with active control forces. Here the first four of these functions can be both passive and active control strategies, while the fifth is obviously only active control strategy. Base isolation in the vibration control is a typical passive control technology based on the function 1. However active base isolation has received more and more attention recently [33, 48-49, 62, 73-74, 80]. Structural damping treatment is also a typical passive vibration control approach that has been using in the practical structural engineering. But active damping has attracted the interests of many researchers during a long period of time [1, 26, 62, 71, 77]. Even dynamic vibration absorber that is a conventional passive controller is updated becoming active absorbers [23, 49, 85]. Devices that have been proposed include active tendon control [84], active tuned mass damper [48], and active bracing system [5]. In addition to the application of the active force to the passive system, some new devices such as electro-rheological fluid damper [77] was recently proposed to be applied to civil engineering structures.

In a passive control system, the reduction of the vibration can be achieved by the addition of materials or devices that can dissipate energy. Hence, passive control does not require an external energy since the energy dissipation can be activated by the passive system itself. In comparison with passive control system, active control system is characterized essentially in

terms of the following two features: i) a certain amount of external power or energy is required; and ii) a decision-making process based on real-time-measured data is involved. It follows that active control contains a broad range of technologies. The most important areas in the active control design are the modeling of control system and control law design.

This dissertation focuses on both the modeling and design of the control system, including development of a discrete model for the active vibration control of multi-story buildings and design of a control law.

1.1 Literature Review

Since the pioneer conceptual study by Yao [97], tremendous progress has been made toward making active vibration control of building structures a viable technology for enhancing structural functionality and safety against natural hazards such as strong earthquakes. The research on active vibration control has been making advances at a miraculous pace, in theory as well as application to real engineering [5, 48-49, 62, 67-68, 71, 73, 80, 83-84, 92].

Early work performed by Yang [93] investigated the vibration control of civil engineering structures subjected to random loading using modern linear feedback control theory. In the references [95-96], Yang, Li, Danielians and Liu proposed a refined version of the instantaneous optimal control algorithm for nonlinear or hysteretic systems. In the investigation they proposed to reduce the response of structures to earthquake excitations by basing the controls on measurements of state and obviating the problem of tracking a time dependent system matrix.

A technique based on an active control algorithm derived from standard numerical integration schemes using corrective pulses or forces to limit the response of a structure that has already

entered the inelastic range was developed by Reinhorn, Manolis and Wen [75]. There, the shape control of structures undergoing inelastic deformations was carried out through the use of an active pulse/force system.

Active energy dissipating system, such as active damping, has been a hot topic of research. Abdel-Mooty and Roorda [1] studied the effect of time delay between sensing the structural motion and applying the control force in an active damping system in analytical and experimental works. Ni, Ko and Ying [68] coupled adjacent building with non-linear hysteretic dampers to mitigate structural seismic response. The research showed that the hysteretic dampers can provide a wideband vibration suppression from the earthquake attack with low- or high-excitation frequencies. Preumont, Dufour, and Malekian [71] developed an active damping system for suppressing structural dynamic response, where a local feedback control force implemented by piezoelectric actuators was used to provide active damping.

Ribakov and Gluck [77] presented an active control system for multi-story structures using Electro-Rheological fluid dampers. When an electric field is applied, the behavior of the electro-rheological fluid is nearly viscoplastic and the shear stress in it must exceed the developed “yield” stress to initiate flow. Significant improvement of the structural response to seismic excitation was obtained using optimal active controlled electro-rheological fluid dampers.

Perhaps the most commonly used active control devices in building structures are active dampers, namely the active mass damper, active tuned mass damper, and the hybrid mass damper. Actually, these dampers should be classified as dynamic vibration absorber rather than dampers, since there exists an auxiliary mass providing a building with the inertia force of the mass damper as control force. Loh and Chao [48] investigated the controlled buildings under earthquake excitations with tuned mass dampers, active tuned mass dampers, passive base

isolation systems and active isolation systems. Nagashima proposed an optimal feedback control law for active mass damper [67].

Spencer, Dyke and Deoskar [83-84] studied a scale model of a three-story building employing an active mass driver and active tendon system, individually. A benchmark structural control problem was utilized for assessing the relative effectiveness and feasibility of various active control algorithms and providing an analytical testbed for evaluation of control design issues such as model order reduction, spill-over, control-structure interaction, limited control authority, sensor noise, available measurements, computational delay, etc.

Wang, Lee, and Chen presented a novel high-performance active mass driver system [88]. Based on an active mass driver system, the device was integrated with a mechanical pulley system for stroke amplification to simultaneously enhance efficiency and save power. Also, an instantaneous direct output feedback control algorithm was derived alongside the hardware development for optimal stability.

For many years, the emphasis of active vibration control has been on developing the combinations of base isolation systems with active control systems for building structures subjected to seismic excitation. In fact, a good deal of the research has concentrated exclusively on hybrid control strategy [40, 62-63, 73-75, 87, 95-96].

Kelly, Leitmann and Soldatos [40] studied the use of base isolation in conjunction with active control for reducing the vibration of structure subjected to earthquake excitation both experimentally and analytically. They adopted a nonlinear controller to minimize the vibration of a structure in experiments where a multilayer natural rubber bearing base isolation system was utilized. To actively suppress the vibration of based-isolated structures, two techniques were

proposed by Reihorn, Soong and Wen [73], one using pulse to maintain the response of the structure within prescribed bound and another using active tendon system.

Pu and Hsu [72] presented an analysis of optimal modal control for tall buildings subjected to earthquake excitation, in which it was demonstrated that the effect of the active control mechanism on the structural response can be represented by the so-called influence matrix in the modal control approach. Pu and Kelly [73] employed a base isolation in conjunction with optimal control, with emphasis on the influence of time delay. They also investigated the possibility of combining passive base isolation control systems and an active control system that exerts control forces only on the base and induces artificial damping without increasing the stiffness to the isolated structure. The various combinations of a base isolation system used in conjunction with active control systems were investigated by Luco, Wong and Mita [49]. In this case the hybrid control design consists of an absorbing boundary at the top of the building structure and nonreflecting or reflecting boundaries at the base.

Tadjbakhsh and Rofooei [87] worked with instantaneous optimal control, in which an optimal control algorithm using acceleration, velocity and displacement feedback was proposed and applied to base-isolated structures. In order to control the response of building structure to strong earthquakes, two hybrid control systems were developed by Yang, Danielians and Liu [94].

Fur, Yang and Ankireddi [24] applied active control to building structures in three examples, one of which involves a base isolated building subjected to earthquake excitation. It is shown that velocity feedback is more effective than acceleration or displacement feedback in reducing interstory displacements and absolute accelerations. A three degree of freedom model of a rigid base-isolated building with actuators located between the base and the ground was studied by Jaliha, Utku and Wada [33], in which numerical simulations were carried out and some useful

results were obtained using the active base isolation system. The same model was studied by Sener and Utku [80]. However, they included the effect of a time delay in the action of the actuator on control performance.

In recent research, Arfiadi and Hadi [5] developed a new procedure to analyze three-dimensional buildings utilizing passive and active control devices, in which two types of active control devices using an active tuned mass damper and an active bracing system were taken into account. The passive parameters of the dampers as well as the controller gain were then optimized using a genetic based optimizer where the H_2 , H_∞ and L_1 norms are taken as the objective function.

The active control problem can be divided into two parts: dynamic modeling of structures and control design. In active vibration control, modeling of controlled structure is an essential issue. Whether or not the modeling of control systems is accurate directly affects the performance of the active control system design. Therefore, many researchers are dedicated to the methodology of control system modeling.

In early research on the modeling of buildings subjected to earthquakes, analyses were carried out mainly using lumped-parameter models in which the mass was concentrated in the floor and stiffness in the columns [18]. Most commonly, damping was modeled as viscous, although this is not very realistic. Lumped-parameter methods lack mathematical rigor.

Meirovitch, in his many books [53, 55, 59 and 64], presented a variety of dynamics modeling methods, including the principle of virtual work, the generalized principle of d'Alembert, the extended Hamilton's principle and Lagrange's equation of motion. Meirovitch and Stemple [61] presented hybrid differential equations by using the principle of virtual work, which model the

controlled motion of a space robot comprised of a rigid base, two flexible arms connected in series, and a rigid end-effector.

As the capacity of all computers is finite, continuous problems can only be solved exactly by mathematical manipulation. However, very few boundary value problems of the partial differential allow a closed-form solution. Indeed, closed-form solutions are possible only in relatively few cases, almost invariably (but not exclusively) involving uniformly distributed parameters and simple boundary conditions [55]. The available mathematical techniques usually limit the possibilities to oversimplified situations. To overcome the intractability of the realistic type of continuum problem, various methods of discretization have from time to time been proposed both by engineers and mathematicians [50, 53, 55, 58, 60]. All involve an approximation which, hopefully, is of such a kind that it approaches, as closely as desired, the true continuum solution as the number of discrete variable increases. In general, structures in engineering are described using a distributed parameter system and complex geometry. Distributed parameter structures can be discretized in two distinct ways [8, 17, 60, 64-65], namely, through lumping of the distributed parameters, or through series discretization. The classical series discretization procedure is the Rayleigh-Ritz method [60], whereby the elastic displacement is assumed to be a linear combination of known admissible functions multiplied by undetermined coefficients. Meirovitch and Stemple [62-63] first derived the equations of motion of a base-isolated structure and associated boundary conditions by means of the extended Hamilton's principle. Then, they discretized the system by mean of the Rayleigh-Ritz method. The control law was a modified on-off with a two-tiered dead zone, a nonlinear control which is more economical and easier to implement than linear control.

The finite element method (FEM) that is a variant of the Rayleigh-Ritz method is by far the most popular series discretization procedure [6-7, 18, 64 and 101]. It was shown by Meirovitch [64] that the FEM has the advantage that the admissible functions tend to be simple, generally

low-degree polynomials, but the disadvantage that it requires a large number of degrees of freedom for good accuracy.

A way of improving the accuracy of the finite element approximation is to keep the width constant and increase the degree of the polynomials that are shape functions. The approach whereby the degree of the polynomials is increased is known as the p -version [6-7]. The p -version of the FEM has been of growing interest over the past 30 years. In the p -version of the FEM, the mesh of the structure is fixed and the degree p of the interpolation functions is progressively increased until the desired degree of convergence is reached. The p -version of the FEM presents many advantages compared with the classical FEM called h -version [7, 102], in which h is the maximum diameter of the element. Firstly, the mesh of the structure has to be generated one time for all; then convergence is reached by increasing the p -order, which improves accuracy by keeping the number of finite elements constant and increasing the number of interpolation functions per element. Second input data can be reduced to the minimum, which greatly simplifies pre-post-processing. Finally adaptive processes for reaching convergence can be realized by increasing automatically the order, which is much easier than adaptive meshing.

In the p -version of the FEM it is possible to choose from a variety of different sets of polynomials, provided the sets are complete. Particularly desirable is the so-called Hierarchical Finite Element Method (HFEM) [12, 23, 56, 64-65, 70, 78-79, 102], which has the property that the set of polynomials in the approximation of degree p represents a subset of the polynomials in the approximation of degree $p+1$. The HFEM combines many of the advantages of both the classical Rayleigh-Ritz method and the FEM, which presents a supplementary advantage in improving accuracy by keeping the number of finite elements constant while increasing the number of interpolation functions per element. In the HFEM, because the interpolation functions set of order p constitutes a subset of the interpolation functions set of

order $p+1$, the mass and stiffness matrix elements that were calculated for the p order set can be re-used for the $p+1$ order set. This is the reason why such elements are called “hierarchical”.

Meirovitch and Baruh [56] have shown that the HFEM’s linear matrices possess the embedding property and that HFEM tends to yield a better accuracy with fewer degrees of freedom than the h -version FEM for eigenvalue problems of the same order.

Zhu [99] proposed a hierarchical polynomials set built from integrated Legendre polynomials. Bardell [10-11] used this set to predict natural flexural vibrations of rectangular plates and skew plates.

A new hierarchical functions set was proposed by Beslin and Nicolas to predict flexural motion of plate-like structures in the medium frequency range [12]. The functions set was built from trigonometric functions instead of polynomials as classically encountered. They showed that such a trigonometric set presented all the advantages of a classical hierarchical polynomials set and additional ones which were of interest if very high order functions were intended to be used. It was stated that the trigonometric set can be used at very high orders, up to 2048 without taking care of computer round-off errors, while the classical polynomials set failed at order 46 because of the limited numerical dynamics of computers.

Houmat [28] applied the trigonometric hierarchical shape functions to plate vibration analysis. The results confirmed that the solutions always converge as the numbers of the hierarchical terms were increased, and that highly accurate values were obtained with the use of a very few hierarchical terms.

Meirovitch and Stemple [65] proposed a new set of hierarchical functions consisting of the Hermite cubics and admissible functions that were constituted by complicated functions. The research demonstrated the new hierarchical functions set could enhance the speed of convergence.

Ribeiro and Petyt [78] used the HFEM and the harmonic balance methods to investigate the geometrically non-linear free and steady-state forced vibrations of uniform, slender beams. In the research, the HFEM model was favorably compared with the traditional FEM models. With the HFEM, convergence was achieved with fewer degrees of freedom, which significantly reduced the computational time. More recently, Ribeiro [79] studied geometrically non-linear vibrations of beams and plane frameworks. Three different hierarchical interpolation function, polynomials, trigonometric functions, and beam eigenfunctions, were investigated. In addition, the suitability of the HFEM for time domain non-linear analysis was examined.

In the last two to three decades, various control methodologies used to reduce active structural vibrations due to earthquakes have become an area of interest to researchers and practicing engineers. A large number of new control strategies have been developed and applied to practical control systems [3, 4, 14, 40-42, 47, 72, 76-77, 91-96 and 98].

Modal control is an important control technique that is based on the ideal of changing the modal characteristics of a system to achieve satisfactory performance. Martin and Soong [51] applied the concept of modal control to large flexible structures. They demonstrated that a great deal of freedom exists in terms of eigenvalue assignments and control policy decision. Juang, Sae-Ung, and Yang [39] applied the pole assignment method to the control design of the critical modes of large structures, where the control design was carried in coupled form.

Meirovitch and Öz [54] and Meirovitch and Baruh [56] developed a different type of modal control methodology, referred to as independent modal-space control (IMSC). The control that they designed is applied to each mode independently. Later, optimal IMSC was employed for controlling structures under earthquake excitations by Meirovitch and Silverberg [57].

Analytical and experimental research on different models revealed important features of the dynamic behavior of civil engineering structures with active control devices. Miller, Masri, Dehghanyar and Caughey [66] illustrated the feasibility, reliability and robustness of the optimal pulse-control method in active vibration control of large civil structures through numerical and experimental investigation.

Much effort has been devoted to the development of robust control algorithms and their application to the active vibration control of the building structure subjected to the seismic excitation. Young and Bienkiewicz [98] developed a robust controller design for the active mass driver benchmark problem. The design process was based on the D-K iteration procedure for complex m synthesis, together with a balanced truncation procedure to reduce the controller order. The final design was a third-order linear controller, which utilized only four accelerometer measurements, and had desirable rolloff properties.

Ankireddi and Yang considered an optimal control method using a sampled data control system for a structural control application [4]. In the study, a discrete time controller using zero-order sample-and-hold device was developed and an H_2 optimal control method was used for designing the control gain. The results suggested that such systems were potentially suited for implementation in the active vibration control of civil infrastructures. Such potentiality became more realistic with the current trends in software development and the increased use of digital computers.

The Linear Quadratic Gaussian (LQG) control strategy using dynamic output feedback controller has been applied to the 310m tall Nanjing TV transmission tower in China equipped with an active mass driver [92]. Wu and Yang presented the LQG control strategy for the acceleration reduction of the tower equipped an active mass driver, taking into account the coupled lateral-torsional motion. It was demonstrated that the LQG controller was quite suitable for practical implementations and the performance of the active mass driver using the LQG strategy was remarkable.

Mixed-norm designs, such as H_2/H_∞ , H_2/LQG and l_1/H_∞ , have started to be introduced to the active vibration control of building system under the seismic excitation due to low cost controllers with significant robustness characteristics [38]. This is because the optimization algorithm more readily relaxes the constraints than restricts them, causing a less likelihood to get stuck at local minima. Standard H_2/LQG optimal control excels at noise and disturbance rejection, but may have difficulty with actuator saturation and plant uncertainty. Johnson, Voulgaris and Bergman [38] developed reduced-order, multi-objective optimal controller for the Notre Dame structural control building model benchmark using l_1 and H_∞ constrains to improve controller performance. They especially attempted to reduce peak responses, avoid saturation, and improve robustness to unmodeled dynamics.

Neural network control has successfully been adopted in structural active control by Faravelli, Chen, Bani-Han, Joghataie, Liut [21], because it is able to produce a desired output by training the network. The goal of a neural network based controller is to generate control forces such that they cause a desired reduction in the response. One of ways to obtain the neural network based active control forces is to emulate the structural system to be controlled by a separate neural network for which the performance function gradients can be easily obtained [21]. Thus

two neural networks are usually required, one to generate efficient control actions, and another to emulate the structural system.

Liu, Matheu, Singh and Mook [47] presented a method to generate an efficient law for a neural network controller to reduce the dynamic response of buildings exposed to earthquake-induced ground excitations. In this research, a training approach, referred to as the force-matching approach, was introduced. Its remarkable advantage lies in a non-necessary requirement of the emulation of the structure by an additional neural network. This technique not only eliminated some of the approximations and uncertainties in the emulation stage but also speeded up the training procedure. The numerical simulations illustrated a good performance with significant response reductions and feasible control requirements.

1.2 Dissertation Outline

The most frequently encountered problem in the control of large flexible structures is to produce a relatively accurate model with as few degrees of freedom as possible and find an appropriate control law to reduce the induced vibration due to seismic excitation that occurs in a short time history. The objectives of this investigation are:

- Develop a discrete model of multi-story building structures under seismic excitation for the active vibration control system design;
- Find a control law for preventing injury to occupants and damage to contents and protecting the integrity of the structure.

In this research, the model of an N -story building structure was considered, which is regarded as a large flexible distributed parameter structure claimed to a base in the form of a rigid slab capable of moving horizontally relative to the ground while restrained by a viscous damper and an elastic spring.

The ideal base isolation is one in which the base lies on a perfectly smooth foundation, so that forces due to ground motion are not transmitted to the base. Clearly, this ideal situation cannot be realized in practice. To prevent the structure from moving in response to wind forces, some restraints must be placed on the base. To this end, it is assumed that the base lies on a viscoelastic support, modeled as a viscous damper and an elastic spring connected to the ground in parallel. In addition, horizontal control forces act on the base and throughout the entire structure to attenuate the vibration of the building due to the ground motion.

The building has distributed stiffness and mass properties, and is regarded as a two-dimensional assemblage of partial frames consisting of distributed-parameter beams and columns, modeled as Euler-Bernoulli beams. For simplicity, the motion of the ground and base are assumed to take place in the horizontal direction of the vertical plane only. Moreover, the motion of a typical point on the structure can be regarded as a superposition of the motion of the base and the elastic displacement of the point relative to the base. All frames as substructures of the flexible structure act independently of one another. The substructures are coupled by constraining them to work together as a single structure. All displacements are small, including the rotations.

The boundary value problem will be derived by means of the extended Hamilton's principle in conjunction with the discretization of the distributed parameter structures using the hierarchical finite element method. It follows that the discrete equations of motion in the matrix form are obtained. Then, a model reduction designed to eliminate the effect of higher modes is carried out. After that the truncated equations of motion are obtained, which have only far fewer degrees of freedom than the original discrete system.

In control design, three structural dynamic models in the state space are developed to actively control the vibration of the multi story building structure: Multiple Channel Control (MCC)

model, Single Channel Control (SCC) model and Special Single Channel Control (SSCC) model. The MCC model is a general multiple input/multiple output (MIMO) dynamic system, while the SCC and SSCC models are single input/multiple output (SIMO) dynamic system.

Then, the Linear Quadratic Gaussian (LQG), the Disturbance Accommodation Control (DAC) and the hybrid LQG/DAC controls have been successfully developed to mitigate the structural vibration, where the Kalman filter is used as an optimal estimator. The main difference of the control systems lie in the use of different algorithm to optimize the state feedback gain matrix. At the same time, the system identification technique is adopted for modeling the disturbance state equation that is indispensable in the state space feedback control.

Finally, a few of computer codes is developed, which is capable of simulating the controlled response of a flexible structure clamped a rigid base to arbitrary unknown disturbance are developed. In order to verify the performance of the control law developed in this investigation, extensive numerical simulations are performed in nine cases.

Although the proposed methods utilize many well-known concepts and methodologies, some significant contributions of the dissertation are:

- 1) Hierarchical Finite Element Method (HFEM) is utilized for modeling control system with fewer degree of freedom without losing accuracy;
- 2) Three control models, MCC, SCC and SSCC models, are proposed. It is shown that the standard state-space control design techniques, such as the LQG control techniques, can be straightforwardly employed for the active suppression of persistent disturbance, provided the model of the controlled system is generated appropriately.
- 3) The DAC technique is developed to suppress the steady state response of the building structure to seismic excitation.

- 4) The hybrid LQG/DAC is presented. The advantage of the hybrid control is that the transient response of the structure was attenuated by using the LQG control while the steady state response to seismic excitation was suppressed by using the DAC approach.

It should be emphasized that the proposed approaches are different from other techniques that are based on disturbance estimation.

CHAPTER TWO

FUNDAMENTAL MODELING THEORY

2.1 The Extended Hamilton's Principle

In this research, a boundary-value problem is derived by means of the extended Hamilton's principle [64], which results from the generalized principle of d'Alembert expressed in the form

$$\sum_{i=1}^N (\mathbf{F}_i - m_i \ddot{\mathbf{R}}_i) \delta \mathbf{R}_i = 0 \quad (2-1)$$

where \mathbf{F}_i are applied forces, \mathbf{R}_i position vectors, $-m_i \ddot{\mathbf{R}}_i$ inertial forces, and $\delta \mathbf{R}_i$ the virtual displacements. This states that the work performed by the effective forces that are the sum of the applied force and the inertial force through infinitesimal virtual displacements compatible with the system constraints is zero. It is first recognized that

$$\sum_{i=1}^N \mathbf{F}_i \delta \mathbf{R}_i = \delta W \quad (2-2)$$

is the virtual work by the applied forces. Then, assuming the mass m_i is constant, it is arrived at

$$\begin{aligned} \frac{d}{dt} (m_i \dot{\mathbf{R}}_i \cdot \delta \mathbf{R}_i) &= m_i \ddot{\mathbf{R}}_i \cdot \delta \mathbf{R}_i + m_i \dot{\mathbf{R}}_i \cdot \delta \dot{\mathbf{R}}_i \\ &= m_i \ddot{\mathbf{R}}_i \cdot \delta \mathbf{R}_i + \delta \left(\frac{1}{2} m_i \dot{\mathbf{R}}_i \cdot \dot{\mathbf{R}}_i \right) \\ &= m_i \ddot{\mathbf{R}}_i \cdot \delta \mathbf{R}_i + \delta T_i \end{aligned} \quad (2-3)$$

where T_i is the kinetic energy of particle m_i . Summing over the entire system of particles and rearranging, it can be obtained:

$$\sum_{i=1}^N \frac{d}{dt} (m_i \dot{\mathbf{R}}_i \cdot \delta \mathbf{R}_i) = \sum_{i=1}^N m_i \ddot{\mathbf{R}}_i \cdot \delta \mathbf{R}_i + \delta T \quad (2-4)$$

where T is the kinetic energy of the entire system of particles. Inserting Eqs. (2-2) and (2-4) into Eq. (2-1) yields:

$$\delta T + \delta W = \sum_{i=1}^N \frac{d}{dt} (m_i \dot{\mathbf{R}}_i \cdot \delta \mathbf{R}_i) \quad (2-5)$$

Multiplying the above equation by $d\tau$ and integrating between the times t_1 and t_2 leads to:

$$\begin{aligned}
\int_{t_1}^{t_2} (\delta T + \delta W) dt &= \int_{t_1}^{t_2} \sum_{i=1}^N \frac{d}{dt} (m_i \dot{\mathbf{R}}_i \cdot \delta \mathbf{R}_i) dt \\
&= \sum_{i=1}^N m_i \dot{\mathbf{R}}_i \cdot \delta \mathbf{R}_i \Big|_{t_1}^{t_2}
\end{aligned} \tag{2-6}$$

Of all the possible varied paths, now only those that coincide with the true path at the two instants t_1 and t_2 is considered, so that Eq. (2-6) reduces to

$$\int_{t_1}^{t_2} (\delta T + \delta W) dt = 0, \quad \delta \mathbf{R}_i = \mathbf{0}, \quad i = 1, 2, \dots, N, \quad t = t_1, t_2 \tag{2-7}$$

In many problems, for systems with constraints the virtual displacements $\delta \mathbf{R}_i$, $i = 1, 2, \dots, N$ are not all independent. In such cases, it is advisable to describe the motion in terms of independent generalized coordinates, denotes by q_j , $j = 1, 2, \dots, M$, where M is the number of degree of freedom of the system, instead of \mathbf{R}_i , $i = 1, 2, \dots, N$. However, no explicit transformation is required here, as the principle has the same form regardless of the coordinates used to express dT and dW . In view of this, dT and dW can be directly expressed in terms of independent generalized coordinates, and the same can be said about the conditions on the virtual displacements at t_1 and t_2 . Hence, the extended Hamilton's principle can be represented in the form

$$\int_{t_1}^{t_2} (dT + dW) dt = 0, \quad dq_j = 0, \quad j = 1, 2, \dots, M, \quad t = t_1, t_2 \tag{2-8}$$

Generally, the virtual work dW includes contributions from both conservative and nonconservative forces, that is

$$dW = dW_c + dW_{nc} \tag{2-9}$$

where the subscripts c and nc denote the virtual work performed by conservative and nonconservative forces, respectively. As we know, the virtual work done by the conservative forces is as usual represented in the form

$$\delta W_c = -\delta V \tag{2-10}$$

in which $V = V(q_1, q_2, \dots, q_M)$ is the potential energy. Finally, the extended Hamilton's principle can be rewritten in the equivalent form:

$$\int_{t_1}^{t_2} (\delta T - \delta V + \delta W_{nc}) dt = 0, \quad \delta q_j = 0, \quad j = 1, 2, \dots, M, \quad t = t_1, t_2 \quad (2-11)$$

Eq. (2-11) is known as the Extended Hamilton's Principle.

2.2 The Hierarchical Finite Element Method (HFEM)

In general, structures in engineering are described using distributed parameter system with complex geometry. Distributed parameter structures can be discretized in two distinct ways [17, 60 and 65], namely, through lumping of the distributed parameters, or through series discretization. Lumped-parameter models tend to be very inaccurate, which can cause problems in control of structures. The classical series discretization procedure is the Rayleigh-Ritz method [64], whereby the elastic displacement is assumed to be a linear combination of known admissible functions multiplied by undetermined coefficients. The finite element method (FEM) that is a variant of the Rayleigh-Ritz method, is by far the most popular series discretization procedure [18, 101]. The basic difference between the two discretization methods is that the classical Rayleigh-Ritz method uses global functions as admissible functions, defined over the entire elastic member, and the FEM uses local functions, defined over a finite element and referred to as interpolation functions. The Rayleigh-Ritz method improves accuracy by increasing the number of admissible functions, whereas the FEM enhances accuracy by increasing the number of the finite elements. For single elastic members, the classical Rayleigh-Ritz method has the advantage that it can yield good accuracy with relatively small number of degrees of freedom, but the disadvantage that the admissible functions tend to be complicated. By contrast, the FEM has the advantage that the admissible functions tend to be simple, generally low-degree polynomials, but the painful disadvantage that it requires a large number of degrees of freedom for good accuracy. The accuracy of the discretization can be only improved in the finite element method by refining the mesh, which implies a reduction in the width of the element, or equivalently an increase in the number of elements. The procedure is characterized by the fact that the degree of the elements is a fixed, generally low number.

Another way of improving the accuracy of the finite element approximation is to keep the width constant and increase the order of the interpolation functions that are also called the shape functions. To distinguish between the two methods, the approach whereby the accuracy is improved by refining the finite element mesh is referred to as the h -version of the finite element method [6-7, 101], in which h is the maximum diameter of the element and the approach whereby the degree of the polynomials is increased is known as the p -version.

The p -version of the FEM has been of growing interest over the past 30 years [6-7]. In the p -version of the FEM, the mesh of the structure is fixed and the degree p of the interpolation functions is progressively increased until the desired degree of convergence is reached. The p -version of the FEM combines many of the advantages of both the classical Rayleigh-Ritz method and the FEM. First of all, the mesh of the structure has to be generated one time for all; then convergence is reached by increasing the p -order, which improves accuracy by keeping the number of finite elements constant and increasing the number of interpolation functions per element. Second input data can be reduced to the minimum, which greatly simplifies pre-post-processing. Finally adaptive processes for reaching convergence can be realized by increasing automatically the order, which is much easier than adaptive meshing. In the p -version of the FEM, it is possible to choose the interpolation functions from a variety of different sets of polynomials, provided the sets are complete.

Another very useful discretization procedure is the Hierarchical Finite Element Method (HFEM) [27, 64-65, 70, 78-79, 99, 102], which belongs to the p -version of the FEM. In addition to improvement of accuracy also by keeping the number of finite elements constant and increasing the number of interpolation functions per element, the HFEM has the property that the set of interpolation functions in the approximation of order p represents a subset of the polynomials in the approximation of order $p+1$. In the HFEM, because the interpolation functions set of order p constitutes a subset of the interpolation functions set of order $p+1$, consequently the mass and

stiffness matrix elements that were calculated for the p order set can be re-used for the $p+1$ order set. This is the reason why such elements are called “hierarchical”.

Advantages of the HFEM is characterized by the fact that i) the mass and stiffness matrices possess the embedding property, in which when one adds a shape function the mass and stiffness matrices are extended only one row and column, the remainder of the matrices keeps unchanged; ii) having higher rate of convergence; iii) the system has less number of degrees of freedom.

In early works, the hierarchical functions as the interpolation functions consist of a set of polynomials [6-7, 10-11, 99, 101-102]. Zhu [99] proposed a hierarchical polynomials set built from integrated Legendre polynomials. Afterwards, Bardell used this hierarchical polynomials set to predict natural flexural vibrations of rectangular plates [10] and skew plates [11].

The Legendre orthogonal polynomial set $\{L_n(x)\}$ used in literature [99] can be represented by

$$L_n(x) = \sum_{m=0}^{n/2} \frac{(-1)^m}{2^m m!} \frac{(2n - 2m - 1)!!}{(n - 2m)!} x^{n-2m}, \quad x \in [-1, 1] \quad (2-12)$$

The s -multiple integral of $L_{n-s}(x)$ denoted by $L_n^s(x)$ can be expressed by [99]

$$\begin{aligned} L_n^s(x) &= \int_{-1}^x \cdots \int_{-1}^x L_{n-s}(y) dy \cdots dy \\ &= \sum_{m=0}^{n/2} \frac{(-1)^m}{2^m m!} \frac{(2n - 2m - 2s - 1)!!}{(n - 2m)!} x^{n-2m} \end{aligned} \quad (2-13)$$

The importance of the polynomials set $\{L_n^s(x)\}$ lies in that they can constitute hierarchical interpolation functions because all their derivatives of order lower than s vanish at the two boundaries $x = \pm 1$.

Bardell [10] proposed a hierarchical interpolation functions set from Zhu's polynomials $\{L_n^s(x)\}$, in which the particular value $s = 2$ was taken. Bardell's polynomials set consists of the classical FEM first four cubic displacement functions and Zhu's polynomials $\{L_n^s(x)\}$ shown in Eq. (2-13), expressed by

$$\begin{aligned} \mathbf{j}_1(\mathbf{z}) &= \frac{1}{2} - \frac{1}{4}\mathbf{z} + \frac{1}{4}\mathbf{z}^3 & \mathbf{z} \in [-1, 1] \\ \mathbf{j}_2(\mathbf{z}) &= \frac{1}{8} - \frac{1}{8}\mathbf{z} - \frac{1}{8}\mathbf{z}^2 + \frac{1}{8}\mathbf{z}^3 \\ \mathbf{j}_3(\mathbf{z}) &= \frac{1}{2} + \frac{3}{4}\mathbf{z} - \frac{1}{4}\mathbf{z}^3 & (2-14) \\ \mathbf{j}_4(\mathbf{z}) &= -\frac{1}{8} - \frac{1}{8}\mathbf{z} + \frac{1}{8}\mathbf{z}^2 + \frac{1}{8}\mathbf{z}^3 \\ \mathbf{j}_i(\mathbf{z}) &\equiv L_{n=i-1}^{s=2}(\mathbf{z}) = \sum_{m=0}^{(i-1)/2} \frac{(-1)^m}{2^m m!} \frac{(2i-2m-7)!!}{(i-2m-1)!} \mathbf{z}^{i-2m-1} & i > 4 \quad (2-15) \end{aligned}$$

It can be observed that all the functions represented by Eq. (2-15) have zero displacement and zero slope at each end of the element. As a result, boundary conditions on displacement and rotation at the edges of the beam are entirely controlled by the first four basics functions. Thus particular boundary conditions such as simple supports and clamps can be treated only by removing some basis functions from this polynomials set.

In discretization procedure, the main interest lies in the convergence speed. The question of convergence speed is related to the completeness. However, a set of polynomials can be

complete in energy and still exhibit poor convergence characteristics. Beslin and Nicolas presented a new hierarchical functions set to predict flexural motion of plate-like structures in the medium frequency range [12]. The functions set was built from trigonometric functions instead of polynomials as classically encountered. They showed that such a trigonometric set presented all the advantages of a classical hierarchical polynomials set and additional ones which were of interest if very high order functions were intended to be used. The trigonometric hierarchical functions set $\{y_i(z)\}$ was defined as [12]

$$y_i(z) = \sin(a_i z + b_i) \sin(c_i z + d_i), \quad i = 1, 2, \dots \quad (2-16)$$

where the coefficients a_i , b_i , c_i and d_i are listed in **Table 2-1**.

Table 2-1. Coefficients a_i , b_i , c_i and d_i

i	a_i	b_i	c_i	d_i
1	$\frac{p}{4}$	$\frac{3p}{4}$	$\frac{p}{4}$	$\frac{3p}{4}$
2	$\frac{p}{4}$	$\frac{3p}{4}$	$-\frac{p}{2}$	$-\frac{3p}{2}$
3	$\frac{p}{4}$	$-\frac{3p}{4}$	$\frac{p}{4}$	$-\frac{3p}{4}$
4	$\frac{p}{4}$	$-\frac{3p}{4}$	$\frac{p}{2}$	$-\frac{3p}{2}$
$i > 4$	$\frac{p}{2} (i - 4)$	$\frac{p}{2} (i - 4)$	$\frac{p}{2}$	$\frac{p}{2}$

In terms of shapes, this trigonometric set has the same tendency as Bardell's polynomials. Because the order of a $y_i(z)$ function is not related to a power of z but to the number of oscillations of a trigonometric function it is numerically more stable than polynomials.

In order to further speed up the convergence, Meirovitch and Stemple proposed a new set of hierarchical functions consisting of the Hermite cubics and admissible functions that are constituted by complicated functions to enhance the speed of convergence [65].

As we know, the most common polynomials for beams in bending are the Hermite cubics. In terms of a non-dimensional local coordinate \mathbf{x} , $0 \leq \mathbf{x} \leq 1$, they are given by

$$\begin{aligned} h_1(\mathbf{x}) &= 1 - 3\mathbf{x}^2 + 2\mathbf{x}^3 \\ h_2(\mathbf{x}) &= 3\mathbf{x}^2 - 2\mathbf{x}^3 \\ h_3(\mathbf{x}) &= \mathbf{x} - 2\mathbf{x}^2 + \mathbf{x}^3 \\ h_4(\mathbf{x}) &= -\mathbf{x}^2 + \mathbf{x}^3 \end{aligned} \quad (2-17)$$

It should be noticed that Eq. (2-17) is the same as Eq. (2-14) in essential, except that the difference in the domain, Eq. (2-17) defined in $[0, 1]$ but Eq. (2-14) defined in $[-1, 1]$. Moreover, as hierarchical functions, the eigenfunction of a uniform fixed-fixed Euler-Bernoulli beam are used, which can be expressed in the computationally useful form

$$\begin{aligned} f_i(\mathbf{x}) &= (\cos I_i + \sin I_i - e^{-I_i}) \sin I_i \mathbf{x} + (\cos I_i - \sin I_i - e^{-I_i}) \cos I_i \mathbf{x} \\ &\quad + (e^{-I_i} \cos I_i - 1) e^{-I_i(1-\mathbf{x})} + \sin I_i e^{-I_i \mathbf{x}} \\ &\quad i = 1, 2, \dots ; 0 \leq \mathbf{x} \leq 1 \end{aligned} \quad (2-18)$$

where I_i satisfies the characteristic equation

$$\cos I_i \cosh I_i = 1 \quad (2-19)$$

The fixed-fixed shape functions given by Eq. (2-18) satisfy the orthogonality properties

$$\int_0^1 \mathbf{f}_i(\mathbf{x}) \mathbf{f}_j(\mathbf{x}) d\mathbf{x} = 0, \quad i \neq j \quad (2-20)$$

$$\int_0^1 \mathbf{f}_i''(\mathbf{x}) \mathbf{f}_j''(\mathbf{x}) d\mathbf{x} = 0, \quad i \neq j \quad (2-21)$$

Moreover, the second derivative of the fixed-fixed shape functions are orthogonal to the second derivative of the Hermite cubics, or

$$\int_0^1 h_i''(\mathbf{x}) \mathbf{f}_j''(\mathbf{x}) d\mathbf{x} = 0, \quad i \neq j \quad (2-22)$$

The hierarchical finite element method in conjunction with the interpolation functions given by Eqs. (2-17) and (2-18) permit accurate modeling of the structure with far fewer degrees of freedom than the h -version of the finite element method.

CHAPTER THREE

THE EQUATIONS OF MOTION

3.1 Basic Assumption

A building consisting of a given number of stories N labeled $i = 1, 2, \dots, N$ can be regarded as a flexible structure of the type shown in **Figure 3-1**, claimed to a base in the form of a rigid slab capable of moving horizontally relative to the ground. The ideal base isolation is one in which the base lies on a perfectly smooth foundation, so that forces due to ground motion are not transmitted to the base. Clearly, this ideal situation cannot be realized in practice. In addition, to prevent the structure from moving in response to wind forces, some restraints must be placed on the base. To this end, it is assumed that the base lies on a viscoelastic support, modeled as a viscous damper and an elastic spring connected to the ground in parallel, as shown in **Figure 3-1**. In addition, horizontal control forces act on the base and throughout the entire structure to attenuate the vibration of the building due to the ground motion.

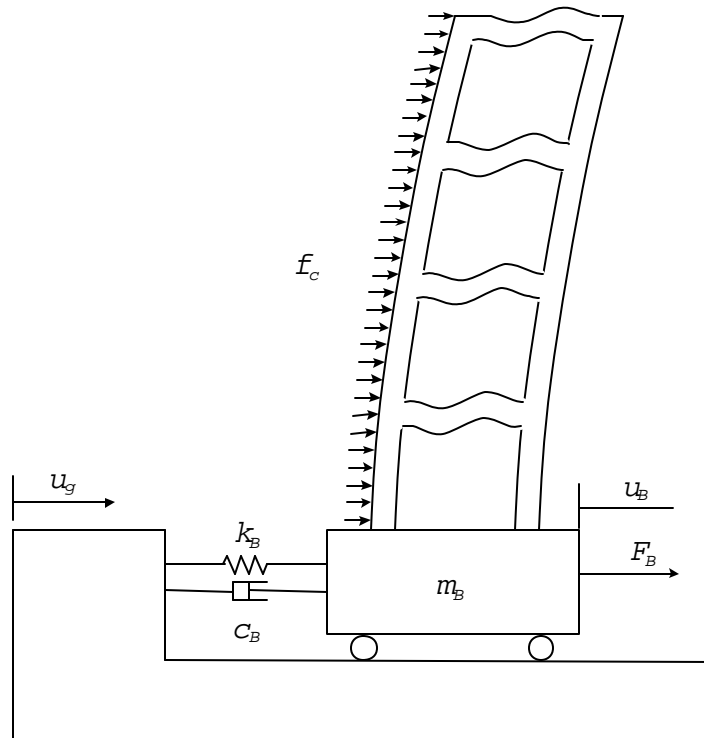


Figure 3-1. Model of building structure with a base subjected to ground motion

The building has distributed stiffness and mass properties and is regarded as a two-dimensional assemblage of portal frames consisting of distributed-parameter beams and columns, modeled as Euler-Bernoulli beams. For simplicity, the motion of the ground and the motion of the base is assumed to take place in the horizontal direction of the vertical plane alone. Moreover, the motion of a typical point on the structure can be regarded as a superposition of the motion of the base and the elastic displacement of the point relative to the base. In view of this, a distinction must be made between points on beams, which undergo only elastic displacement in the vertical direction with rigid-body displacements in the horizontal direction, and points on the columns, which undergo both rigid-body and elastic displacements in the horizontal direction. Moreover, it is assumed that the elastic members do not deform axially. Beams and columns connected at given joint undergo the same displacement and rotation at that joint. The axial extension of both the beams and columns is neglected, and consequently the both ends of a beam undergo no transverse displacement, and the tips of columns corresponding to the same story undergo the same horizontal displacement. However, the effect of axial forces working throughout the shortening of the columns due to bending is included in the model.

Here, all substructure frames of the flexible structure are considered to act independently of one another, and they are coupled by constraining them to work together as a single structure. Our interest lies in linear equations of motion, which necessitates that all displacements must be small, including the rotations.

3.2 Analysis of Disjoint Substructures

Consider a typical substructure i as a two-dimensional portal frame shown in *Figure 3-2*. This substructure consists of three distributed parameter beam and columns, modeled as uniform Euler-Bernoulli beams. In order to describe the motion of the system, the absolute

displacement of the ground is denoted by $u_g(t)$, the absolute displacement of the base by $u_B(t)$ and the rigid-body displacements of the floors relative to the base by $u_o^{(i)}(t)$, $i = 1, 2, \dots, N$, all three types of displacement taking place in the horizontal direction. Moreover, the elastic displacement of a typical point on the floor is denoted by $w_0^{(i)}(x, t)$, the elastic displacement of a typical point on the left column on the i th substructure relative to the base, by $w_1^{(i)}(x, t)$, and the elastic displacement of a typical point on the right column by $w_2^{(i)}(x, t)$, where $i = 1, 2, \dots, N$.

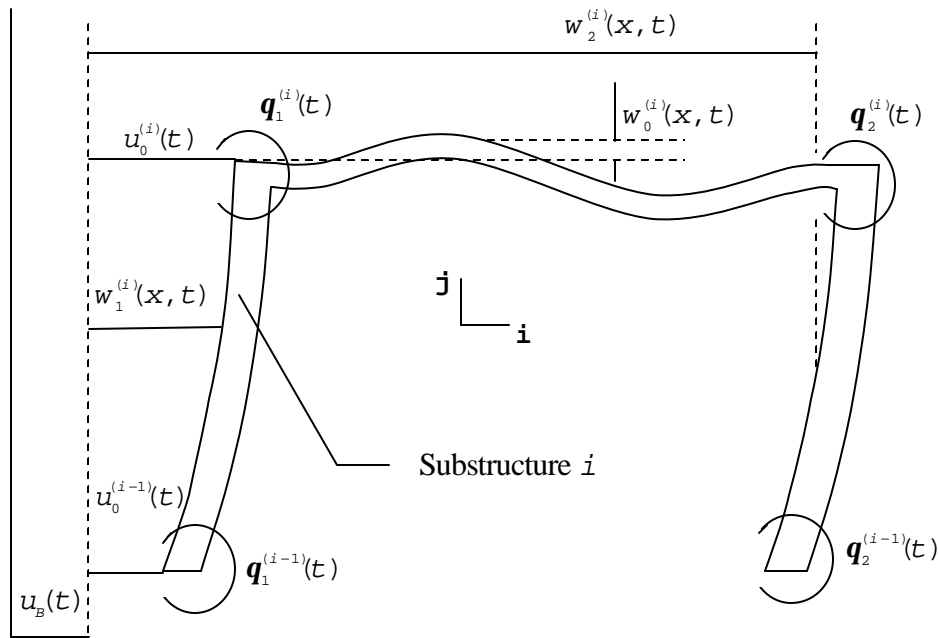


Figure 3-2. Model of the i th substructure

It is proposed to use the hierarchical finite element method (HFEM) to discretize the substructure [64]. For a typical point on the floor of the i th substructure, its position vector with subscript 0, $\mathbf{R}_0^{(i)}(x, t)$, can be expressed as

$$\mathbf{R}_0^{(i)}(\mathbf{x}, t) = (u_B(t) + u_0^{(i)}(t))\mathbf{i} + w_0^{(i)}(\mathbf{x}, t)\mathbf{j} \quad (3-1)$$

where $u_B(t)$ denotes the motion of the base, $u_0^{(i)}$ denotes the rigid-body displacements of the floor in the i th substructure relative to the base, and $w_0^{(i)}(\mathbf{x}, t)$ denotes the elastic displacement of a typical point on the floor in the i th substructure, which can be further written as

$$w_0^{(i)}(\mathbf{x}, t) = h_3\left(\frac{\mathbf{x}}{l_0^{(i)}}\right)l_0^{(i)}\mathbf{q}_1^{(i)} + h_4\left(\frac{\mathbf{x}}{l_0^{(i)}}\right)l_0^{(i)}\mathbf{q}_2^{(i)} + \mathbf{f}_1\left(\frac{\mathbf{x}}{l_0^{(i)}}\right)\mathcal{Q}_{01}^{(i)}(t) + \cdots + \mathbf{f}_{n_0}\left(\frac{\mathbf{x}}{l_0^{(i)}}\right)\mathcal{Q}_{0n_0}^{(i)}(t) \quad (3-2)$$

where $h_i, i = 1, \dots, 4$, indicate the Hermite cubics as shown in Eqs. (2-12), and $\mathbf{f}_j, j = 1, \dots, n_0$, the hierarchical functions as shown in Eqs. (2-13). Introduce a set of generalized coordinate vectors

$$\mathbf{q}^{(i)} = \left\{ u_B \quad u_0^{(i)} \quad u_0^{(i-1)} \quad \mathbf{q}_1^{(i)} \quad \mathbf{q}_1^{(i-1)} \quad \mathbf{q}_2^{(i)} \quad \mathbf{q}_2^{(i-1)} \quad \mathbf{q}_0^{(i)} \quad \mathbf{q}_1^{(i)} \quad \mathbf{q}_2^{(i)} \right\}^T \quad (3-3)$$

$$i = 1, \dots, N$$

in which

$$\mathbf{q}_0^{(i)}(t) = \left\{ \mathcal{Q}_{01}^{(i)}(t) \quad \mathcal{Q}_{02}^{(i)}(t) \quad \cdots \quad \mathcal{Q}_{0n_0}^{(i)}(t) \right\}^T$$

$$\mathbf{q}_1^{(i)}(t) = \left\{ \mathcal{Q}_{11}^{(i)}(t) \quad \mathcal{Q}_{12}^{(i)}(t) \quad \cdots \quad \mathcal{Q}_{1n_1}^{(i)}(t) \right\}^T$$

$$\mathbf{q}_2^{(i)}(t) = \left\{ \mathcal{Q}_{21}^{(i)}(t) \quad \mathcal{Q}_{22}^{(i)}(t) \quad \cdots \quad \mathcal{Q}_{2n_2}^{(i)}(t) \right\}^T$$

are n_0 and n_1 dimension generalized coordinate vectors associated with the hierarchical functions, respectively. It should be noted that $u_0^{(0)}, \mathbf{q}_1^{(0)}$ and $\mathbf{q}_2^{(0)}$ vanish identically.

Letting

$$\mathbf{F}_0^{(i)}(\mathbf{x}) = \left\{ 0 \quad 0 \quad 0 \quad h_3\left(\frac{\mathbf{x}}{l_0^{(i)}}\right)l_0^{(i)} \quad 0 \quad h_4\left(\frac{\mathbf{x}}{l_0^{(i)}}\right)l_0^{(i)} \quad 0 \quad \mathbf{f}\left(\frac{\mathbf{x}}{l_0^{(i)}}\right) \quad \mathbf{0} \quad \mathbf{0} \right\} \quad (3-4)$$

in which $\mathbf{f}(\mathbf{x}) = \{\mathbf{f}_1(\mathbf{x}) \quad \mathbf{f}_2(\mathbf{x}) \quad \cdots \quad \mathbf{f}_{n_0}(\mathbf{x})\}$ is a n_0 dimension hierarchical function vector while $\mathbf{f}_k(\mathbf{x})$, $k = 1, 2, \dots, n_0$, are a suitable set of the hierarchical functions, Eq. (3-2) can be rewritten as following:

$$\mathbf{w}_0^{(i)}(\mathbf{x}, t) = \Phi_0^{(i)}(\mathbf{x}) \cdot \mathbf{q}^{(i)}(t) \quad (3-5)$$

For a typical point in the left column of the i th substructure, its position vector with subscript 1 can be expressed as

$$\mathbf{R}_1^{(i)}(\mathbf{x}, t) = (\mathbf{u}_B(t) + \mathbf{w}_1^{(i)}(\mathbf{x}, t))\mathbf{i} \quad (3-6)$$

where $\mathbf{w}_1^{(i)}(\mathbf{x}, t)$ denotes the elastic displacement of a typical point on the left column in the i th substructure, which can be further written as

$$\begin{aligned} \mathbf{w}_1^{(i)}(\mathbf{x}, t) = & h_1\left(\frac{\mathbf{x}}{l_1^{(i)}}\right)\mathbf{u}_0^{(i)}(t) + h_2\left(\frac{\mathbf{x}}{l_1^{(i)}}\right)\mathbf{u}_0^{(i-1)}(t) + h_3\left(\frac{\mathbf{x}}{l_1^{(i)}}\right)l_1^{(i)}\mathbf{q}_1^{(i)}(t) + h_4\left(\frac{\mathbf{x}}{l_1^{(i)}}\right)l_1^{(i)}\mathbf{q}_1^{(i-1)}(t) \\ & + \mathbf{y}_1\left(\frac{\mathbf{x}}{l_1^{(i)}}\right)\mathbf{q}_{11}^{(i)}(t) + \cdots + \mathbf{y}_{n_1}\left(\frac{\mathbf{x}}{l_1^{(i)}}\right)\mathbf{q}_{1n_1}^{(i)}(t) \end{aligned} \quad (3-7)$$

where $h_j(\mathbf{x})$, $j = 1, \dots, 4$, are Hermite cubics expressed in Eqs. (2-12). In introducing the following notations,

$$\tilde{\mathbf{F}}_1^{(i)}(\mathbf{x}) = \left\{ 0 \quad h_1\left(\frac{\mathbf{x}}{l_1^{(i)}}\right) \quad h_2\left(\frac{\mathbf{x}}{l_1^{(i)}}\right) \quad h_3\left(\frac{\mathbf{x}}{l_1^{(i)}}\right)l_1^{(i)} \quad h_4\left(\frac{\mathbf{x}}{l_1^{(i)}}\right)l_1^{(i)} \quad 0 \quad 0 \quad 0 \quad \mathbf{y}\left(\frac{\mathbf{x}}{l_1^{(i)}}\right) \quad \mathbf{0} \right\} \quad (3-8)$$

where $\mathbf{y}(\mathbf{x}) = \{\mathbf{y}_1(\mathbf{x}) \ \mathbf{y}_2(\mathbf{x}) \ \cdots \ \mathbf{y}_{n_1}(\mathbf{x})\}$ is a n_1 dimension hierarchical function vector while $\mathbf{y}_k(\mathbf{x})$, $k = 1, 2, \dots, n_1$, are a set of the hierarchical functions, Eq. (3-7) can be written in the more compact form as

$$\mathbf{w}_1^{(i)}(\mathbf{x}, t) = \tilde{\mathbf{F}}_1^{(i)}(\mathbf{x}) \cdot \mathbf{q}^{(i)} \quad (3-9)$$

Similarly, for a typical point on the right column of the i th substructure, its position vector with subscript 2 can be expressed as

$$\mathbf{R}_2^{(i)}(\mathbf{x}, t) = (\mathbf{u}_B(t) + \mathbf{w}_2^{(i)}(\mathbf{x}, t))\mathbf{i} \quad (3-10)$$

where $\mathbf{w}_2^{(i)}(\mathbf{x}, t)$ denotes the elastic displacement of the typical point, which can be written as

$$\begin{aligned} \mathbf{w}_2^{(i)}(\mathbf{x}, t) = & h_1\left(\frac{\mathbf{x}}{l_1^{(i)}}\right)\mathbf{u}_0^{(i)}(t) + h_2\left(\frac{\mathbf{x}}{l_1^{(i)}}\right)\mathbf{u}_0^{(i-1)}(t) + h_3\left(\frac{\mathbf{x}}{l_1^{(i)}}\right)l_1^{(i)}\mathbf{q}_2^{(i)}(t) + h_4\left(\frac{\mathbf{x}}{l_1^{(i)}}\right)l_1^{(i)}\mathbf{q}_2^{(i-1)}(t) \\ & + \mathbf{y}_1\left(\frac{\mathbf{x}}{l_1^{(i)}}\right)\mathbf{q}_{21}^{(i)}(t) + \cdots + \mathbf{y}_{n_1}\left(\frac{\mathbf{x}}{l_1^{(i)}}\right)\mathbf{q}_{2n_1}^{(i)}(t) \end{aligned} \quad (3-11)$$

or

$$\mathbf{w}_2^{(i)}(\mathbf{x}, t) = \tilde{\mathbf{F}}_2^{(i)}(\mathbf{x}) \cdot \mathbf{q}^{(i)} \quad (3-12)$$

where

$$\tilde{\mathbf{F}}_2^{(i)}(\mathbf{x}) = \left\{ 0 \quad h_1\left(\frac{\mathbf{x}}{l_1^{(i)}}\right) \quad h_2\left(\frac{\mathbf{x}}{l_1^{(i)}}\right) \quad 0 \quad 0 \quad h_3\left(\frac{\mathbf{x}}{l_1^{(i)}}\right)l_1^{(i)} \quad h_4\left(\frac{\mathbf{x}}{l_1^{(i)}}\right)l_1^{(i)} \quad \mathbf{0} \quad \mathbf{0} \quad \mathbf{y}\left(\frac{\mathbf{x}}{l_1^{(i)}}\right) \right\} \quad (3-13)$$

In introducing the following notations

$$\mathbf{F}_1^{(i)}(\mathbf{x}) = \left\{ 1 \quad h_1\left(\frac{\mathbf{x}}{l_1^{(i)}}\right) \quad h_2\left(\frac{\mathbf{x}}{l_1^{(i)}}\right) \quad h_3\left(\frac{\mathbf{x}}{l_1^{(i)}}\right)l_1^{(i)} \quad h_4\left(\frac{\mathbf{x}}{l_1^{(i)}}\right)l_1^{(i)} \quad 0 \quad 0 \quad 0 \quad y\left(\frac{\mathbf{x}}{l_1^{(i)}}\right) \quad 0 \right\} \quad (3-14)$$

$$\mathbf{F}_2^{(i)}(\mathbf{x}) = \left\{ 1 \quad h_1\left(\frac{\mathbf{x}}{l_1^{(i)}}\right) \quad h_2\left(\frac{\mathbf{x}}{l_1^{(i)}}\right) \quad 0 \quad 0 \quad h_3\left(\frac{\mathbf{x}}{l_1^{(i)}}\right)l_1^{(i)} \quad h_4\left(\frac{\mathbf{x}}{l_1^{(i)}}\right)l_1^{(i)} \quad 0 \quad 0 \quad y\left(\frac{\mathbf{x}}{l_1^{(i)}}\right) \right\} \quad (3-15)$$

Eqs. (3-1), (3-6) and (3-10) can be rewritten in the form:

$$\mathbf{R}_0^{(i)}(\mathbf{x}, t) = (\dot{u}_B(t) + \dot{u}_O^{(i)}(t))\mathbf{i} + \mathbf{F}_0^{(i)}(\mathbf{x}) \cdot \mathbf{q}^{(i)}(t)\mathbf{j} \quad (3-16)$$

$$\mathbf{R}_1^{(i)}(\mathbf{x}, t) = \mathbf{F}_1^{(i)}(\mathbf{x}) \cdot \mathbf{q}^{(i)}(t)\mathbf{i} \quad (3-17)$$

$$\mathbf{R}_2^{(i)}(\mathbf{x}, t) = \mathbf{F}_2^{(i)}(\mathbf{x}) \cdot \mathbf{q}^{(i)}(t)\mathbf{i} \quad (3-18)$$

Furthermore, the corresponding velocities can be obtained by simply derivating Eqs. (3-16), (3-17) and (3-18) with respect to time t

$$\dot{\mathbf{R}}_0^{(i)}(\mathbf{x}, t) = (\dot{\dot{u}}_B(t) + \dot{\dot{u}}_O^{(i)}(t))\mathbf{i} + \mathbf{F}_0^{(i)}(\mathbf{x}) \cdot \dot{\mathbf{q}}^{(i)}(t)\mathbf{j} \quad (3-19)$$

$$\dot{\mathbf{R}}_1^{(i)}(\mathbf{x}, t) = \mathbf{F}_1^{(i)}(\mathbf{x}) \cdot \dot{\mathbf{q}}^{(i)}(t)\mathbf{i} \quad (3-20)$$

$$\dot{\mathbf{R}}_2^{(i)}(\mathbf{x}, t) = \mathbf{F}_2^{(i)}(\mathbf{x}) \cdot \dot{\mathbf{q}}^{(i)}(t)\mathbf{i} \quad (3-21)$$

3.3 The Kinetic Energy of the System

The kinetic energy of the i th substructure can be written in the following form

$$\begin{aligned}
T^{(i)} &= \frac{1}{2} \int_0^{l_0^{(i)}} \mathbf{r}_0(\mathbf{x}) (\dot{\mathbf{R}}_0^{(i)}(\mathbf{x}, t))^T \dot{\mathbf{R}}_0^{(i)}(\mathbf{x}, t) d\mathbf{x} \\
&+ \frac{1}{2} \int_0^{l_1^{(i)}} \mathbf{r}_1(\mathbf{x}) (\dot{\mathbf{R}}_1^{(i)}(\mathbf{x}, t))^T \dot{\mathbf{R}}_1^{(i)}(\mathbf{x}, t) d\mathbf{x} \\
&+ \frac{1}{2} \int_0^{l_2^{(i)}} \mathbf{r}_2(\mathbf{x}) (\dot{\mathbf{R}}_2^{(i)}(\mathbf{x}, t))^T \dot{\mathbf{R}}_2^{(i)}(\mathbf{x}, t) d\mathbf{x} \\
&= \frac{1}{2} m_0^{(i)} (\dot{u}_B + \dot{u}_O^{(i)})^2 + \frac{1}{2} \int_0^{l_0^{(i)}} \mathbf{r}_0(\dot{\mathbf{q}}^{(i)})^T (\mathbf{F}_0^{(i)})^T \mathbf{F}_0^{(i)} \dot{\mathbf{q}}^{(i)} d\mathbf{x} \\
&+ \frac{1}{2} \int_0^{l_1^{(i)}} \mathbf{r}_1(\dot{\mathbf{q}}^{(i)})^T (\mathbf{F}_1^{(i)})^T \mathbf{F}_1^{(i)} \dot{\mathbf{q}}^{(i)} d\mathbf{x} + \frac{1}{2} \int_0^{l_2^{(i)}} \mathbf{r}_2(\dot{\mathbf{q}}^{(i)})^T (\mathbf{F}_2^{(i)})^T \mathbf{F}_2^{(i)} \dot{\mathbf{q}}^{(i)} d\mathbf{x} \\
&= \frac{1}{2} m_0^{(i)} (\dot{u}_B + \dot{u}_O^{(i)})^2 \\
&+ \frac{1}{2} (\dot{\mathbf{q}}^{(i)})^T \left[\int_0^{l_0^{(i)}} \mathbf{r}_0(\mathbf{F}_0^{(i)})^T \mathbf{F}_0^{(i)} d\mathbf{x} + \int_0^{l_1^{(i)}} \mathbf{r}_1(\mathbf{F}_1^{(i)})^T \mathbf{F}_1^{(i)} d\mathbf{x} + \int_0^{l_2^{(i)}} \mathbf{r}_2(\mathbf{F}_2^{(i)})^T \mathbf{F}_2^{(i)} d\mathbf{x} \right] \dot{\mathbf{q}}^{(i)}
\end{aligned} \tag{3-22}$$

where

$$m_0^{(i)} = \int_0^{l_0^{(i)}} \mathbf{r}_0 d\mathbf{x} \tag{3-23}$$

is the mass of the beam in the i th substructure. Extending the terms $(\mathbf{F}_0^{(i)})^T \mathbf{F}_0^{(i)}$, $(\mathbf{F}_1^{(i)})^T \mathbf{F}_1^{(i)}$ and $(\mathbf{F}_2^{(i)})^T \mathbf{F}_2^{(i)}$ yields:

$$\begin{aligned}
 & (\mathbf{F}_0^{(i)})^T \mathbf{F}_0^{(i)} = \\
 & \left[\begin{array}{cccccc|ccc}
 0 & 0 & 0 & 0 & 0 & 0 & 0 & 0 & 0 \\
 0 & 0 & 0 & 0 & 0 & 0 & 0 & 0 & 0 \\
 & 0 & 0 & 0 & 0 & 0 & 0 & 0 & 0 \\
 & & h_3^2 \left(\frac{x}{l_0^{(i)}}\right) (l_0^{(i)})^2 & 0 & h_3 \left(\frac{x}{l_0^{(i)}}\right) h_4 \left(\frac{x}{l_0^{(i)}}\right) (l_0^{(i)})^2 & 0 & h_3 \left(\frac{x}{l_0^{(i)}}\right) f \left(\frac{x}{l_0^{(i)}}\right) l_0^{(i)} & 0 & 0 \\
 & & & 0 & 0 & 0 & 0 & 0 & 0 \\
 & & & & h_4^2 \left(\frac{x}{l_0^{(i)}}\right) (l_0^{(i)})^2 & 0 & h_4 \left(\frac{x}{l_0^{(i)}}\right) f \left(\frac{x}{l_0^{(i)}}\right) l_0^{(i)} & 0 & 0 \\
 & & & & & 0 & 0 & 0 & 0 \\
 \hline
 \text{Symmetry} & & & & & & \left(f \left(\frac{x}{l_0^{(i)}}\right) \right)^T f \left(\frac{x}{l_0^{(i)}}\right) & 0 & 0 \\
 & & & & & & & 0 & 0 \\
 & & & & & & & & 0
 \end{array} \right]
 \end{aligned}
 \tag{3-24}$$

$$\begin{aligned}
 & (\mathbf{F}_1^{(i)})^T \mathbf{F}_1^{(i)} = \\
 & \left[\begin{array}{cccccc|ccc}
 1 & h_1 \left(\frac{x}{l_1^{(i)}}\right) & h_2 \left(\frac{x}{l_1^{(i)}}\right) & h_3 \left(\frac{x}{l_1^{(i)}}\right) l_1^{(i)} & h_4 \left(\frac{x}{l_1^{(i)}}\right) l_1^{(i)} & 0 & 0 & y \left(\frac{x}{l_1^{(i)}}\right) & 0 \\
 h_1^2 \left(\frac{x}{l_1^{(i)}}\right) & h_1 \left(\frac{x}{l_1^{(i)}}\right) h_2 \left(\frac{x}{l_1^{(i)}}\right) & h_1 \left(\frac{x}{l_1^{(i)}}\right) h_3 \left(\frac{x}{l_1^{(i)}}\right) l_1^{(i)} & h_1 \left(\frac{x}{l_1^{(i)}}\right) h_4 \left(\frac{x}{l_1^{(i)}}\right) l_1^{(i)} & 0 & 0 & 0 & h_1 \left(\frac{x}{l_1^{(i)}}\right) y \left(\frac{x}{l_1^{(i)}}\right) & 0 \\
 & h_2^2 \left(\frac{x}{l_1^{(i)}}\right) & h_2 \left(\frac{x}{l_1^{(i)}}\right) h_3 \left(\frac{x}{l_1^{(i)}}\right) l_1^{(i)} & h_2 \left(\frac{x}{l_1^{(i)}}\right) h_4 \left(\frac{x}{l_1^{(i)}}\right) l_1^{(i)} & 0 & 0 & 0 & h_2 \left(\frac{x}{l_1^{(i)}}\right) y \left(\frac{x}{l_1^{(i)}}\right) & 0 \\
 & & h_3^2 \left(\frac{x}{l_1^{(i)}}\right) (l_1^{(i)})^2 & h_3 \left(\frac{x}{l_1^{(i)}}\right) h_4 \left(\frac{x}{l_1^{(i)}}\right) (l_1^{(i)})^2 & 0 & 0 & 0 & h_3 \left(\frac{x}{l_1^{(i)}}\right) y \left(\frac{x}{l_1^{(i)}}\right) l_1^{(i)} & 0 \\
 & & & h_4^2 \left(\frac{x}{l_1^{(i)}}\right) (l_1^{(i)})^2 & 0 & 0 & 0 & h_4 \left(\frac{x}{l_1^{(i)}}\right) y \left(\frac{x}{l_1^{(i)}}\right) l_1^{(i)} & 0 \\
 & & & & 0 & 0 & 0 & 0 & 0 \\
 & & & & & 0 & 0 & 0 & 0 \\
 \hline
 \text{Symmetry} & & & & & & & 0 & 0 & 0 \\
 & & & & & & & \left(y \left(\frac{x}{l_1^{(i)}}\right) \right)^T y \left(\frac{x}{l_1^{(i)}}\right) & 0 \\
 & & & & & & & & 0
 \end{array} \right]
 \end{aligned}
 \tag{3-25}$$

$$\left(\mathbf{F}_2^{(i)}\right)^T \mathbf{F}_2^{(i)} =$$

$$\left[\begin{array}{cccccc|cc} 1 & h_1\left(\frac{x}{l_1^{(i)}}\right) & h_2\left(\frac{x}{l_1^{(i)}}\right) & 0 & 0 & h_3\left(\frac{x}{l_1^{(i)}}\right)l_1^{(i)} & h_4\left(\frac{x}{l_1^{(i)}}\right)l_1^{(i)} & 0 & 0 & y\left(\frac{x}{l_1^{(i)}}\right) \\ h_1^2\left(\frac{x}{l_1^{(i)}}\right) & h_1\left(\frac{x}{l_1^{(i)}}\right)h_2\left(\frac{x}{l_1^{(i)}}\right) & h_2^2\left(\frac{x}{l_1^{(i)}}\right) & 0 & 0 & h_1\left(\frac{x}{l_1^{(i)}}\right)h_3\left(\frac{x}{l_1^{(i)}}\right)l_1^{(i)} & h_1\left(\frac{x}{l_1^{(i)}}\right)h_4\left(\frac{x}{l_1^{(i)}}\right)l_1^{(i)} & 0 & 0 & h_1\left(\frac{x}{l_1^{(i)}}\right)y\left(\frac{x}{l_1^{(i)}}\right) \\ & & & 0 & 0 & h_2\left(\frac{x}{l_1^{(i)}}\right)h_3\left(\frac{x}{l_1^{(i)}}\right)l_1^{(i)} & h_2\left(\frac{x}{l_1^{(i)}}\right)h_4\left(\frac{x}{l_1^{(i)}}\right)l_1^{(i)} & 0 & 0 & h_2\left(\frac{x}{l_1^{(i)}}\right)y\left(\frac{x}{l_1^{(i)}}\right) \\ & & & 0 & 0 & 0 & 0 & 0 & 0 & 0 \\ & & & & & 0 & 0 & 0 & 0 & 0 \\ & & & & & h_3^2\left(\frac{x}{l_1^{(i)}}\right)\left(l_1^{(i)}\right)^2 & h_3\left(\frac{x}{l_1^{(i)}}\right)h_4\left(\frac{x}{l_1^{(i)}}\right)\left(l_1^{(i)}\right)^2 & 0 & 0 & h_3\left(\frac{x}{l_1^{(i)}}\right)y\left(\frac{x}{l_1^{(i)}}\right)l_1^{(i)} \\ & & & & & & h_4^2\left(\frac{x}{l_1^{(i)}}\right)\left(l_1^{(i)}\right)^2 & 0 & 0 & h_4\left(\frac{x}{l_1^{(i)}}\right)y\left(\frac{x}{l_1^{(i)}}\right)l_1^{(i)} \\ \hline & & & & & \text{symmetry} & & 0 & 0 & 0 \\ & & & & & & & 0 & 0 & \left(y\left(\frac{x}{l_1^{(i)}}\right)\right)^T y\left(\frac{x}{l_1^{(i)}}\right) \end{array} \right] \quad (3-26)$$

Furthermore, the kinetic energy of the i th substructure can be written in the matrix form as following

$$T^{(i)} = \frac{1}{2} \left(\dot{\mathbf{q}}^{(i)}\right)^T \mathbf{M}^{(i)} \dot{\mathbf{q}}^{(i)} \quad (3-27)$$

where

$$\mathbf{M}^{(i)} = \begin{bmatrix} \mathbf{M}_c^{(i)} & \mathbf{M}_{ch}^{(i)} \\ \left(\mathbf{M}_{ch}^{(i)}\right)^T & \mathbf{M}_h^{(i)} \end{bmatrix} \quad (3-28)$$

$$\begin{aligned}
 \mathbf{M}_c^{(i)} = & \int_0^{l_0^{(i)}} \mathbf{r}_0 \begin{bmatrix} 1 & 1 & 0 & 0 & 0 & 0 \\ 1 & 0 & 0 & 0 & 0 & 0 \\ & 0 & 0 & 0 & 0 & 0 \\ & & h_3^2(\frac{\mathbf{x}}{l_0^{(i)}})(l_0^{(i)})^2 & 0 & h_3(\frac{\mathbf{x}}{l_0^{(i)}})h_4(\frac{\mathbf{x}}{l_0^{(i)}})(l_0^{(i)})^2 & 0 \\ & & & 0 & 0 & 0 \\ & & & & h_4^2(\frac{\mathbf{x}}{l_0^{(i)}})(l_0^{(i)})^2 & 0 \\ & & & & & 0 \end{bmatrix} dx \\
 & + \int_0^{l_1^{(i)}} \mathbf{r}_1 \begin{bmatrix} 1 & h_1(\frac{\mathbf{x}}{l_1^{(i)}}) & h_2^{(i)}(\frac{\mathbf{x}}{l_1^{(i)}}) & h_3^{(i)}(\frac{\mathbf{x}}{l_1^{(i)}})l_1^{(i)} & h_4^{(i)}(\frac{\mathbf{x}}{l_1^{(i)}})l_1^{(i)} & 0 & 0 \\ h_1^2(\frac{\mathbf{x}}{l_1^{(i)}}) & h_1(\frac{\mathbf{x}}{l_1^{(i)}})h_2(\frac{\mathbf{x}}{l_1^{(i)}}) & h_2(\frac{\mathbf{x}}{l_1^{(i)}})h_3(\frac{\mathbf{x}}{l_1^{(i)}})l_1^{(i)} & h_1(\frac{\mathbf{x}}{l_1^{(i)}})h_3(\frac{\mathbf{x}}{l_1^{(i)}})l_1^{(i)} & h_1(\frac{\mathbf{x}}{l_1^{(i)}})h_4(\frac{\mathbf{x}}{l_1^{(i)}})l_1^{(i)} & 0 & 0 \\ & h_2^2(\frac{\mathbf{x}}{l_1^{(i)}}) & h_2(\frac{\mathbf{x}}{l_1^{(i)}})h_3(\frac{\mathbf{x}}{l_1^{(i)}})l_1^{(i)} & h_2(\frac{\mathbf{x}}{l_1^{(i)}})h_4(\frac{\mathbf{x}}{l_1^{(i)}})l_1^{(i)} & & 0 & 0 \\ & & h_3^2(\frac{\mathbf{x}}{l_1^{(i)}})(l_1^{(i)})^2 & h_3(\frac{\mathbf{x}}{l_1^{(i)}})h_4(\frac{\mathbf{x}}{l_1^{(i)}})l_1^{(i)} & & 0 & 0 \\ & & & & h_4^2(\frac{\mathbf{x}}{l_1^{(i)}})(l_1^{(i)})^2 & 0 & 0 \\ & & & & & 0 & 0 \\ & & & & & & 0 \end{bmatrix} dx \\
 & + \int_0^{l_1^{(i)}} \mathbf{r}_2 \begin{bmatrix} 1 & h_1(\frac{\mathbf{x}}{l_1^{(i)}}) & h_2^{(i)}(\frac{\mathbf{x}}{l_1^{(i)}}) & 0 & 0 & h_3^{(i)}(\frac{\mathbf{x}}{l_1^{(i)}})l_1^{(i)} & h_4^{(i)}(\frac{\mathbf{x}}{l_1^{(i)}})l_1^{(i)} \\ h_1^2(\frac{\mathbf{x}}{l_1^{(i)}}) & h_1(\frac{\mathbf{x}}{l_1^{(i)}})h_2(\frac{\mathbf{x}}{l_1^{(i)}}) & h_2(\frac{\mathbf{x}}{l_1^{(i)}})h_3(\frac{\mathbf{x}}{l_1^{(i)}})l_1^{(i)} & 0 & 0 & h_1(\frac{\mathbf{x}}{l_1^{(i)}})h_3(\frac{\mathbf{x}}{l_1^{(i)}})l_1^{(i)} & h_1(\frac{\mathbf{x}}{l_1^{(i)}})h_4(\frac{\mathbf{x}}{l_1^{(i)}})l_1^{(i)} \\ & h_2^2(\frac{\mathbf{x}}{l_1^{(i)}}) & 0 & 0 & h_2(\frac{\mathbf{x}}{l_1^{(i)}})h_3(\frac{\mathbf{x}}{l_1^{(i)}})l_1^{(i)} & h_2(\frac{\mathbf{x}}{l_1^{(i)}})h_4(\frac{\mathbf{x}}{l_1^{(i)}})l_1^{(i)} & \\ & & 0 & 0 & 0 & 0 & 0 \\ & & & 0 & 0 & 0 & 0 \\ & & & h_3^2(\frac{\mathbf{x}}{l_1^{(i)}})(l_1^{(i)})^2 & h_3(\frac{\mathbf{x}}{l_1^{(i)}})h_4(\frac{\mathbf{x}}{l_1^{(i)}})l_1^{(i)} & & \\ & & & & & h_4^2(\frac{\mathbf{x}}{l_1^{(i)}})(l_1^{(i)})^2 & \end{bmatrix} dx
 \end{aligned}$$

(3-29)

$$\begin{aligned}
 \mathbf{M}_{ch}^{(i)} = & \int_0^{l_0^{(i)}} \mathbf{r}_0 \begin{bmatrix} 0 & 0 & 0 \\ 0 & 0 & 0 \\ 0 & 0 & 0 \\ h_3(\frac{x}{l_0^{(i)}})f(\frac{x}{l_0^{(i)}})l_0^{(i)} & 0 & 0 \\ 0 & 0 & 0 \\ h_4(\frac{x}{l_0^{(i)}})f(\frac{x}{l_0^{(i)}})l_0^{(i)} & 0 & 0 \\ 0 & 0 & 0 \end{bmatrix} dx + \int_0^{l_1^{(i)}} \mathbf{r}_1 \begin{bmatrix} 0 & y(\frac{x}{l_1^{(i)}}) & 0 \\ 0 & h_1(\frac{x}{l_1^{(i)}})y(\frac{x}{l_1^{(i)}}) & 0 \\ 0 & h_2(\frac{x}{l_1^{(i)}})y(\frac{x}{l_1^{(i)}}) & 0 \\ 0 & h_3(\frac{x}{l_1^{(i)}})y(\frac{x}{l_1^{(i)}})l_1^{(i)} & 0 \\ 0 & h_4(\frac{x}{l_1^{(i)}})y(\frac{x}{l_1^{(i)}})l_1^{(i)} & 0 \\ 0 & 0 & 0 \\ 0 & 0 & 0 \end{bmatrix} dx \\
 & + \int_0^{l_2^{(i)}} \mathbf{r}_2 \begin{bmatrix} 0 & 0 & y(\frac{x}{l_1^{(i)}}) \\ 0 & 0 & h_1(\frac{x}{l_1^{(i)}})y(\frac{x}{l_1^{(i)}}) \\ 0 & 0 & h_2(\frac{x}{l_1^{(i)}})y(\frac{x}{l_1^{(i)}}) \\ 0 & 0 & 0 \\ 0 & 0 & 0 \\ 0 & 0 & h_3(\frac{x}{l_1^{(i)}})y(\frac{x}{l_1^{(i)}})l_1^{(i)} \\ 0 & 0 & h_4(\frac{x}{l_1^{(i)}})y(\frac{x}{l_1^{(i)}})l_1^{(i)} \end{bmatrix} dx \tag{3-30}
 \end{aligned}$$

$$\begin{aligned}
 \mathbf{M}_h^{(i)} = & \int_0^{l_0^{(i)}} \mathbf{r}_0 \begin{bmatrix} \left(f(\frac{x}{l_0^{(i)}})\right)^T f(\frac{x}{l_0^{(i)}}) & 0 & 0 \\ 0 & 0 & 0 \\ 0 & 0 & 0 \end{bmatrix} dx + \int_0^{l_1^{(i)}} \mathbf{r}_1 \begin{bmatrix} 0 & 0 & 0 \\ 0 & \left(y(\frac{x}{l_1^{(i)}})\right)^T y(\frac{x}{l_1^{(i)}}) & 0 \\ 0 & 0 & 0 \end{bmatrix} dx \\
 & + \int_0^{l_1^{(i)}} \mathbf{r}_2 \begin{bmatrix} 0 & 0 & 0 \\ 0 & 0 & 0 \\ 0 & 0 & \left(y(\frac{x}{l_1^{(i)}})\right)^T y(\frac{x}{l_1^{(i)}}) \end{bmatrix} dx \tag{3-31}
 \end{aligned}$$

It should be noted that the element mass matrices $\mathbf{M}_c^{(i)}$ are only Hermite cubics dependent, independent of the hierarchical functions, while $\mathbf{M}_h^{(i)}$ are hierarchical function dependent, independent of Hermite cubics. When increasing a hierarchical function in discretizing procedure to improve accuracy, only $\mathbf{M}_h^{(i)}$ and $\mathbf{M}_{ch}^{(i)}$ are affected but $\mathbf{M}_c^{(i)}$ keep unchanged.

The kinetic energy of the whole system can be represented by

$$T = \frac{1}{2} m_B \dot{u}_B^2 + \sum_{i=1}^N T^{(i)} = \frac{1}{2} \dot{\tilde{\mathbf{q}}}^T \tilde{\mathbf{M}} \dot{\tilde{\mathbf{q}}} \quad (3-32)$$

where

$$\tilde{\mathbf{q}} = \left\{ u_B^{(N)} \mathbf{q}_1^{(N)} \mathbf{q}_2^{(N)} (\mathbf{q}_0^{(N)})^T (\mathbf{q}_1^{(N)})^T (\mathbf{q}_2^{(N)})^T u_0^{(N-1)} \mathbf{q}_1^{(N-1)} \mathbf{q}_2^{(N-1)} (\mathbf{q}_0^{(N-1)})^T \cdots u_0^{(i)} \mathbf{q}_1^{(i)} \mathbf{q}_2^{(i)} (\mathbf{q}_0^{(i)})^T (\mathbf{q}_1^{(i)})^T (\mathbf{q}_2^{(i)})^T u_0^{(i-1)} \mathbf{q}_1^{(i-1)} \mathbf{q}_2^{(i-1)} (\mathbf{q}_0^{(i-1)})^T \cdots u_0^{(1)} \mathbf{q}_1^{(1)} \mathbf{q}_2^{(1)} (\mathbf{q}_0^{(1)})^T (\mathbf{q}_1^{(1)})^T (\mathbf{q}_2^{(1)})^T \right\}^T \quad (3-33)$$

is a $(1 + N \times (3 + n_0 + 2 \times n_1))$ dimensional global vector, and $\tilde{\mathbf{M}}$ is global mass matrix. In carrying out the assembly of the element matrix, it is observed that displacement of base u_B appears as top component in all $\mathbf{q}^{(i)}$, $i = 1, \dots, N$. Consistent with this, there are N element mass matrix entries corresponding to u_B , the entry (1,1) of $\mathbf{M}^{(i)}$, $i = 1, \dots, N$. Similarly, it is can also observed that nodal displacement $u_0^{(i-1)}$, nodal angular displacements $\mathbf{q}_1^{(i-1)}$ and $\mathbf{q}_2^{(i-1)}$ appear as the 3rd, 5th and 7th components in $\mathbf{q}^{(i)}$ and as the 2nd, 4th and 6th components in $\mathbf{q}^{(i-1)}$, respectively. Consistent with this, there are two element mass matrix entries corresponding to $u_0^{(i-1)}$, the entry (3,3) of $\mathbf{M}^{(i)}$ and the entry (2,2) of $\mathbf{M}^{(i-1)}$, two entries corresponding to $\mathbf{q}_1^{(i-1)}$, the entry (5,5) of $\mathbf{M}^{(i)}$ and the entry (4,4) of $\mathbf{M}^{(i-1)}$, two

entries corresponding to $\mathbf{q}_2^{(i-1)}$, the entry (7,7) of $\mathbf{M}^{(i)}$ and the entry (6,6) of $\mathbf{M}^{(i-1)}$. The assembly consists of elimination of the duplications of u_B , $u_0^{(i-1)}$, $\mathbf{q}_1^{(i-1)}$ and $\theta_2^{(i-1)}$ from the nodal vector $\tilde{\mathbf{q}}$ and adding correspondingly the entries (1,1) in $\mathbf{M}^{(i)}$, $i = 1, \dots, N - 1$, to the entry (1,1) in $\mathbf{M}^{(N)}$ resulting in the mass, m , of the entire system; adding correspondingly the entry (2,2) of $\mathbf{M}^{(i-1)}$ to the entry (3,3) of $\mathbf{M}^{(i)}$, the entry (4,4) of $\mathbf{M}^{(i-1)}$ to the entry (5,5) of $\mathbf{M}^{(i)}$; the entry (6,6) of $\mathbf{M}^{(i-1)}$ to the entry (7,7) of $\mathbf{M}^{(i)}$. The resulting global mass matrix $\tilde{\mathbf{M}}$ is real symmetric and positive definite. It must be pointed out that the entry (1,1) of the global mass matrix $\tilde{\mathbf{M}}$ is the total mass of entire system, m , including the base and the N -stores building.

It is not difficult to observe that in order to improve accuracy, only one row and one column needs to be added to the global mass matrix $\tilde{\mathbf{M}}$ without disturbing the other elements of the matrix $\tilde{\mathbf{M}}$. Hence the global mass matrix $\tilde{\mathbf{M}}$ possesses the embedding property.

3.4 The Potential Energy of the System

The potential energy of the i th substructure can be expressed by

$$\begin{aligned}
 V^{(i)} &= \frac{1}{2} \int_0^{l_0^{(i)}} EI^{(i)} \left(\frac{\partial^2 w_0^{(i)}}{\partial x^2} \right)^2 dx \\
 &+ \frac{1}{2} \int_0^{l_1^{(i)}} \left[EI^{(i)} \left(\frac{\partial^2 w_1^{(i)}}{\partial x^2} \right)^2 - P_1^{(i)} \left(\frac{\partial w_1^{(i)}}{\partial x} \right)^2 \right] dx \\
 &+ \frac{1}{2} \int_0^{l_2^{(i)}} \left[EI^{(i)} \left(\frac{\partial^2 w_2^{(i)}}{\partial x^2} \right)^2 - P_2^{(i)} \left(\frac{\partial w_2^{(i)}}{\partial x} \right)^2 \right] dx
 \end{aligned} \tag{3-34}$$

$$\left(\frac{\partial \tilde{\mathbf{F}}_2^{(i)}}{\partial \mathbf{x}^2}\right)^T \frac{\partial \tilde{\mathbf{F}}_2^{(i)}}{\partial \mathbf{x}^2} =$$

$\begin{bmatrix} 0 & 0 & 0 & 0 & 0 & 0 \\ h_1'^2(\frac{\mathbf{x}}{l_1^{(i)}}) & h_1'(\frac{\mathbf{x}}{l_1^{(i)}})h_2'(\frac{\mathbf{x}}{l_1^{(i)}}) & 0 & 0 & h_1'(\frac{\mathbf{x}}{l_1^{(i)}})h_3'(\frac{\mathbf{x}}{l_1^{(i)}})l_1^{(i)} & h_1'(\frac{\mathbf{x}}{l_1^{(i)}})h_4'(\frac{\mathbf{x}}{l_1^{(i)}})l_1^{(i)} \\ & h_2'^2(\frac{\mathbf{x}}{l_1^{(i)}}) & 0 & 0 & h_2'(\frac{\mathbf{x}}{l_1^{(i)}})h_3'(\frac{\mathbf{x}}{l_1^{(i)}})l_1^{(i)} & h_2'(\frac{\mathbf{x}}{l_1^{(i)}})h_4'(\frac{\mathbf{x}}{l_1^{(i)}})l_1^{(i)} \\ & & 0 & 0 & 0 & 0 \\ & & 0 & 0 & 0 & 0 \\ & & & h_3'^2(\frac{\mathbf{x}}{l_1^{(i)}})(l_1^{(i)})^2 & h_3'(\frac{\mathbf{x}}{l_1^{(i)}})h_4'(\frac{\mathbf{x}}{l_1^{(i)}})(l_1^{(i)})^2 & h_4'^2(\frac{\mathbf{x}}{l_1^{(i)}})(l_1^{(i)})^2 \end{bmatrix}$	$\begin{bmatrix} 0 & 0 \\ 0 & h_1'(\frac{\mathbf{x}}{l_1^{(i)}})y'(\frac{\mathbf{x}}{l_1^{(i)}}) \\ 0 & h_2'(\frac{\mathbf{x}}{l_1^{(i)}})y'(\frac{\mathbf{x}}{l_1^{(i)}}) \\ 0 & 0 \\ 0 & 0 \\ 0 & 0 \\ 0 & h_3'(\frac{\mathbf{x}}{l_1^{(i)}})y'(\frac{\mathbf{x}}{l_1^{(i)}})l_1^{(i)} \\ 0 & h_4'(\frac{\mathbf{x}}{l_1^{(i)}})y'(\frac{\mathbf{x}}{l_1^{(i)}})l_1^{(i)} \end{bmatrix} / (l_1^{(i)})^2$	
symmetry		$\begin{bmatrix} 0 & 0 \\ 0 & 0 \\ \left(y'(\frac{\mathbf{x}}{l_1^{(i)}})\right)^T & y'(\frac{\mathbf{x}}{l_1^{(i)}}) \end{bmatrix}$

(3-39)

$$\left(\frac{\partial^2 \tilde{\mathbf{F}}_2^{(i)}}{\partial \mathbf{x}^2}\right)^T \frac{\partial^2 \tilde{\mathbf{F}}_2^{(i)}}{\partial \mathbf{x}^2} =$$

$\begin{bmatrix} 0 & 0 & 0 & 0 & 0 & 0 \\ h_1''^2(\frac{\mathbf{x}}{l_1^{(i)}}) & h_1''(\frac{\mathbf{x}}{l_1^{(i)}})h_2''(\frac{\mathbf{x}}{l_1^{(i)}}) & 0 & 0 & h_1''(\frac{\mathbf{x}}{l_1^{(i)}})h_3''(\frac{\mathbf{x}}{l_1^{(i)}})l_1^{(i)} & h_1''(\frac{\mathbf{x}}{l_1^{(i)}})h_4''(\frac{\mathbf{x}}{l_1^{(i)}})l_1^{(i)} \\ & h_2''^2(\frac{\mathbf{x}}{l_1^{(i)}}) & 0 & 0 & h_2''(\frac{\mathbf{x}}{l_1^{(i)}})h_3''(\frac{\mathbf{x}}{l_1^{(i)}})l_1^{(i)} & h_2''(\frac{\mathbf{x}}{l_1^{(i)}})h_4''(\frac{\mathbf{x}}{l_1^{(i)}})l_1^{(i)} \\ & & 0 & 0 & 0 & 0 \\ & & 0 & 0 & 0 & 0 \\ & & & h_3''^2(\frac{\mathbf{x}}{l_1^{(i)}})(l_1^{(i)})^2 & h_3''(\frac{\mathbf{x}}{l_1^{(i)}})h_4''(\frac{\mathbf{x}}{l_1^{(i)}})(l_1^{(i)})^2 & h_4''^2(\frac{\mathbf{x}}{l_1^{(i)}})(l_1^{(i)})^2 \end{bmatrix}$	$\begin{bmatrix} 0 & 0 \\ 0 & h_1''(\frac{\mathbf{x}}{l_1^{(i)}})y''(\frac{\mathbf{x}}{l_1^{(i)}}) \\ 0 & h_2''(\frac{\mathbf{x}}{l_1^{(i)}})y''(\frac{\mathbf{x}}{l_1^{(i)}}) \\ 0 & 0 \\ 0 & 0 \\ 0 & 0 \\ 0 & h_3''(\frac{\mathbf{x}}{l_1^{(i)}})y''(\frac{\mathbf{x}}{l_1^{(i)}})l_1^{(i)} \\ 0 & h_4''(\frac{\mathbf{x}}{l_1^{(i)}})y''(\frac{\mathbf{x}}{l_1^{(i)}})l_1^{(i)} \end{bmatrix} / (l_1^{(i)})^4$	
symmetry		$\begin{bmatrix} 0 & 0 \\ 0 & 0 \\ \left(y''(\frac{\mathbf{x}}{l_1^{(i)}})\right)^T & y''(\frac{\mathbf{x}}{l_1^{(i)}}) \end{bmatrix}$

3-40)

$$V^{(i)} = \frac{1}{2} (\mathbf{q}^{(i)})^T \mathbf{K}^{(i)} \mathbf{q}^{(i)} \quad (3-41)$$

where

$$\mathbf{K}^{(i)} = \begin{bmatrix} \mathbf{K}_c^{(i)} & \mathbf{K}_{ch}^{(i)} \\ (\mathbf{K}_{ch}^{(i)})^T & \mathbf{K}_h^{(i)} \end{bmatrix} \quad (3-42)$$

in which

$$\mathbf{K}_c^{(i)} = \int_0^{l_0^{(i)}} \frac{EI^{(i)}}{(l_0^{(i)})^4} \begin{bmatrix} 0 & 0 & 0 & 0 & 0 & 0 \\ 0 & 0 & 0 & 0 & 0 & 0 \\ & 0 & 0 & 0 & 0 & 0 \\ & & h_3''^2 \left(\frac{x}{l_0^{(i)}}\right) (l_0^{(i)})^2 & 0 & h_3'' \left(\frac{x}{l_0^{(i)}}\right) h_4'' \left(\frac{x}{l_0^{(i)}}\right) (l_0^{(i)})^2 & 0 \\ & & & 0 & 0 & 0 \\ & & & & h_4''^2 \left(\frac{x}{l_0^{(i)}}\right) (l_0^{(i)})^2 & 0 \\ & & & & & 0 \end{bmatrix} dx +$$

$$+ \int_0^{l_1^{(i)}} \frac{EI^{(i)}}{(l_0^{(i)})^4} \begin{bmatrix} 0 & 0 & 0 & 0 & 0 & 0 & 0 & 0 \\ h_1''^2 \left(\frac{x}{l_1^{(i)}}\right) h_1' \left(\frac{x}{l_1^{(i)}}\right) h_2'' \left(\frac{x}{l_1^{(i)}}\right) h_1' \left(\frac{x}{l_1^{(i)}}\right) h_3'' \left(\frac{x}{l_1^{(i)}}\right) h_1'' \left(\frac{x}{l_1^{(i)}}\right) h_4'' \left(\frac{x}{l_1^{(i)}}\right) h_1'' \left(\frac{x}{l_1^{(i)}}\right) & 0 & 0 & 0 & 0 & 0 & 0 \\ & h_2''^2 \left(\frac{x}{l_1^{(i)}}\right) & h_2' \left(\frac{x}{l_1^{(i)}}\right) h_3'' \left(\frac{x}{l_1^{(i)}}\right) h_1'' \left(\frac{x}{l_1^{(i)}}\right) & h_2'' \left(\frac{x}{l_1^{(i)}}\right) h_4'' \left(\frac{x}{l_1^{(i)}}\right) h_1'' \left(\frac{x}{l_1^{(i)}}\right) & 0 & 0 & 0 & 0 \\ & & h_3''^2 \left(\frac{x}{l_1^{(i)}}\right) (l_1^{(i)})^2 & h_3' \left(\frac{x}{l_1^{(i)}}\right) h_4'' \left(\frac{x}{l_1^{(i)}}\right) (l_1^{(i)})^2 & 0 & 0 & 0 & 0 \\ & & & & h_4''^2 \left(\frac{x}{l_1^{(i)}}\right) (l_1^{(i)})^2 & 0 & 0 & 0 \\ & & & & & 0 & 0 & 0 \\ & & & & & & 0 & 0 \end{bmatrix} -$$

$$- \frac{P_1^{(i)}}{(l_0^{(i)})^2} \begin{bmatrix} 0 & 0 & 0 & 0 & 0 & 0 & 0 & 0 \\ h_1''^2 \left(\frac{x}{l_1^{(i)}}\right) h_1' \left(\frac{x}{l_1^{(i)}}\right) h_2'' \left(\frac{x}{l_1^{(i)}}\right) h_1' \left(\frac{x}{l_1^{(i)}}\right) h_3'' \left(\frac{x}{l_1^{(i)}}\right) h_1'' \left(\frac{x}{l_1^{(i)}}\right) h_4'' \left(\frac{x}{l_1^{(i)}}\right) h_1'' \left(\frac{x}{l_1^{(i)}}\right) & 0 & 0 & 0 & 0 & 0 & 0 & 0 \\ & h_2''^2 \left(\frac{x}{l_1^{(i)}}\right) & h_2'' \left(\frac{x}{l_1^{(i)}}\right) h_3'' \left(\frac{x}{l_1^{(i)}}\right) h_1'' \left(\frac{x}{l_1^{(i)}}\right) & h_2'' \left(\frac{x}{l_1^{(i)}}\right) h_4'' \left(\frac{x}{l_1^{(i)}}\right) h_1'' \left(\frac{x}{l_1^{(i)}}\right) & 0 & 0 & 0 & 0 \\ & & h_3''^2 \left(\frac{x}{l_1^{(i)}}\right) (l_1^{(i)})^2 & h_3'' \left(\frac{x}{l_1^{(i)}}\right) h_4'' \left(\frac{x}{l_1^{(i)}}\right) (l_1^{(i)})^2 & 0 & 0 & 0 & 0 \\ & & & & h_4''^2 \left(\frac{x}{l_1^{(i)}}\right) (l_1^{(i)})^2 & 0 & 0 & 0 \\ & & & & & 0 & 0 & 0 \\ & & & & & & 0 & 0 \end{bmatrix} dx +$$

$$\begin{aligned}
 & + \int_0^{l_1^{(i)}} \left\{ \frac{EI^{(i)}}{(l_0^{(i)})^4} \begin{bmatrix} 0 & 0 & 0 & 0 & 0 & 0 \\ h_1''^2(\frac{x}{l_1^{(i)}}) h_1''(\frac{x}{l_1^{(i)}}) h_2''(\frac{x}{l_1^{(i)}}) & 0 & 0 & h_1'(\frac{x}{l_1^{(i)}}) h_3''(\frac{x}{l_1^{(i)}}) l_1^{(i)} & h_1''(\frac{x}{l_1^{(i)}}) h_4''(\frac{x}{l_1^{(i)}}) l_1^{(i)} \\ & h_2''^2(\frac{x}{l_1^{(i)}}) & 0 & 0 & h_2'(\frac{x}{l_1^{(i)}}) h_3''(\frac{x}{l_1^{(i)}}) l_1^{(i)} & h_2''(\frac{x}{l_1^{(i)}}) h_4''(\frac{x}{l_1^{(i)}}) l_1^{(i)} \\ & & 0 & 0 & 0 & 0 \\ & & 0 & 0 & 0 & 0 \\ & \text{symmetry} & & h_3''^2(\frac{x}{l_1^{(i)}}) (l_1^{(i)})^2 & h_3'(\frac{x}{l_1^{(i)}}) h_4''(\frac{x}{l_1^{(i)}}) (l_1^{(i)})^2 \\ & & & & & h_4''^2(\frac{x}{l_1^{(i)}}) (l_1^{(i)})^2 \end{bmatrix} \right. \\
 & - \frac{P_2^{(i)}}{(l_0^{(i)})^2} \left. \begin{bmatrix} 0 & 0 & 0 & 0 & 0 & 0 \\ h_1'^2(\frac{x}{l_1^{(i)}}) h_1'(\frac{x}{l_1^{(i)}}) h_2'(\frac{x}{l_1^{(i)}}) & 0 & 0 & h_1'(\frac{x}{l_1^{(i)}}) h_3'(\frac{x}{l_1^{(i)}}) l_1^{(i)} & h_1'(\frac{x}{l_1^{(i)}}) h_4'(\frac{x}{l_1^{(i)}}) l_1^{(i)} \\ & h_2'^2(\frac{x}{l_1^{(i)}}) & 0 & 0 & h_2'(\frac{x}{l_1^{(i)}}) h_3'(\frac{x}{l_1^{(i)}}) l_1^{(i)} & h_2'(\frac{x}{l_1^{(i)}}) h_4'(\frac{x}{l_1^{(i)}}) l_1^{(i)} \\ & & 0 & 0 & 0 & 0 \\ & & 0 & 0 & 0 & 0 \\ & \text{symmetry} & & h_3'^2(\frac{x}{l_1^{(i)}}) (l_1^{(i)})^2 & h_3'(\frac{x}{l_1^{(i)}}) h_4'(\frac{x}{l_1^{(i)}}) (l_1^{(i)})^2 \\ & & & & & h_4'^2(\frac{x}{l_1^{(i)}}) (l_1^{(i)})^2 \end{bmatrix} dx \right. \\
 & \left. \right\} \quad (3-43)
 \end{aligned}$$

$$\begin{aligned}
 \mathbf{K}_{ch}^{(i)} = & \int_0^{l_0^{(i)}} \frac{EI^{(i)}}{(l_0^{(i)})^4} \begin{bmatrix} 0 & 0 & 0 \\ h_3''^{(i)}(\frac{x}{l_0^{(i)}}) f''(\frac{x}{l_0^{(i)}}) l_0^{(i)} & 0 & 0 \\ 0 & 0 & 0 \\ h_3''^{(i)}(\frac{x}{l_0^{(i)}}) f''(\frac{x}{l_0^{(i)}}) l_0^{(i)} & 0 & 0 \\ 0 & 0 & 0 \end{bmatrix} dx + \\
 & + \int_0^{l_1^{(i)}} \left\{ \frac{EI^{(i)}}{(l_1^{(i)})^4} \begin{bmatrix} 0 & 0 & 0 \\ 0 & h_1''(\frac{x}{l_1^{(i)}}) y''(\frac{x}{l_1^{(i)}}) & 0 \\ 0 & h_2''(\frac{x}{l_1^{(i)}}) y''(\frac{x}{l_1^{(i)}}) & 0 \\ 0 & h_3''(\frac{x}{l_1^{(i)}}) y''(\frac{x}{l_1^{(i)}}) l_1^{(i)} & 0 \\ 0 & h_4''(\frac{x}{l_1^{(i)}}) y''(\frac{x}{l_1^{(i)}}) l_1^{(i)} & 0 \\ 0 & 0 & 0 \\ 0 & 0 & 0 \end{bmatrix} - \frac{P_1^{(i)}}{(l_1^{(i)})^2} \begin{bmatrix} 0 & 0 & 0 \\ 0 & h_1'(\frac{x}{l_1^{(i)}}) y'(\frac{x}{l_1^{(i)}}) & 0 \\ 0 & h_2'(\frac{x}{l_1^{(i)}}) y'(\frac{x}{l_1^{(i)}}) & 0 \\ 0 & h_3'(\frac{x}{l_1^{(i)}}) y'(\frac{x}{l_1^{(i)}}) l_1^{(i)} & 0 \\ 0 & h_4'(\frac{x}{l_1^{(i)}}) y'(\frac{x}{l_1^{(i)}}) l_1^{(i)} & 0 \\ 0 & 0 & 0 \\ 0 & 0 & 0 \end{bmatrix} dx \right\} +
 \end{aligned}$$

$$+ \int_0^{l_1^{(i)}} \left\{ \frac{EI^{(i)}}{(l_1^{(i)})^4} \begin{bmatrix} 0 & 0 & 0 \\ 0 & 0 & h_1''(\frac{x}{l_1^{(i)}})y'(\frac{x}{l_1^{(i)}}) \\ 0 & 0 & h_2''(\frac{x}{l_1^{(i)}})y'(\frac{x}{l_1^{(i)}}) \\ 0 & 0 & 0 \\ 0 & 0 & 0 \\ 0 & 0 & h_3''(\frac{x}{l_1^{(i)}})y'(\frac{x}{l_1^{(i)}})l_1^{(i)} \\ 0 & 0 & h_4''(\frac{x}{l_1^{(i)}})y'(\frac{x}{l_1^{(i)}})l_1^{(i)} \end{bmatrix} - \frac{P_2^{(i)}}{(l_1^{(i)})^2} \begin{bmatrix} 0 & 0 & 0 \\ 0 & 0 & h_1'(\frac{x}{l_1^{(i)}})y'(\frac{x}{l_1^{(i)}}) \\ 0 & 0 & h_2'(\frac{x}{l_1^{(i)}})y'(\frac{x}{l_1^{(i)}}) \\ 0 & 0 & 0 \\ 0 & 0 & 0 \\ 0 & 0 & h_3'(\frac{x}{l_1^{(i)}})y'(\frac{x}{l_1^{(i)}})l_1^{(i)} \\ 0 & 0 & h_4'(\frac{x}{l_1^{(i)}})y'(\frac{x}{l_1^{(i)}})l_1^{(i)} \end{bmatrix} \right\} dx \quad (3-44)$$

$$\mathbf{K}_h^{(i)} = \int_0^{l_0^{(i)}} \frac{EI^{(i)}}{(l_0^{(i)})^4} \begin{bmatrix} \left(f''(\frac{x}{l_0^{(i)}}) \right)^T f''(\frac{x}{l_0^{(i)}}) & 0 & 0 \\ 0 & 0 & 0 \\ 0 & 0 & 0 \end{bmatrix} dx +$$

$$+ \int_0^{l_1^{(i)}} \left\{ \frac{EI^{(i)}}{(l_1^{(i)})^4} \begin{bmatrix} 0 & 0 & 0 \\ 0 & \left(y''(\frac{x}{l_1^{(i)}}) \right)^T y''(\frac{x}{l_1^{(i)}}) & 0 \\ 0 & 0 & 0 \end{bmatrix} - \frac{P_1^{(i)}}{(l_1^{(i)})^2} \begin{bmatrix} 0 & 0 & 0 \\ 0 & \left(y'(\frac{x}{l_1^{(i)}}) \right)^T y'(\frac{x}{l_1^{(i)}}) & 0 \\ 0 & 0 & 0 \end{bmatrix} \right\} dx$$

$$+ \int_0^{l_1^{(i)}} \left\{ \frac{EI^{(i)}}{(l_1^{(i)})^4} \begin{bmatrix} 0 & 0 & 0 \\ 0 & 0 & 0 \\ 0 & 0 & \left(y''(\frac{x}{l_1^{(i)}}) \right)^T y''(\frac{x}{l_1^{(i)}}) \end{bmatrix} - \frac{P_2^{(i)}}{(l_1^{(i)})^2} \begin{bmatrix} 0 & 0 & 0 \\ 0 & 0 & 0 \\ 0 & 0 & \left(y'(\frac{x}{l_1^{(i)}}) \right)^T y'(\frac{x}{l_1^{(i)}}) \end{bmatrix} \right\} dx \quad (3-45)$$

It should be noted that the element mass matrices $\mathbf{K}_c^{(i)}$ are only Hermite cubics dependent, independent of the hierarchical functions, while $\mathbf{K}_h^{(i)}$ are hierarchical function dependent, independent of the Hermite cubics.

Thus, the potential energy of the entire system can be represented as

$$V = \frac{1}{2} k_B (u_B - u_g)^2 + \sum_{i=1}^N V^{(i)} = \frac{1}{2} \tilde{\mathbf{q}}^T \tilde{\mathbf{K}} \tilde{\mathbf{q}} - k_B u_g u_B + \frac{1}{2} k_B u_g^2 \quad (3-46)$$

where k_B is the spring constant of the isolation system, u_g indicates the motion of the ground, $\tilde{\mathbf{K}}$ is the global stiffness matrix of the entire system, the entry (1, 1) of which is k_B . In carrying out the assembly of the element matrix, there are two element stiffness matrix entries corresponding to $u_0^{(i-1)}$, the entry (3,3) of $\mathbf{K}^{(i)}$ and the entry (2,2) of $\mathbf{K}^{(i-1)}$, two entries corresponding to $\mathbf{q}_1^{(i-1)}$, the entry (5,5) of $\mathbf{K}^{(i)}$ and the entry (4,4) of $\mathbf{K}^{(i-1)}$, two entries corresponding to $\mathbf{q}_2^{(i-1)}$, the entry (7,7) of $\mathbf{K}^{(i)}$ and the entry (6,6) of $\mathbf{K}^{(i-1)}$. Thus, the assembly consists of adding the entry (2,2) of $\mathbf{K}^{(i-1)}$ to the entry (3,3) of $\mathbf{K}^{(i)}$, the entry (4,4) of $\mathbf{K}^{(i-1)}$ to the entry (5,5) of $\mathbf{K}^{(i)}$, and the entry (6,6) of $\mathbf{K}^{(i-1)}$ to the entry (7,7) of $\mathbf{K}^{(i)}$. The resulting global stiffness matrix $\tilde{\mathbf{K}}$ is real symmetric and positive definite. It must be pointed out that the entry (1,1) of the global stiffness matrix $\tilde{\mathbf{K}}$ is k_B , although the entry (1,1) of all element stiffness matrix $\mathbf{K}^{(i)}$ are zero. This arises from the effect of elastic spring by which the base is connected to the ground.

3.5 Virtual Work of the Nonconservative Forces

The virtual work of the nonconservative forces consisting of the damping and the control forces acting on the i th substructure can be written as

$$\begin{aligned} \delta W_{nc}^{(i)} &= \int_0^{l_0^{(i)}} f_{d0}^{(i)}(x, t) \delta w_0^{(i)} dx + \int_0^{l_1^{(i)}} f_{d1}^{(i)}(x, t) \delta w_1^{(i)} dx + \int_0^{l_2^{(i)}} f_{d2}^{(i)}(x, t) \delta w_2^{(i)} dx \\ &+ F_c^{(i)} (\delta u_B + \delta u_0^{(i)}) + \int_0^{l_1^{(i)}} f_{c1}^{(i)}(x, t) (\delta u_B + \delta w_1^{(i)}) dx + \int_0^{l_2^{(i)}} f_{c2}^{(i)}(x, t) (\delta u_B + \delta w_2^{(i)}) dx \end{aligned} \quad (3-47)$$

where $f_{d0}^{(i)}(x, t)$, $f_{d1}^{(i)}(x, t)$ and $f_{d2}^{(i)}(x, t)$ denote the damping force densities on the floor, the left and right elastic columns on the i th substructure, respectively, $F_c^{(i)}(t)$ is the horizontal control force applying on the i th floor, $f_{c1}^{(i)}(x, t)$ and $f_{c2}^{(i)}(x, t)$ are the control force densities on the left and right elastic columns on the i th substructure, respectively. Since damping forces can be generated by means of a Rayleigh's dissipation function and accounted for separately in the virtual work [64], the Rayleigh dissipation function has the form

$$\begin{aligned} f(t) = & \frac{1}{2} c_B (\dot{u}_B(t) - \dot{u}_g(t))^2 \\ & + \frac{1}{2} \sum_{i=1}^N \left[\int_0^{l_0^{(i)}} c_0^{(i)}(x) (\dot{w}_0^{(i)}(x, t))^2 dx + \int_0^{l_1^{(i)}} c_1^{(i)}(x) (\dot{w}_1^{(i)}(x, t))^2 dx \right. \\ & \left. + \int_0^{l_2^{(i)}} c_2^{(i)}(x) (\dot{w}_2^{(i)}(x, t))^2 dx \right] \end{aligned} \quad (3-48)$$

where c_B is the coefficient of viscous damping of the isolation system, $c_0^{(i)}$, $c_1^{(i)}$ and $c_2^{(i)}$ are coefficients of viscous damping per unit length of the floor, the left and right elastic columns of the i th substructure, respectively. Then, the damping forces can be generated from $f(t)$ by writing

$$F_d = - \frac{\partial f}{\partial \dot{u}_B} = -c_B (\dot{u}_B - \dot{u}_g) \quad (3-49)$$

$$f_{d0}^{(i)} = -c_0^{(i)} \dot{w}_0^{(i)}, \quad f_{d1}^{(i)} = -c_1^{(i)} \dot{w}_1^{(i)}, \quad f_{d2}^{(i)} = -c_2^{(i)} \dot{w}_2^{(i)} \quad (3-50)$$

Introducing the above damping forces into Eq. (3-47), it is obtained

$$\begin{aligned} \delta W_{nc}^{(i)} = & - \int_0^{l_0^{(i)}} c_0^{(i)} \dot{w}_0^{(i)} \delta w_0^{(i)} dx - \int_0^{l_1^{(i)}} c_1^{(i)} \dot{w}_1^{(i)} \delta w_1^{(i)} dx - \int_0^{l_2^{(i)}} c_2^{(i)} \dot{w}_2^{(i)} \delta w_2^{(i)} dx \\ & + F_c^{(i)} (\delta u_B + \delta u_O) + \int_0^{l_1^{(i)}} f_{c1}^{(i)}(x, t) (\delta u_B + \delta w_1^{(i)}) dx + \int_0^{l_2^{(i)}} f_{c2}^{(i)}(x, t) (\delta u_B + \delta w_2^{(i)}) dx \end{aligned} \quad (3-51)$$

Considering the expressions of the elastic displacements relative to the base in Eqs. (3-5), (3-9) and (3-12), the virtual work can be expressed in the following form:

$$\begin{aligned}
\delta W_{nc}^{(i)} &= -\int_0^{l_0^{(i)}} c_0^{(i)} (\dot{\mathbf{q}}^{(i)})^T (\mathbf{F}_0)^T \mathbf{F}_0 \delta \mathbf{q}^{(i)} dx - \int_0^{l_1^{(i)}} c_1^{(i)} (\dot{\mathbf{q}}^{(i)})^T (\tilde{\mathbf{F}}_1^{(i)})^T \tilde{\mathbf{F}}_1^{(i)} \delta \mathbf{q}^{(i)} dx \\
&\quad - \int_0^{l_2^{(i)}} c_2^{(i)} (\dot{\mathbf{q}}^{(i)})^T (\tilde{\mathbf{F}}_2^{(i)})^T \tilde{\mathbf{F}}_2^{(i)} \delta \mathbf{q}^{(i)} dx + F_c^{(i)} (\delta u_B + \delta u_0^{(i)}) \\
&\quad + \int_0^{l_1^{(i)}} f_{c1}^{(i)}(x, t) (\delta u_B + \tilde{\mathbf{F}}_1^{(i)} \delta \mathbf{q}^{(i)}) dx + \int_0^{l_2^{(i)}} f_{c2}^{(i)}(x, t) (\delta u_B + \tilde{\mathbf{F}}_2^{(i)} \delta \mathbf{q}^{(i)}) dx \\
&= -(\dot{\mathbf{q}}^{(i)})^T \left[\int_0^{l_0^{(i)}} c_0^{(i)} (\mathbf{F}_0)^T \mathbf{F}_0 dx + \int_0^{l_1^{(i)}} c_1^{(i)} (\tilde{\mathbf{F}}_1^{(i)})^T \tilde{\mathbf{F}}_1^{(i)} dx + \int_0^{l_2^{(i)}} c_2^{(i)} (\tilde{\mathbf{F}}_2^{(i)})^T \tilde{\mathbf{F}}_2^{(i)} dx \right] \delta \mathbf{q}^{(i)} \\
&\quad + \left[F_c^{(i)} + \int_0^{l_1^{(i)}} f_{c1}^{(i)} dx + \int_0^{l_2^{(i)}} f_{c2}^{(i)} dx \right] \delta u_B + F_c^{(i)} \delta u_0^{(i)} + \left[\int_0^{l_1^{(i)}} f_{c1}^{(i)} \tilde{\mathbf{F}}_1^{(i)} dx + \int_0^{l_2^{(i)}} f_{c2}^{(i)} \tilde{\mathbf{F}}_2^{(i)} dx \right] \delta \mathbf{q}^{(i)}
\end{aligned} \tag{3-52}$$

In order to be concise, the previous equation can be rewritten as following:

$$\delta W_{nc}^{(i)} = [\mathbf{Q}_d^{(i)} + \mathbf{Q}_c^{(i)}]^T \delta \mathbf{q}^{(i)} \tag{3-53}$$

where

$$\mathbf{Q}_d^{(i)} = - \left[\int_0^{l_0^{(i)}} c_0^{(i)} (\mathbf{F}_0^{(i)})^T \mathbf{F}_0^{(i)} dx + \int_0^{l_1^{(i)}} c_1^{(i)} (\tilde{\mathbf{F}}_1^{(i)})^T \tilde{\mathbf{F}}_1^{(i)} dx + \int_0^{l_2^{(i)}} c_2^{(i)} (\tilde{\mathbf{F}}_2^{(i)})^T \tilde{\mathbf{F}}_2^{(i)} dx \right] \dot{\mathbf{q}}^{(i)} \tag{3-54}$$

is a generalized damping force vector on the i th substructure,

$$\mathbf{Q}_c^{(i)} = \begin{Bmatrix} F_c^{(i)} \\ F_c^{(i)} \\ \mathbf{0} \\ \vdots \\ \mathbf{0} \end{Bmatrix} + \int_0^{l_1^{(i)}} f_{c1}^{(i)} (\mathbf{F}_1^{(i)})^T dx + \int_0^{l_2^{(i)}} f_{c2}^{(i)} (\mathbf{F}_2^{(i)})^T dx \tag{3-55}$$

is a generalized control force vector on the i th substructure.

Introducing Eqs. (3-28), (3-29) and (3-30) into the above generalized vectors arrives at

$$\mathbf{Q}_d^{(i)} = -\mathbf{C}^{(i)} \dot{\mathbf{q}}^{(i)} \quad (3-56)$$

where

$$\mathbf{C}^{(i)} = -\left[\int_0^{t_0^{(i)}} c_0^{(i)} (\mathbf{F}_0^{(i)})^T \mathbf{F}_0^{(i)} dx + \int_0^{t_1^{(i)}} c_1^{(i)} (\tilde{\mathbf{F}}_1^{(i)})^T \tilde{\mathbf{F}}_1^{(i)} dx + \int_0^{t_2^{(i)}} c_2^{(i)} (\tilde{\mathbf{F}}_2^{(i)})^T \tilde{\mathbf{F}}_2^{(i)} dx \right] \quad (3-57)$$

In assembling $\delta W_{nc}^{(i)}$, the total virtual work of the damping and the control forces exerted on the entire system can be represented by

$$\begin{aligned} \delta W_{nc} &= (F_d + F_{cB}) \delta u_B + \sum_{i=1}^N \delta W_{nc}^{(i)} \\ &= [-c_B (\dot{u}_B - \dot{u}_g) + F_{cB}] \delta u_B + \sum_{i=1}^N (\mathbf{Q}_d^{(i)} + \mathbf{Q}_c^{(i)})^T \delta \mathbf{q}^{(i)} \quad (3-58) \\ &= (\tilde{\mathbf{Q}}_d + \tilde{\mathbf{Q}}_c + \hat{\mathbf{Q}}_g)^T \delta \tilde{\mathbf{q}} \end{aligned}$$

where c_B is the coefficient of viscous damping of the isolation system, F_{cB} is the horizontal force on the base, $\tilde{\mathbf{Q}}_d = -\tilde{\mathbf{C}} \dot{\tilde{\mathbf{q}}}$ is a generalized global damping vector, $\tilde{\mathbf{Q}}_c$ a generalized global control force vector, $\hat{\mathbf{Q}}_g$ a generalized global disturbance vector due to external excitation. It should be pointed out that in the global disturbance vector $\hat{\mathbf{Q}}_g$, all elements are zero except for the first entry being $c_B \dot{u}_g$. In carrying out the assembly of the element vectors $\mathbf{Q}_d^{(i)}$ (or $\mathbf{C}^{(i)}$) and $\mathbf{Q}_c^{(i)}$, similar carrying out the assembly of the element matrices $\mathbf{M}^{(i)}$ and $\mathbf{K}^{(i)}$, the second entry of $\mathbf{Q}_d^{(i-1)}$ (or $\mathbf{C}^{(i-1)}$) and $\mathbf{Q}_c^{(i-1)}$ must be added to the third entry of $\mathbf{Q}_d^{(i)}$ (or $\mathbf{C}^{(i)}$) and $\mathbf{Q}_c^{(i)}$, respectively. Meanwhile, the fourth entry of $\mathbf{Q}_d^{(i-1)}$ (or $\mathbf{C}^{(i-1)}$) and $\mathbf{Q}_c^{(i-1)}$ is added to the

fifth entry of $\mathbf{Q}_d^{(i)}$ (or $\mathbf{C}^{(i)}$) and $\mathbf{Q}_c^{(i)}$, and the sixth entry of $\mathbf{Q}_d^{(i-1)}$ (or $\mathbf{C}^{(i-1)}$) and $\mathbf{Q}_c^{(i-1)}$ to the seventh entry of $\mathbf{Q}_d^{(i)}$ (or $\mathbf{C}^{(i)}$) and $\mathbf{Q}_c^{(i)}$, respectively.

3.6 Derivation of Discrete Equations of Motion

Inserting the kinetic energy represented by Eq (3-32), the potential energy expressed by Eq. (3-46) and the virtual work performed by nonconservative forces expressed by Eq. (3-58) into the Extended Hamilton's principle Eq. (2-11), the discrete equations of motion can easily obtained. The Extended Hamilton's principle can be expressed in the form

$$\int_{t_1}^{t_2} (\delta T - \delta V + \delta W_{nc}) dt = 0, \quad \delta q_j = 0, \quad j = 1, 2, \dots, M, \quad t = t_1, t_2 \quad (2-11)$$

The variation in the kinetic energy and the potential energy are expressed in the form, respectively

$$\delta T = (\delta \dot{\tilde{\mathbf{q}}})^T \tilde{\mathbf{M}} \dot{\tilde{\mathbf{q}}} \quad (3-59)$$

$$\delta V = (\delta \tilde{\mathbf{q}})^T \tilde{\mathbf{K}} \tilde{\mathbf{q}} - k_b u_g \delta u_B \quad (3-60)$$

In considering

$$\begin{aligned} \int_{t_1}^{t_2} \delta T dt &= \int_{t_1}^{t_2} (\delta \dot{\tilde{\mathbf{q}}})^T \tilde{\mathbf{M}} \dot{\tilde{\mathbf{q}}} dt = \int_{t_1}^{t_2} \frac{d(\delta \tilde{\mathbf{q}})^T}{dt} \tilde{\mathbf{M}} \dot{\tilde{\mathbf{q}}} dt \\ &= (\delta \tilde{\mathbf{q}})^T \tilde{\mathbf{M}} \dot{\tilde{\mathbf{q}}}\Big|_{t_1}^{t_2} - \int_{t_1}^{t_2} (\delta \tilde{\mathbf{q}})^T \tilde{\mathbf{M}} \ddot{\tilde{\mathbf{q}}} dt = - \int_{t_1}^{t_2} (\delta \tilde{\mathbf{q}})^T \tilde{\mathbf{M}} \ddot{\tilde{\mathbf{q}}} dt \end{aligned} \quad (3-61)$$

$$\int_{t_1}^{t_2} \delta V dt = \int_{t_1}^{t_2} [(\delta \tilde{\mathbf{q}})^T \tilde{\mathbf{K}} \tilde{\mathbf{q}} - k_b u_g \delta u_B] dt \quad (3-62)$$

$$\delta W_{nc} = (\delta \tilde{\mathbf{q}})^T (\tilde{\mathbf{Q}}_d + \tilde{\mathbf{Q}}_c + \hat{\mathbf{Q}}_g) \quad (3-63)$$

the Extended Hamilton's principle can be rewritten in the following format

$$\int_{t_1}^{t_2} \left[-(\delta \tilde{\mathbf{q}})^T \tilde{\mathbf{M}} \ddot{\tilde{\mathbf{q}}} - (\delta \tilde{\mathbf{q}})^T \tilde{\mathbf{K}} \tilde{\mathbf{q}} + k_b u_g \delta u_B + (\delta \tilde{\mathbf{q}})^T (\tilde{\mathbf{Q}}_d + \tilde{\mathbf{Q}}_c + \hat{\mathbf{Q}}_g) \right] dt = 0 \quad (3-64)$$

$$\text{Setting} \quad \tilde{\mathbf{Q}}_g = k_b u_g \mathbf{d}u_B + (\mathbf{d}\tilde{\mathbf{q}})^T \hat{\mathbf{Q}}_g \quad (3-65)$$

the following is derived:

$$\int_{t_1}^{t_2} (\delta \tilde{\mathbf{q}})^T \left[-\tilde{\mathbf{M}} \ddot{\tilde{\mathbf{q}}} - \tilde{\mathbf{C}} \dot{\tilde{\mathbf{q}}} - \tilde{\mathbf{K}} \tilde{\mathbf{q}} + \tilde{\mathbf{Q}}_c + \tilde{\mathbf{Q}}_g \right] dt = 0 \quad (3-66)$$

The generalized coordinates are independent, so that the virtual displacements δq_i in the $\delta \mathbf{q}$ are entirely arbitrary. It follows that the integral can be zero for all δq_i if and only if the coefficients of δq_i identically zero, which yields the equations of motion

$$\tilde{\mathbf{M}} \ddot{\tilde{\mathbf{q}}} + \tilde{\mathbf{C}} \dot{\tilde{\mathbf{q}}} + \tilde{\mathbf{K}} \tilde{\mathbf{q}} = \tilde{\mathbf{Q}}_c + \tilde{\mathbf{Q}}_g \quad (3-67)$$

3.7 Model Reduction

In the preceding section, the discrete equations of motion were derived in the matrix form. For the convenience of control design, rewrite the global mass matrix $\tilde{\mathbf{M}}$, the global damping matrix $\tilde{\mathbf{C}}$ and the global stiffness matrix $\tilde{\mathbf{K}}$ in the following form:

$$\tilde{\mathbf{M}} = \begin{bmatrix} m & \mathbf{Q} \\ \mathbf{Q}^T & \tilde{\mathbf{M}}_e \end{bmatrix}, \quad \tilde{\mathbf{C}} = \begin{bmatrix} c_b & \mathbf{0} \\ \mathbf{0} & \tilde{\mathbf{C}}_e \end{bmatrix}, \quad \tilde{\mathbf{K}} = \begin{bmatrix} k_b & \mathbf{0} \\ \mathbf{0} & \tilde{\mathbf{K}}_e \end{bmatrix} \quad (3-68)$$

Assume that the global mass matrix $\tilde{\mathbf{M}}$, the global damping matrix $\tilde{\mathbf{C}}$ and the global stiffness matrix $\tilde{\mathbf{K}}$ are $(m+1) \times (m+1)$ dimensional matrices, in which $m = N \times (3 + n_0 + 2 \times n_1)$. Moreover, rewrite the generalized displacement vector, the generalized control vector and the generalized disturbance vector in the following form

$$\tilde{\mathbf{q}}(t) = \begin{Bmatrix} u_B(t) \\ \tilde{\mathbf{q}}_e(t) \end{Bmatrix} \quad (3-69)$$

$$\tilde{\mathbf{Q}}_c = \begin{Bmatrix} F_B + \sum_{i=1}^N \left(\int_0^{l_1^{(i)}} f_{c1}^{(i)} dx + \int_0^{l_2^{(i)}} f_{c2}^{(i)} dx \right) \\ \mathbf{f}_c \end{Bmatrix} \quad (3-70)$$

$$\tilde{\mathbf{Q}}_g = \begin{Bmatrix} c_B \dot{u}_g + k_B u_g + \sum_{i=1}^N \left(\int_0^{l_1^{(i)}} f_w^{(i)} dx + \int_0^{l_2^{(i)}} f_w^{(i)} dx \right) \\ \mathbf{f}_w \end{Bmatrix} \quad (3-71)$$

which are $(m+1)$ -dimensional vectors.

The HFEM yields a discrete model with far fewer degrees of freedom than the ordinary finite element method. Still, the number of degree of freedom tends to be large relation to the useful information contained in such a discrete model. Indeed, it is a well-known fact that higher modes are difficult to excite, as they require a great deal of energy. Moreover, higher modes tend to be inaccurate, which is a characteristic of discretized models [64]. Hence, a model reduction designed to eliminate the effect of higher modes seems in order. To this end, the eigenvalue problem corresponding to the undamped structure is considered separate, which can

be obtained by assuming that the base is held fixed and by ignoring damping. The eigenvalue problem has the form

$$\tilde{\mathbf{K}}_e \mathbf{U} = \tilde{\mathbf{M}}_e \mathbf{U} \mathbf{L} \quad (3-72)$$

where \mathbf{U} is a $m \times m$ dimensional modal matrix and \mathbf{L} the $m \times m$ dimensional diagonal matrix of eigenvalues of the elastic structure clamped at the base. The modal matrix is orthonormal with respect to both the mass matrix and stiffness matrix, or

$$\mathbf{U}^T \tilde{\mathbf{M}}_e \mathbf{U} = \mathbf{I}, \quad \mathbf{U}^T \tilde{\mathbf{K}}_e \mathbf{U} = \mathbf{L} \quad (3-73)$$

in which \mathbf{I} is the $m \times m$ identity matrix.

It is assumed that the structure alone has m degrees of freedom, so that \mathbf{U} and \mathbf{L} are $m \times m$ matrices. Consistent with the above discussion, it is proposed to retain only n modes, $n \ll m$. To this end, the submatrix of \mathbf{U} is denoted by \mathbf{U}_{tr} containing the first n columns alone and introduce the linear transformation

$$\tilde{\mathbf{q}}_e(t) = \mathbf{U}_{tr} \mathbf{q}_e(t) \quad (3-73)$$

or

$$\tilde{\mathbf{q}}(t) = \begin{bmatrix} 1 & \mathbf{0} \\ \mathbf{0} & \mathbf{U}_{tr} \end{bmatrix} \mathbf{q}(t) = \begin{bmatrix} 1 & \mathbf{0} \\ \mathbf{0} & \mathbf{U}_{tr} \end{bmatrix} \begin{Bmatrix} u_B \\ \mathbf{q}_e \end{Bmatrix} \quad (3-74)$$

where \mathbf{q}_e is an n dimensional vector of elastic modal coordinates, $\mathbf{q} = \left\{ u_B \ \mathbf{q}_e^T \right\}^T$ is the displacement vector of the truncated system. Introducing Eq. (3-74) into Eq. (3-67) and premultiplying through by $\begin{bmatrix} 1 & \mathbf{0} \\ \mathbf{0} & \mathbf{U}_{tr} \end{bmatrix}^T$, the truncated equations of motion are:

$$\mathbf{M}\ddot{\mathbf{q}} + \mathbf{C}\dot{\mathbf{q}} + \mathbf{K}\mathbf{q} = \mathbf{Q}_c + \mathbf{Q}_g \quad (3-75)$$

in which

$$\mathbf{M} = \begin{bmatrix} 1 & \mathbf{0} \\ \mathbf{0} & \mathbf{U}_{tr} \end{bmatrix}^T \begin{bmatrix} m & \mathbf{Q} \\ \mathbf{Q}^T & \tilde{\mathbf{M}}_e \end{bmatrix} \begin{bmatrix} 1 & \mathbf{0} \\ \mathbf{0} & \mathbf{U}_{tr} \end{bmatrix} = \begin{bmatrix} m & \mathbf{Q}\mathbf{U} \\ (\mathbf{Q}\mathbf{U})^T & \mathbf{I} \end{bmatrix} \quad (3-76)$$

$$\mathbf{C} = \begin{bmatrix} 1 & \mathbf{0} \\ \mathbf{0} & \mathbf{U}_{tr} \end{bmatrix}^T \begin{bmatrix} c_b & \mathbf{0} \\ \mathbf{0} & \tilde{\mathbf{C}}_e \end{bmatrix} \begin{bmatrix} 1 & \mathbf{0} \\ \mathbf{0} & \mathbf{U}_{tr} \end{bmatrix} = \begin{bmatrix} c_b & \mathbf{0} \\ \mathbf{0} & \mathbf{C}_e \end{bmatrix} \quad (3-77)$$

$$\mathbf{K} = \begin{bmatrix} 1 & \mathbf{0} \\ \mathbf{0} & \mathbf{U}_{tr} \end{bmatrix}^T \begin{bmatrix} k_b & \mathbf{0} \\ \mathbf{0} & \tilde{\mathbf{K}}_e \end{bmatrix} \begin{bmatrix} 1 & \mathbf{0} \\ \mathbf{0} & \mathbf{U}_{tr} \end{bmatrix} = \begin{bmatrix} k_b & \mathbf{0} \\ \mathbf{0} & \mathbf{L}_{tr} \end{bmatrix} \quad (3-78)$$

are the truncated mass, damping and stiffness matrices, respectively, where

$$\mathbf{C}_e = \mathbf{U}_{tr}^T \tilde{\mathbf{C}}_e \mathbf{U}_{tr} \quad (3-79)$$

\mathbf{L}_{tr} is the truncated diagonal matrix of the lowest eigenvalues and

$$\mathbf{Q}_c = \begin{bmatrix} 1 & \mathbf{0} \\ \mathbf{0} & \mathbf{U}_{tr} \end{bmatrix}^T \tilde{\mathbf{Q}}_c = \left\{ \begin{array}{l} F_B + \sum_{i=1}^N \left(\int_0^{l_1^{(i)}} f_{c1}^{(i)} dx + \int_0^{l_2^{(i)}} f_{c2}^{(i)} dx \right) \\ \mathbf{U}_{tr}^T \mathbf{f}_c \end{array} \right\} \quad (3-80)$$

$$\mathbf{Q}_g = \begin{bmatrix} 1 & \mathbf{0} \\ \mathbf{0} & \mathbf{U}_{tr} \end{bmatrix}^T \tilde{\mathbf{Q}}_g = \left\{ \left[c_B \dot{u}_g + k_B u_g + \sum_{i=1}^N \left(\int_0^{t_1^{(i)}} \mathbf{f}_w^{(i)} dx + \int_0^{t_2^{(i)}} \mathbf{f}_w^{(i)} dx \right) \right] \mathbf{U}_{tr}^T \mathbf{f}_w \right\} \quad (3-81)$$

are truncated control and disturbance vectors, respectively. Observe that the truncated discrete system, Eq.(3-75) has only $n + 1$ degrees of freedom, as opposed to $m + 1$ degrees of freedom of the original discrete system.

CHAPTER FOUR

State Space Realization of Dynamic System

4.1 Introduction

One of the most important tasks confronting a control system analyst is to develop a mathematical model of the dynamic system of interest. In many situations the essence of the analytical design problem is in the modeling; once that is done the rest of analysis falls quickly into place. There are two modeling and analysis approaches customary for use in linear systems: the transfer function approach and the state space approach. In this dissertation, the state space model will be considered. The state variable model of a system includes a description of the internal status of that system, in addition to the input-output behavior. Therefore, state variable models represent a more complete description in general.

The feature of the state space approach that sets it apart from the transfer function approach is the representation of the process under examination by systems of first-order differential equations. The state space is the model of representation of a dynamic system that would be most natural to a modern control system analyst.

The basic premise of Newtonian dynamics, on which equation of motion developed in the previous chapter, is based that the future evolution of a dynamic process is entirely determined by its present state. Indeed this premise might be considered as the basis of an abstract definition of the state of a dynamic system. The state of a dynamic system is a set of physical quantities, the specification of which completely determines the evolution of the system. The difficulty with this definition, as well as its major advantage, is that the specific physical quantities that define the system state are not unique, although their number called the system order is unique. In many situation there is an obvious choice of the state variables to define the system state, but there are also many cases in which the choice of state variables is by no means obvious.

In the very beginning of control system design, the mathematical model of dynamic systems is generally represented in differential equations. Afterwards the mathematical model needs frequently to be transferred to the state space. The transformation of dynamic systems from differential equations to the state space representation is preferred to as the state space realization of the dynamic systems.

In the previous chapter the mathematical model of the building system has been presented using differential equations. In this chapter, the concept of state is introduced and methods of writing state variable forms of the system models are presented. Three state variable models of the dynamic system will be developed based on the truncated equations of motion developed in the preceding chapter, one of which is referred to as Multiple Channel Control (MCC) model, another is the Single Channel Control (SCC) model and the final one is the Special Single Channel Control (SSCC) model.

4.2 Differential Equation of Motion

Before beginning the state space realization of the building system, differential equation of motion needs rewritten. In the previous chapter, the truncated equations of motion were derived in the matrix form were given by

$$\mathbf{M}\ddot{\mathbf{q}} + \mathbf{C}\dot{\mathbf{q}} + \mathbf{K}\mathbf{q} = \mathbf{Q}_c + \mathbf{Q}_g \quad (3-75)$$

This equation in the matrix form is essentially systems of ordinary differential equations characterizing the behavior of the dynamic system. For the sake of convenience of control design, the truncated mass matrix \mathbf{M} , the truncated damping matrix \mathbf{C} and the truncated stiffness matrix \mathbf{K} is rewritten in the following form

$$\mathbf{M} = \begin{bmatrix} m & \bar{\mathbf{f}} \\ \bar{\mathbf{f}}^T & \mathbf{M}_e \end{bmatrix}, \quad \mathbf{C} = \begin{bmatrix} c_b & \mathbf{0} \\ \mathbf{0} & \mathbf{C}_e \end{bmatrix}, \quad \mathbf{K} = \begin{bmatrix} k_b & \mathbf{0} \\ \mathbf{0} & \mathbf{K}_e \end{bmatrix} \quad (4-1)$$

The truncated mass matrix \mathbf{M} , the truncated damping matrix \mathbf{C} and the truncated stiffness matrix \mathbf{K} are assumed $(n+1) \times (n+1)$ dimensional matrices. Moreover, the truncated displacement vector, the truncated control vector and the truncated disturbance vector take on following form

$$\mathbf{q}(t) = \begin{Bmatrix} u_B(t) \\ \mathbf{q}_e(t) \end{Bmatrix} \quad (4-2)$$

$$\mathbf{Q}_c = \begin{Bmatrix} F_B + \sum_{i=1}^N \left(\int_0^{l_1^{(i)}} f_{c1}^{(i)} dx + \int_0^{l_2^{(i)}} f_{c2}^{(i)} dx \right) \\ \mathbf{U}_{tx}^T \mathbf{f}_c \end{Bmatrix} \quad (4-3)$$

$$\mathbf{Q}_g = \begin{Bmatrix} c_B \dot{u}_g + k_B u_g + \sum_{i=1}^N \left(\int_0^{l_1^{(i)}} f_w^{(i)} dx + \int_0^{l_2^{(i)}} f_w^{(i)} dx \right) \\ \mathbf{U}_{tx}^T \mathbf{f}_w \end{Bmatrix} \quad (4-4)$$

which are $(n+1)$ -dimensional vectors. The goal of this research work is to seek a suitable control law for minimizing the response of the elastic structure to the ground motion with the most economic control force.

The following notations are introduced

$$\mathbf{C}_g = \begin{Bmatrix} c_b \\ \mathbf{0} \end{Bmatrix}, \quad \mathbf{K}_g = \begin{Bmatrix} k_b \\ \mathbf{0} \end{Bmatrix} \quad (4-5)$$

into Eq. (4-3) and assume that the wind force \mathbf{Q}_w can be described as filtered white noise, and can be written as

$$\mathbf{Q}_w(t) = \left\{ \sum_{i=1}^N \left(\int_0^{l_1^{(i)}} \mathbf{f}_w^{(i)} d\mathbf{x} + \int_0^{l_2^{(i)}} \mathbf{f}_w^{(i)} d\mathbf{x} \right) \right\} = \mathbf{W}\mathbf{g}(t) \quad (4-6)$$

$$\mathbf{U}_{tr}^T \mathbf{f}_w$$

where \mathbf{W} is an $(n+1)$ -dimensional constant vector, $\mathbf{g}(t)$ is white noise with variance \mathbf{S}_g . Thus, Eq. (4-3) can be rewritten as

$$\mathbf{Q}_g = \mathbf{C}_g \dot{u}_g + \mathbf{K}_g u_g + \mathbf{W}\mathbf{g} \quad (4-7)$$

Assuming that the control forces are implemented by means of r discrete actuators, the control density function f_c can be expressed by

$$f_c = \sum_{i=1}^r F_i(t) \delta(P - P_i) \quad (4-8)$$

where P_i denote the location of the actuators, then

$$\sum_{i=1}^N \left(\int_0^{l_1^{(i)}} f_{c1}^{(i)} d\mathbf{x} + \int_0^{l_2^{(i)}} f_{c2}^{(i)} d\mathbf{x} \right) = \sum_{r=1}^r F_i(t) = \mathbf{1}_{1 \times r} \cdot \mathbf{F}_e \quad (4-9)$$

where $\mathbf{1}_{1 \times r}$ denotes a row vector all elements of which are unity, and

$$\mathbf{F}_e = \begin{Bmatrix} F_1 \\ F_2 \\ \vdots \\ F_r \end{Bmatrix} \quad (4-10)$$

is a r dimensional vector of actual controls acting on the elastic structure, and the truncated control vector written as

$$\mathbf{U}_{tr}^T \mathbf{f}_c = \mathbf{B}_e \mathbf{F}_e \quad (4-11)$$

where

$$\mathbf{B}_e = \begin{bmatrix} \mathbf{F}_1(p_1) & \mathbf{F}_1(p_2) & \dots & \mathbf{F}_1(p_r) \\ \mathbf{F}_2(p_1) & \mathbf{F}_2(p_2) & \dots & \mathbf{F}_2(p_r) \\ \vdots & \vdots & \dots & \vdots \\ \mathbf{F}_n(p_1) & \mathbf{F}_n(p_2) & \dots & \mathbf{F}_n(p_r) \end{bmatrix} \quad (4-12)$$

is an $n \times r$ dimensional control influence matrix for the elastic structure. Inserting Eqs. (4-9) and (4-11) into Eq.(4-4), the generalized control vector \mathbf{Q}_c in terms of actual control forces is as follows:

$$\mathbf{Q}_c = \mathbf{B}_c \mathbf{u}(t) \quad (4-13)$$

where

$$\mathbf{B}_c = \begin{bmatrix} 1 & \mathbf{1}_{1 \times r} \\ \mathbf{0}_{n \times 1} & \mathbf{B}_e \end{bmatrix}, \quad \mathbf{u}(t) = \begin{Bmatrix} \mathbf{F}_b(t) \\ \mathbf{F}_e(t) \end{Bmatrix} \quad (4-14)$$

are an $(n + 1) \times (r + 1)$ control influence matrix for the system and a $(r+1)$ dimensional actual control vector for the system, respectively. Thus, when substituting Eqs. (4-7) and (4-13) into Eq. (4-1), Eq. (4-1) can be rewritten in the form

$$\mathbf{M}\ddot{\mathbf{q}} + \mathbf{C}\dot{\mathbf{q}} + \mathbf{K}\mathbf{q} = \mathbf{C}_g \dot{u}_g + \mathbf{K}_g u_g + \mathbf{B}_c \mathbf{u} + \mathbf{W}\mathbf{g} \quad (4-15)$$

or

$$\mathbf{M}\ddot{\mathbf{q}} + \mathbf{C}\dot{\mathbf{q}} + \mathbf{K}\mathbf{q} = \mathbf{C}_g \dot{u}_g + \mathbf{K}_g u_g + \mathbf{Q}_c + \mathbf{Q}_w \quad (4-16)$$

It is noted that derivative of the ground motion appear \dot{u}_g in the system differential equations (4-15) and (4-16).

4.3 Multiple Channel Control (MCC) Model

The most commonly used state variables in structural dynamics are phase-variables-type state variables [63]. However, when derivatives of the input appear in the system differential equation, phase-variables-type state selection must be modified. If the method is applied without modification, a set of first-order differential equations is obtained as desired, but the input derivatives will still be present. The state equations must express the derivative of the state variable vector as a function of the state variable vector and input but not the derivative of the input. A serious mistake that is sometimes made is to define a new vector with components made up of u_g and its derivatives. This is incorrect because the inputs to the state equations must be actual physical inputs to the system. Arbitrary mathematical redefinition is not allowed here or in the output [13]. This differs from the situation for the internal state variables, which may or may not correspond to real physical variables. The input components must be independently selectable variables. Clearly when $u_g(t)$ is specified, there is no freedom left in specifying its derivatives $\dot{u}_g(t)$. The correct method of dealing with input derivatives is to absorb the derivatives terms into the definitions of the state variables.

To this end, taking the Laplace's transform of both sides of the foregoing equation, Eq.(4-16) can be expressed as following:

$$(\mathbf{M}s^2 + \mathbf{C}s + \mathbf{K})\mathbf{q}(s) = (\mathbf{C}_g s + \mathbf{K}_g)u_g(s) + \mathbf{Q}_c(s) + \mathbf{Q}_w(s) \quad (4-17)$$

Multiplying both of sides of the above equation by s^{-2} and \mathbf{M}^{-1} leads to

$$\mathbf{q} = s^{-1}(\mathbf{M}^{-1}\mathbf{C}_g u_g - \mathbf{M}^{-1}\mathbf{C}\mathbf{q}) + s^{-2}(\mathbf{M}^{-1}\mathbf{Q}_c + \mathbf{M}^{-1}\mathbf{Q}_w + \mathbf{M}^{-1}\mathbf{K}_g u_g - \mathbf{M}^{-1}\mathbf{K}\mathbf{q}) \quad (4-18)$$

Eq. (4-18) can be represented by a block diagram shown in **Figure 4-1**.

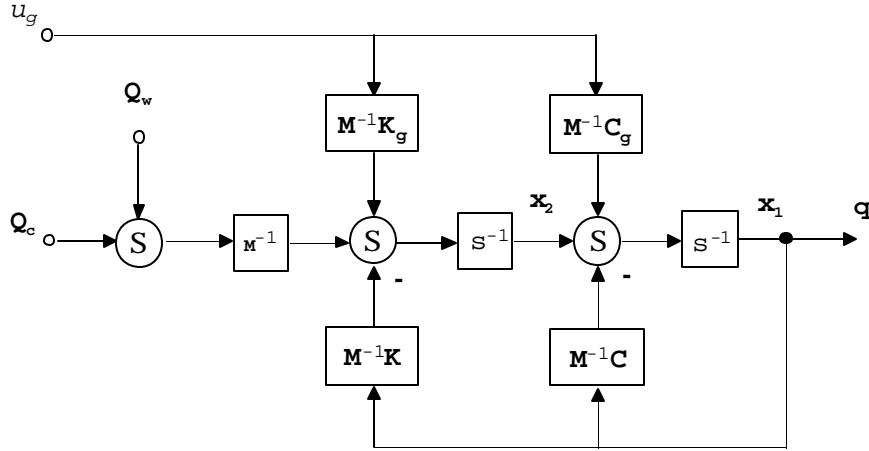


Figure. 4-1. Block diagram of the system

According to the simulation diagram corresponding to Eq. (4-18), shown in the above scheme, it is not difficult for us to arrive at

$$\begin{aligned}\dot{\mathbf{x}}_1 &= -\mathbf{M}^{-1}\mathbf{C}\mathbf{x}_1 + \mathbf{x}_2 + \mathbf{M}^{-1}\mathbf{C}_g u_g \\ \dot{\mathbf{x}}_2 &= -\mathbf{M}^{-1}\mathbf{K}\mathbf{x}_1 + \mathbf{M}^{-1}\mathbf{K}_g u_g + \mathbf{M}^{-1}\mathbf{Q}_c + \mathbf{M}^{-1}\mathbf{Q}_w\end{aligned}\quad (4-19)$$

$$\mathbf{q} = \mathbf{x}_1 \quad (4-20)$$

Introducing the notation $\mathbf{x}_0 = \begin{Bmatrix} \mathbf{x}_1 \\ \mathbf{x}_2 \end{Bmatrix}$ into Eqs. (4-19) and (4-20), it can be arrived at

$$\dot{\mathbf{x}}_0 = \begin{bmatrix} -\mathbf{M}^{-1}\mathbf{C} & \mathbf{I} \\ -\mathbf{M}^{-1}\mathbf{K} & \mathbf{0} \end{bmatrix} \mathbf{x}_0 + \begin{bmatrix} \mathbf{M}^{-1}\mathbf{C}_g \\ \mathbf{M}^{-1}\mathbf{K}_g \end{bmatrix} u_g + \begin{bmatrix} \mathbf{0} \\ \mathbf{M}^{-1} \end{bmatrix} \mathbf{Q}_c + \begin{bmatrix} \mathbf{0} \\ \mathbf{M}^{-1} \end{bmatrix} \mathbf{Q}_w \quad (4-21)$$

$$\mathbf{q} = [\mathbf{I} \ \mathbf{0}] \mathbf{x}_0$$

Introducing the following notations

$$\mathbf{A}_a = \begin{bmatrix} -\mathbf{M}^{-1}\mathbf{C} & \mathbf{I} \\ -\mathbf{M}^{-1}\mathbf{K} & \mathbf{0} \end{bmatrix}, \quad \mathbf{B}_a = \begin{bmatrix} \mathbf{0} \\ \mathbf{M}^{-1}\mathbf{B}_c \end{bmatrix}, \quad \mathbf{F}_a = \begin{bmatrix} \mathbf{M}^{-1}\mathbf{C}_g \\ \mathbf{M}^{-1}\mathbf{K}_g \end{bmatrix} \quad (4-22)$$

$$\mathbf{G}_a = \begin{bmatrix} \mathbf{0} \\ \mathbf{M}^{-1}\mathbf{W} \end{bmatrix}, \quad \mathbf{C}_a = [\mathbf{I} \quad \mathbf{0}]$$

Eqs. (4-20) and (4-21) can be written in the standard form of the feedback control of dynamic system in state space

$$\begin{aligned} \dot{\mathbf{x}}_0 &= \mathbf{A}_a \mathbf{x}_0 + \mathbf{B}_a \mathbf{u} + \mathbf{F}_a u_g + \mathbf{G}_a \mathbf{g} \\ \mathbf{q} &= \mathbf{C}_a \mathbf{x}_0 \end{aligned} \quad (4-23)$$

Figure 4-2 illustrates the corresponding block diagram.

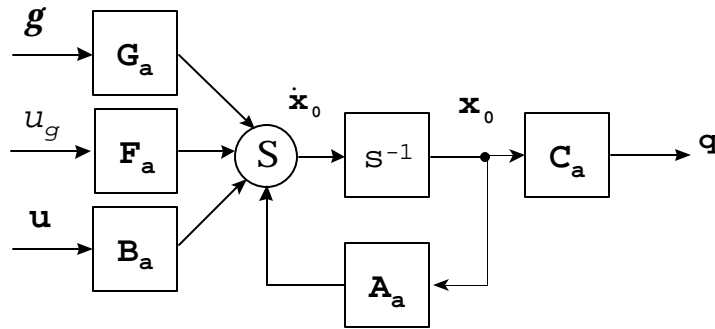


Figure 4-2. Block diagram of the MCC model

Note that the system is a multiple-input and multiple-output (MIMO) system. In addition, the system is also a multivariable control system since \mathbf{u} is a vector.

4.4 Single Channel Control (SCC) Model

Section 4.1 mentioned that the selection of the state variables is not unique process, other choices could be made. If the actual control vector $\mathbf{u}(t)$ in Eqs. (4-14) can be written in the form

$$\mathbf{u}(t) = \begin{Bmatrix} F_b(t) \\ \mathbf{F}_e(t) \end{Bmatrix} = \begin{bmatrix} U_b \\ \mathbf{U}_e \end{bmatrix} \cdot [u(t) + \mathbf{a}\dot{u}(t)] = \mathbf{U} \cdot [u(t) + \mathbf{a}\dot{u}(t)] \quad (4-24)$$

where $\mathbf{U} = \begin{Bmatrix} U_b \\ \mathbf{U}_e \end{Bmatrix}$ is a constant vector called control force distribution vector, \mathbf{a} is a constant to be determined, and $u(t)$ is a single control signal. In this model, it is noted the input signal $u(t)$ is a scalar being different from that in the MCC model where the input signal is a vector $\mathbf{u}(t)$. Therefore only one control channel is needed, which is very valuable in real practice engineering. Hence, Eq. (4-12) can be rearranged as

$$\mathbf{M}\ddot{\mathbf{q}} + \mathbf{C}\dot{\mathbf{q}} + \mathbf{K}\mathbf{q} = \mathbf{C}_g\dot{u}_g + \mathbf{K}_g u_g + \mathbf{a}\mathbf{B}_c \mathbf{U}\dot{u} + \mathbf{B}_c \mathbf{U}u + \mathbf{W}\mathbf{g} \quad (4-25)$$

Let $\mathbf{F}_k = \mathbf{B}_c \mathbf{U}$, and $\mathbf{F}_e = \mathbf{a}\mathbf{F}_k = \mathbf{a}\mathbf{B}_c \mathbf{U}$ (4-26)

Eq. (4-25) can be rewritten as

$$\mathbf{M}\ddot{\mathbf{q}} + \mathbf{C}\dot{\mathbf{q}} + \mathbf{K}\mathbf{q} = \mathbf{C}_g\dot{u}_g + \mathbf{K}_g u_g + \mathbf{F}_e\dot{u} + \mathbf{F}_k u + \mathbf{W}\mathbf{g} \quad (4-27)$$

In the same way as stated in MCC model, taking the Laplace's transform and multiplying both of sides of the previous equation by s^{-2} and \mathbf{M}^{-1} , Eq.(4-27) can be expressed as following

$$\mathbf{q} = s^{-1}(\mathbf{M}^{-1}\mathbf{C}_g u_g + \mathbf{M}^{-1}\mathbf{F}_c u - \mathbf{M}^{-1}\mathbf{C}\mathbf{q}) + s^{-2}(\mathbf{M}^{-1}\mathbf{K}_g u_g + \mathbf{M}^{-1}\mathbf{F}_k u + \mathbf{M}^{-1}\mathbf{W}\mathbf{g} - \mathbf{M}^{-1}\mathbf{K}\mathbf{q}) \quad (4-28)$$

Eq. (4-28) can also be represented by a block diagram shown in *Figure 4-3*.

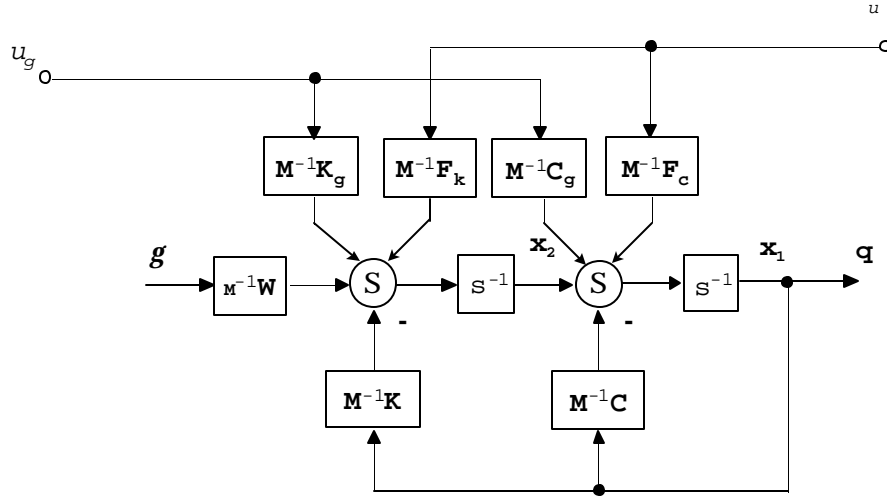


Figure 4-3. Block diagram of the system in the SCC model

According to the block diagram above, it is not difficult to arrive at

$$\begin{aligned} \dot{\mathbf{x}}_1 &= -\mathbf{M}^{-1}\mathbf{C}\mathbf{x}_1 + \mathbf{x}_2 + \mathbf{M}^{-1}\mathbf{F}_c u + \mathbf{M}^{-1}\mathbf{C}_g u_g \\ \dot{\mathbf{x}}_2 &= -\mathbf{M}^{-1}\mathbf{K}\mathbf{x}_1 + \mathbf{M}^{-1}\mathbf{F}_k u + \mathbf{M}^{-1}\mathbf{K}_g u_g + \mathbf{M}^{-1}\mathbf{W}\mathbf{g} \\ \mathbf{q} &= \mathbf{x}_1 \end{aligned} \quad (4-29)$$

Introducing the following notations

$$\mathbf{x}_0 = \begin{Bmatrix} \mathbf{x}_1 \\ \mathbf{x}_2 \end{Bmatrix}, \quad \mathbf{A}_a = \begin{bmatrix} -\mathbf{M}^{-1}\mathbf{C} & \mathbf{I} \\ -\mathbf{M}^{-1}\mathbf{K} & \mathbf{0} \end{bmatrix}, \quad \mathbf{B}_a = \begin{bmatrix} \mathbf{M}^{-1}\mathbf{F}_c \\ \mathbf{M}^{-1}\mathbf{F}_k \end{bmatrix},$$

(4-30)

$$\mathbf{F}_a = \begin{bmatrix} \mathbf{M}^{-1}\mathbf{C}_g \\ \mathbf{M}^{-1}\mathbf{K}_g \end{bmatrix}, \quad \mathbf{G}_a = \begin{bmatrix} \mathbf{0} \\ \mathbf{M}^{-1}\mathbf{W} \end{bmatrix}, \quad \mathbf{C}_a = [\mathbf{I} \quad \mathbf{0}]$$

Eqs. (4-29) can be written in the standard form of the feedback control of dynamic system in state space

$$\begin{aligned} \dot{\mathbf{X}}_0 &= \mathbf{A}_a \mathbf{X}_0 + \mathbf{B}_a u + \mathbf{F}_a u_g + \mathbf{G}_a \mathbf{g} \\ \mathbf{q} &= \mathbf{C}_a \mathbf{X}_0 \end{aligned} \quad (4-31)$$

which has the same form as Eq. (4-23), except that the control vector $\mathbf{u}(t)$ is replaced by the single control signal $u(t)$. It must be pointed out that the control matrix \mathbf{B}_a in Eqs. (4-30) is different from that in Eqs. (4-22), which is the most important distinction between the MCC model and the SCC model.

It is noticed that the Laplace's transform of Eq. (4-24) gives

$$\mathbf{u}(s) = \mathbf{U}(as + 1)u(s) \quad (4-32)$$

From the above equation, a filter with transfer function $D(s)$ is obtained

$$\mathbf{U}D(s) = \frac{\mathbf{u}(s)}{u(s)} = \mathbf{U}(as + 1) \quad (4-33)$$

in which $D(s)$ appears to be a typical Proportional Derivative (PD) compensator, although it functions for achieving a different goal in this problem. This implies the control law developed in this section is realizable in the physical world since the PD compensator is widely used in the industry. Essentially, the PD compensator serves as a combined active damper and active spring.

4.5 Special Single Channel Control (SSCC) Model

In the SCC model, the control force distribution vector \mathbf{U} and the constant \mathbf{a} were introduced. These parameters play an important role in control system design, however their determination is a parameter optimization problem that is out of the scope of this dissertation. Here only a special control force distribution vector \mathbf{U} and constant \mathbf{a} are discussed.

Allowing $u = u_g$, one can minimize the effect of the ground motion u_g on the system, as long as the following relations are satisfied

$$\mathbf{F}_c = -\mathbf{C}_g \quad \text{and} \quad \mathbf{F}_k = -\mathbf{K}_g \quad (4-34)$$

From $\mathbf{F}_k = -\mathbf{K}_g$,

$$\begin{bmatrix} 1 & \mathbf{1}_{1 \times r} \\ \mathbf{0} & \mathbf{B}_e \end{bmatrix} \begin{Bmatrix} U_b \\ \mathbf{U}_e \end{Bmatrix} = - \begin{Bmatrix} k_b \\ \mathbf{0} \end{Bmatrix} \quad (4-35)$$

The following must hold true

$$U_b = -k_b \quad \text{and} \quad \mathbf{U}_e = \mathbf{0} \quad (4-36)$$

if the previous equation is valid. Similarly, in order to satisfy $\mathbf{F}_c = -\mathbf{C}_g$, that is

$$\mathbf{a} \begin{bmatrix} 1 & \mathbf{1}_{1 \times r} \\ \mathbf{0} & \mathbf{B}_e \end{bmatrix} \begin{Bmatrix} U_b \\ \mathbf{U}_e \end{Bmatrix} = - \begin{Bmatrix} C_b \\ \mathbf{0} \end{Bmatrix} \quad (4-37)$$

the statement

$$\mathbf{a} = \frac{c_b}{k_b} \tag{4-38}$$

must hold true as well. Hence, a very simple control model is obtained based on the SCC model, given by Eqs. (4-36) and (4-38), only a control force $F_b(t) = -c_b\dot{u}(t) - k_b u(t)$ acting on the base is needed. The conclusion is reasonable. Since the external effect on the system is merely $c_b\dot{u}_g(t) + k_b u_g(t)$ acting on the base, which arises from the ground motion and exerts disturbance force through the viscous damper and the elastic spring, only a control force that suppress $c_b\dot{u}_g(t) + k_b u_g(t)$ is necessary.

The SSCC model is very challenging in real engineering because only one control force is needed and it is placed on the base. Its significance lies not only in engineering cost reduction, but also in the fact that implementation of the control system is simpler than other models.

CHAPTER FIVE

CONTROL SYSTEM DESIGN

5.1 Introduction to Optimum Feedback Control Theory

In a typical control system design problem, inputs are a dynamic system to be controlled (plant), a description of the types of inputs to be encountered, and specifications regarding acceptable values of system errors, i.e., the difference between desired and actual responses. What is then required is to design a controller so that the plant-controller combination satisfies the specifications. If the inputs are known precisely, e.g., steps, ramps, exponentials in the deterministic case or random processes with known means and covariances in the stochastic case and specifications can be translated into a quadratic performance index, then optimal feedback control theory will furnish a useful design tool.

Over the past decades, optimum feedback control approach has been applied increasingly to the physical engineering. The design of optimal feedback control systems for linear plants by using quadratic penalties on the state and control variables represents one of the most studied class problems in dynamic deterministic and stochastic optimal control theory. Results are available for both the time-varying and the time invariant cases, as well as for the continuous-time and discrete-time system models.

This chapter describes three control methodologies based on the MCC, SCC and SSCC control models developed in the previous chapter. These three control approaches are the Linear Quadratic Gaussian (LQG) control, the Disturbance Accommodating Control (DAC) and hybrid LQG/DAC control.

The LQG control is a modern state space technique for designing optimal dynamic regulators. It enables a trade off in performance and control effort, and takes into account process and measurement noise. *Figure 5-1* shows the schematic of a typical dynamic system with a regulator.

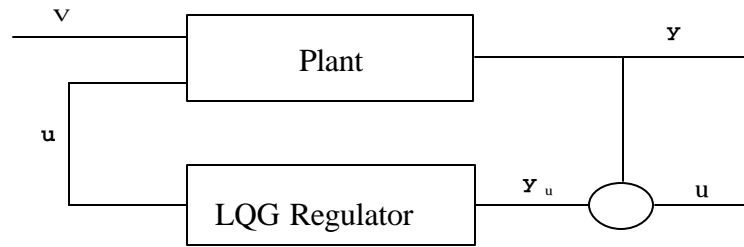


Figure 5-1. Schematic of a typical dynamic system with a regulator

The goal is to regulate the output \mathbf{y} around zero. The plant is driven by the process noise \mathbf{v} and the controls \mathbf{u} , and the regulator relies on the noisy measurements $\mathbf{y}_u = \mathbf{y} + \mathbf{u}$ to generate these controls. The plant state and measurement equations are of the form

$$\dot{\mathbf{x}} = \mathbf{A}\mathbf{x} + \mathbf{B}\mathbf{u} + \mathbf{G}\mathbf{v} \quad (5-1)$$

$$\mathbf{y}_u = \mathbf{C}\mathbf{x} + \mathbf{u} \quad (5-2)$$

and both \mathbf{v} and \mathbf{u} are modeled as white noise. The LQG regulator consists of an optimal state feedback gain and Kalman state estimator. The design of these two components independently is shown below.

Optimal state feedback gain

In the optimal feedback control, a gain matrix is sought to minimize a specified quadratic performance criterion $J(\mathbf{u})$ expressed as the integral of a quadratic form in the state vector \mathbf{x} plus a second quadratic form in the control vector \mathbf{u} , i.e.

$$J(\mathbf{u}) = \int_0^{\infty} (\mathbf{x}^T \mathbf{Q} \mathbf{x} + \mathbf{u}^T \mathbf{R} \mathbf{u}) dt \quad (5-3)$$

The weighting matrices \mathbf{Q} and \mathbf{R} are user-specified and define the trade-off between regulation performance (how fast $\mathbf{x}(t)$ goes to zero) and control effort. The first design step seeks a state feedback law $\mathbf{u} = -\mathbf{K}\mathbf{x}$ that minimizes the cost function $J(\mathbf{u})$. The minimizing gain matrix \mathbf{K} is obtained by solving an algebraic Riccati equation [20]. This gain is usually called the LQ-optimal gain. Sometimes, the process seeking the LQ state feedback regulator, i.e. LQ-optimal gain matrix \mathbf{K} , is called Linear Quadratic Regulator (LQR) design.

Kalman state estimator

It is clear that the LQ-optimal state feedback $\mathbf{u} = -\mathbf{K}\mathbf{x}$ is not implementable without full state measurement. However, one can derive a state estimate $\hat{\mathbf{x}}$ such that $\mathbf{u} = -\mathbf{K}\hat{\mathbf{x}}$ remains optimal for output feedback problem. This state estimate is generated by Kalman filter [22] as shown below:

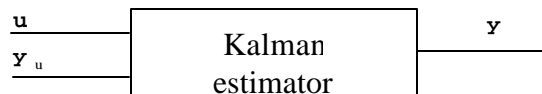


Figure 5-2. Block diagram of the Kalman estimator

Mathematically, the Kalman state estimator can be expressed by

$$\dot{\hat{\mathbf{x}}} = \mathbf{A}\hat{\mathbf{x}} + \mathbf{B}\mathbf{u} + \mathbf{L}(\mathbf{y}_u - \mathbf{C}\hat{\mathbf{x}}) \quad (5-4)$$

with two inputs, controls \mathbf{u} and measurements $\mathbf{y}_u = \mathbf{y} + \mathbf{u}$. The noise covariance data represented by

$$\mathbf{Q}_n = E(\mathbf{v}\mathbf{v}^T), \quad \mathbf{R}_n = E(\mathbf{u}\mathbf{u}^T) \quad (5-5)$$

determines the Kalman gain \mathbf{L} in conjunction with dynamic systems through an algebraic Riccati equation. The Kalman filter is an optimal estimator when dealing with Gaussian white noise. Specifically, it minimizes the asymptotic covariance of the estimation error $\mathbf{x} - \hat{\mathbf{x}}$, i.e.

$$\lim_{t \rightarrow \infty} E((\mathbf{x} - \hat{\mathbf{x}})(\mathbf{x} - \hat{\mathbf{x}})^T) \quad (5-6)$$

LQG regulator

To form the LQG regulator, simply connect the Kalman filter and LQ optimal gain \mathbf{K} as shown in *Figure 5-3*.

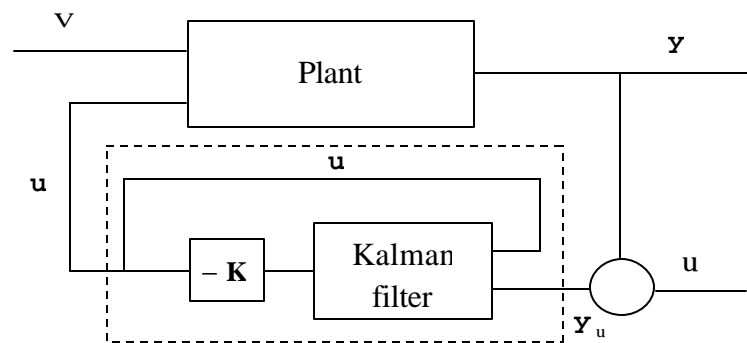


Figure 5-3. Block diagram of LQG regulator

This regulator has state space equations:

$$\dot{\hat{\mathbf{x}}} = (\mathbf{A} - \mathbf{L}\mathbf{C} - \mathbf{B}\mathbf{K})\hat{\mathbf{x}} + \mathbf{L}\mathbf{y}_u \quad (5-7)$$

$$\mathbf{u} = -\mathbf{K}\hat{\mathbf{x}} \quad (5-8)$$

In addition to LQG design, a Disturbance Accommodate Control (DAC) design and a hybrid LQG/DAC control system are also studied in this chapter. Hence, nine cases will have to be discussed, which are three control systems, the LQG, the DAC and the hybrid LQG/DAC, in conjunction with three different control models, the MCC model, the SCC model and the SSCC model, respectively.

5.2 Disturbance Rejection Problem

In general control system design, the design of regulators is considered. Here performance objective is to control the plant to achieve a specified, desired closed-loop dynamic behavior of the system in response to arbitrary initial disturbances. A more general design objective is to control the system error not only for initial disturbances, but also for persistent disturbances. This is a disturbance rejection problem. The disturbance rejection is an important factor in the design of many control systems, especially in the active vibration and noise control systems. In active vibration and noise control system design, generally there always exist the persistent disturbances, with no specified desired output. In the disturbance rejection problem, it is assumed that the dynamic system

$$\dot{\mathbf{X}}_0 = \mathbf{A}_a \mathbf{X}_0 + \mathbf{B}_a \mathbf{u}$$

is disturbed by a disturbance $\mathbf{d}(t)$, i.e., the system dynamic equations are given by

$$\dot{\mathbf{X}}_0 = \mathbf{A}_a \mathbf{X}_0 + \mathbf{B}_a \mathbf{u} + \mathbf{d}(t) \quad (5-9)$$

The objective is to determine the control input $\mathbf{u}(t)$ that minimizes the effect of the disturbance $\mathbf{d}(t)$ on the value of a performance.

As shown in *Figure 5-1*, the plant is driven by the process noise \mathbf{v} and the controls \mathbf{u} in general. The dynamic process considered here as elsewhere in the dissertation is, as usual, characterized by the vector-matrix differential equation

$$\begin{aligned} \dot{\mathbf{X}}_0 &= \mathbf{A}_a \mathbf{X}_0 + \mathbf{B}_a \mathbf{u} + \mathbf{F}_a u_g + \mathbf{G}_a \mathbf{g} \\ \mathbf{q} &= \mathbf{C}_a \mathbf{X}_0 \end{aligned} \quad (4-23)$$

It is noticed that being different from Eq. (5-1) there are two terms $\mathbf{F}_a u_g$ and $\mathbf{G}_a \mathbf{g}$ representing the influence of the ground motion and the wind force besides the state variable term $\mathbf{A}_a \mathbf{X}_0$ and control term $\mathbf{B}_a \mathbf{u}$. In Eq. (5-1), however, there is only one term $\mathbf{G}\mathbf{v}$ representing the process noise. The $\mathbf{F}_a u_g$ can be not viewed directly as the process noise, although the $\mathbf{G}_a \mathbf{g}$ can be treated as a process noise. Clearly, the problem is a disturbance rejection problem as shown in Eq. (4-23), where $\mathbf{d}(t) = \mathbf{F}_a u_g + \mathbf{G}_a \mathbf{g}$ is the disturbance signal.

If the ground motion can be viewed as the impulse response of a certain system expressed as

$$\begin{aligned} \dot{\mathbf{z}} &= \mathbf{A}_z \mathbf{z} + \mathbf{B}_z \mathbf{d} + \mathbf{G}_z \mathbf{q} \\ u_g &= \mathbf{C}_z \mathbf{z} \end{aligned} \quad (5-10)$$

where $\mathbf{d}(t)$ is a unit impulse function at time $t = 0$, \mathbf{q} is white noise with variance \mathbf{S}_q , then combining Eqs. (4-23) and (5-10), the following can be obtained:

$$\begin{cases} \begin{bmatrix} \dot{\mathbf{x}}_0 \\ \dot{\mathbf{z}} \end{bmatrix} = \begin{bmatrix} \mathbf{A}_a & \mathbf{F}_a \mathbf{C}_z \\ \mathbf{0} & \mathbf{A}_z \end{bmatrix} \begin{bmatrix} \mathbf{x}_0 \\ \mathbf{z} \end{bmatrix} + \begin{bmatrix} \mathbf{B}_a \\ \mathbf{0} \end{bmatrix} \mathbf{u} + \begin{bmatrix} \mathbf{G}_a & \mathbf{0} \\ \mathbf{0} & \mathbf{G}_z \end{bmatrix} \begin{bmatrix} \mathbf{g} \\ \mathbf{q} \end{bmatrix} \\ \mathbf{q} = \begin{bmatrix} \mathbf{C}_a & \mathbf{0} \end{bmatrix} \begin{bmatrix} \mathbf{x}_0 \\ \mathbf{z} \end{bmatrix} \end{cases} \quad (5-11)$$

The corresponding block diagram is drawn in *Figure 5-4*.

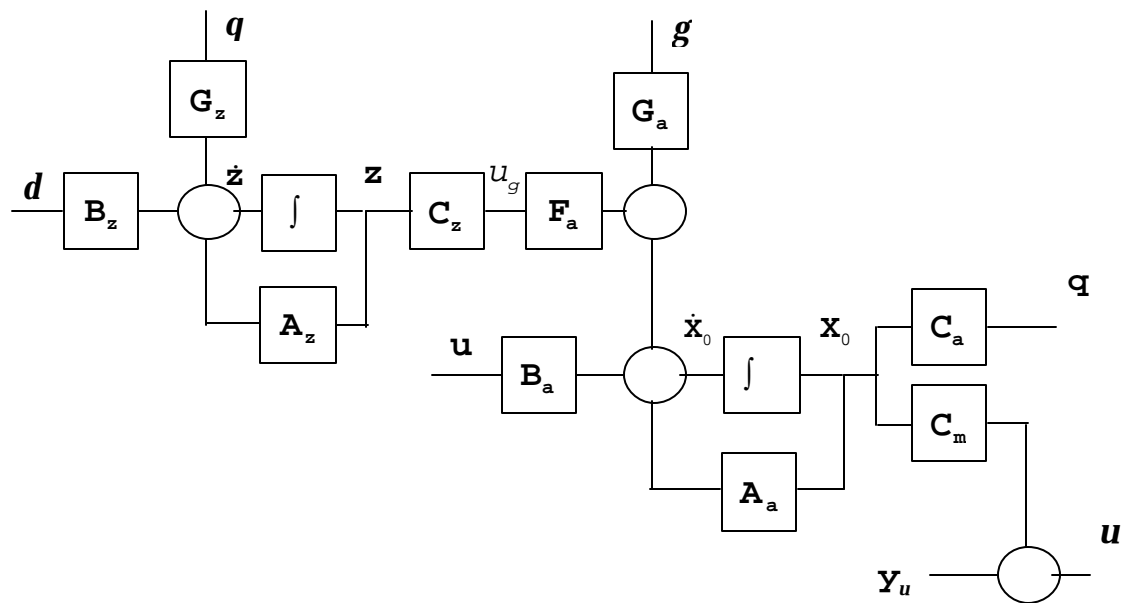


Figure 5-4. Block diagram of the system in the disturbance rejection problem

Thus, the disturbance rejection problem becomes the LQR problem represented by

$$\dot{\mathbf{X}} = \mathbf{A}\mathbf{X} + \mathbf{B}\mathbf{u} + \mathbf{G}\mathbf{v} \quad (5-12)$$

$$\mathbf{q} = \mathbf{C}_o \mathbf{X} \quad (5-13)$$

where

$$\mathbf{A} = \begin{bmatrix} \mathbf{A}_a & \mathbf{F}_a \mathbf{C}_z \\ \mathbf{0} & \mathbf{A}_z \end{bmatrix}, \quad \mathbf{B} = \begin{bmatrix} \mathbf{B}_a \\ \mathbf{0} \end{bmatrix}, \quad \mathbf{G} = \begin{bmatrix} \mathbf{G}_a & \mathbf{0} \\ \mathbf{0} & \mathbf{G}_z \end{bmatrix}, \quad \mathbf{C}_o = [\mathbf{C}_a \quad \mathbf{0}] \quad (5-14)$$

$$\mathbf{x} = \begin{Bmatrix} \mathbf{x}_0 \\ \mathbf{z} \end{Bmatrix}, \quad \mathbf{v} = \begin{Bmatrix} \mathbf{g} \\ \mathbf{q} \end{Bmatrix}$$

with

$$\mathbf{E}[\mathbf{v}] = \mathbf{0}, \quad \mathbf{E}[\mathbf{v}\mathbf{v}^T] = \begin{bmatrix} \mathbf{S}_g^2 & \mathbf{0} \\ \mathbf{0} & \mathbf{S}_q^2 \end{bmatrix} \quad (5-15)$$

where \mathbf{E} denotes mathematical expectation. The block diagram corresponding to Eqs. (5-12) and (5-13) is shown in *Figure 5-5*:

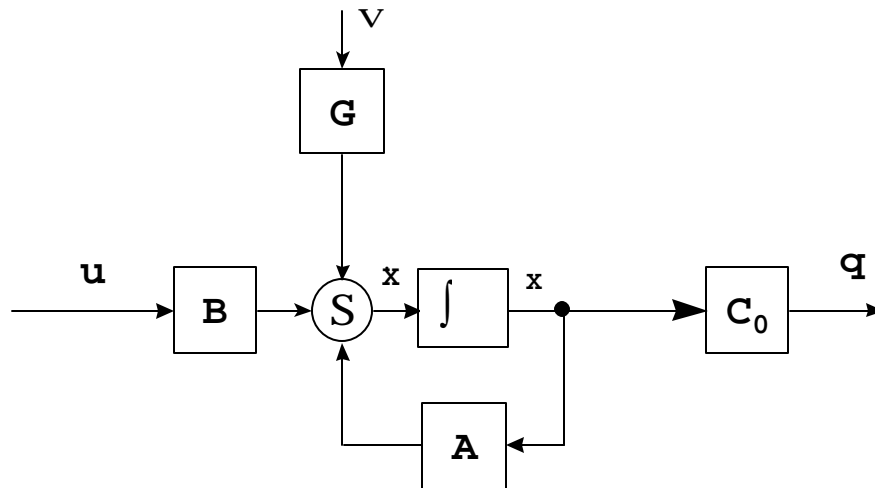


Figure 5-5. Block diagram of the system in the form of the LQR problem with noise

5.3 Linear Quadratic Regulator (LQR) Problem

During LQR design study, determination of the active control force is based on the minimization of a given performance objective with respect to the control force under the

constraint conditions defined by the equation of motion and the initial conditions. In this study, the performance objective is represented by a quadratic cost function

$$J(\mathbf{u}) = \int_0^{\infty} (\mathbf{x}^T \mathbf{Q} \mathbf{x} + \mathbf{u}^T \mathbf{R} \mathbf{u}) dt \quad (5-16)$$

where \mathbf{Q} is a symmetric and positive semi-definite matrix, \mathbf{R} is a symmetric and positive definite matrix. They are often called the state weighting matrix and control weighting matrix, respectively. In the cost function defined by Eq. (5-16) two terms contribute to the integrated cost of control: the quadratic form $\mathbf{x}^T \mathbf{Q} \mathbf{x}$ that represents a penalty on the deviation of the state \mathbf{x} from the origin and the term $\mathbf{u}^T \mathbf{R} \mathbf{u}$ that represents the cost of control. This means, of course, that the desired state is the origin, not some other place. The state weighting matrix \mathbf{Q} specifies the importance of the various components of the state vector relative to each other. It should be obvious that the choice of the state weighting matrix \mathbf{Q} depends on what the system designer is trying to achieve. In this study, the interest is only the state and its influence on the system output, and a suitable performance criterion might well be

$$\mathbf{q} = \mathbf{C}_o \mathbf{x} \quad (5-13)$$

So in this case

$$\mathbf{Q} = \mathbf{C}_o^T \mathbf{C}_o \quad (5-17)$$

The considerations alluded above with regard to \mathbf{Q} apply as well to the control weighting matrix \mathbf{R} . The term $\mathbf{u}^T \mathbf{R} \mathbf{u}$ in the performance index (5-16) is included in an attempt to limit the magnitude of the control signal \mathbf{u} . Unless a “cost” is imposed for use of

control, the design that emerges is liable to generate control signals that cannot be achieved by the actuator. Actuator is the physical device that produces the control signal. And the result will be that the control signal will saturate at the maximum signal that can be produced. Thus in a desire to avoid saturation and its consequences, the control signal weighting matrix is selected large enough to avoid saturation of the control signal under normal conditions of operation. The relationship between the weighting matrices \mathbf{Q} and \mathbf{R} and the dynamic behavior of the closed-loop system depends of course on the matrices \mathbf{A} and \mathbf{B} and are quite complex. It is impractical to predict the effect on closed-loop behavior of a given pair of weighting matrices. A suitable approach would be to solve for the gain matrix \mathbf{K} that result from a range of weighting matrices \mathbf{Q} and \mathbf{R} , and simulate the corresponding closed-loop response. The gain matrix \mathbf{K} that produces the response closest to meeting the design objectives is the ultimate selection. With the software that is now widely available, such as Matlab, it is a simple matter to solve for \mathbf{K} given \mathbf{A} , \mathbf{B} , \mathbf{Q} and \mathbf{R} . In a few hours time, the gain matrices and transient response that result for dozen or more combinations of \mathbf{Q} and \mathbf{R} can be determined, and a suitable selection of \mathbf{K} can be made.

Now the optimal gain matrix \mathbf{K} can be calculated such that the state feedback law

$$\mathbf{u} = -\mathbf{K}\mathbf{x} \quad (5-18)$$

minimizes the quadratic cost function under the constraint conditions defined by the equation of motion

$$\dot{\mathbf{x}} = \mathbf{A}\mathbf{x} + \mathbf{B}\mathbf{u} \quad (5-19)$$

Thus, the problem becomes a standard the linear quadratic regulator (LQR) problem. It can be shown that a state feedback solution of the LQR problem is obtained in terms of the solution of a differential, matrix Riccati equation [20]. The interest lies in the steady state LQR problem. Therefore, the unique position definite solution to the associated algebraic matrix Riccati equation:

$$0 = \mathbf{S}\mathbf{A} + \mathbf{A}^T\mathbf{S} + \mathbf{Q} - \mathbf{S}\mathbf{B}\mathbf{R}^{-1}\mathbf{B}^T\mathbf{S} \quad (5-20)$$

Consequently, the optimal feedback gain matrix \mathbf{K} can be obtained as following

$$\mathbf{K} = \mathbf{R}^{-1}\mathbf{B}^T\mathbf{S}, \quad \mathbf{u} = -\mathbf{R}^{-1}\mathbf{B}^T\mathbf{S}\mathbf{x} \quad (5-21)$$

For convenience, \mathbf{K} can be partitioned into two components

$$\mathbf{K} = [\mathbf{k}_x \quad \mathbf{k}_z] \quad (5-22)$$

so that Eq. (5-17) can be rewritten as

$$\mathbf{u} = -\mathbf{k}_x\mathbf{x}_0 - \mathbf{k}_z\mathbf{z} \quad (5-23)$$

The control law given by Eqs. (5-23) constitutes the solution to the steady state LQR problem.

5.4 Linear Quadratic Estimator (LQE) Problem

It is obvious that regardless of the success of the LQR regulator, a key element in our design of control is to seek an on-line, real-time state $\mathbf{x}(t)$. It is clear that the LQR optimal state feedback $\mathbf{u} = -\mathbf{K}\mathbf{x}$ is not implemented without full state measurement. In

the real world, it is difficult to find the true state $\mathbf{x}(t)$, if it is not impossible. However, a state estimate $\hat{\mathbf{x}}$ can be derived such that $\mathbf{u} = -\mathbf{K}\hat{\mathbf{x}}$ remains optimal. In practice only a state estimator needs to be constructed that produces a state estimate $\hat{\mathbf{x}}_0$ of \mathbf{x}_0 . This is because the system expressed by Eq. (5-10) is essentially an estimator that estimates the ground motion $u_g(t)$. Thus since such system being able to produce the disturbance state \mathbf{z} has been constructed by Eq. (5-10), then there is no need to reconstruct another device to estimate \mathbf{z} . Now start to construct a data processing device that can produce estimates of the state $\mathbf{x}_0(t)$, such that the feedback law expressed by Eq. (5-23) is changed as

$$\mathbf{u} = \mathbf{u}_x + \mathbf{u}_z = -\mathbf{k}_x \hat{\mathbf{x}}_0 - \mathbf{k}_z \mathbf{z} \quad (5-24)$$

where $\mathbf{u}_x = -\mathbf{k}_x \hat{\mathbf{x}}_0$, $\mathbf{u}_z = -\mathbf{k}_z \mathbf{z}$, and $\hat{\mathbf{x}}_0$ is the output of the estimator. Consider the continuous-time system with state and measurement equation

$$\begin{cases} \dot{\mathbf{x}}_0 = \mathbf{A}_a \mathbf{x}_0 + \mathbf{B}_a \mathbf{u}_x + \mathbf{G}_a \mathbf{v} \\ \mathbf{y} = \mathbf{C}_m \mathbf{x}_0 + \mathbf{u} \end{cases} \quad (5-25)$$

where \mathbf{C}_m is a measurement output matrix, which in general differs from the output matrix \mathbf{C}_a , \mathbf{v} and \mathbf{u} that is sensor noise vector with variance \mathbf{S}_u are white noise processes, having known spectral density matrices represented by

$$E[\mathbf{v}\mathbf{v}^T] = \mathbf{Q}_f, \quad E[\mathbf{u}\mathbf{u}^T] = \mathbf{R}_f \quad (5-26)$$

Here, the control input $\mathbf{u}_x(t)$ can be measured directly, but the state $\mathbf{x}_0(t)$ is available indirectly through the noisy output $\mathbf{y}(t) = \mathbf{C}_m \mathbf{x}_0 + \mathbf{u}$. The LQE problem is to find a dynamic system that optimally estimates the state of the system given the above measurements. One would like to seek the optimum state estimator for the state $\mathbf{x}_0(t)$.

Let $\hat{\mathbf{x}}_0(t)$ denote the state estimate. The solution of the LQE problem is a Kalman filter. It can be expressed by the differential equation

$$\dot{\hat{\mathbf{x}}}_0 = \mathbf{A}_a \hat{\mathbf{x}}_0 + \mathbf{B}_a \mathbf{u}_x + \mathbf{L}(\mathbf{y} - \mathbf{C}_m \hat{\mathbf{x}}_0) \quad (5-27)$$

A remarkable property of the Kalman filter is that it is optimum under any reasonable performance criterion, provided the random processes, \mathbf{v} and \mathbf{u} , are white and Gaussian. It can be shown that the \mathbf{L} is the solution to the Ricutti equation as shown in following

$$\mathbf{0} = \mathbf{A}_a \mathbf{P} + \mathbf{P} \mathbf{A}_a^T + \mathbf{G}_a \mathbf{Q}_f \mathbf{G}_a^T - \mathbf{P} \mathbf{C}_m^T \mathbf{R}_f^{-1} \mathbf{C}_m \mathbf{P} \quad (5-28)$$

$$\mathbf{L} = \mathbf{P} \mathbf{C}_m^T \mathbf{R}_f^{-1} \quad (5-29)$$

The block diagram of the LQE is depicted in *Figure 5-6*, in which a dashed frame indicates the Kalman filter. The input into the estimator consists of the noisy measurement of the plant $\mathbf{y} = \mathbf{C}_m \mathbf{x}_0 + \mathbf{u}$ and the control component \mathbf{u}_x , while the output of the estimator is the estimate of the state $\hat{\mathbf{x}}_0$.

5.5 Steady State LQG Problem

The steady state LQG problem is to find a compensator that uses measurements $\mathbf{u}(t)$ and $\mathbf{y}(t)$ to generate a control input $\mathbf{u}(t)$ that minimizes the performance measure represented by Eq. (5-16) given the stochastic system Eq. (5-25) and noise matrices \mathbf{Q}_f and \mathbf{R}_f for white noise processes \mathbf{v} and \mathbf{u} . The solution of this LQG problem depends on a separation principle that states the optimal LQG problem may be solved by separately solving the optimal estimation problem and deterministic certainty equivalence control problem. The separation principle guarantees the LQG problem can be reduced

to the solution of two decoupled Riccati equations, (5-20) and (5-28). So far, the full procedure of the LQG problem has been described. The block diagram of the procedure is drawn in *Figure 5-7*.

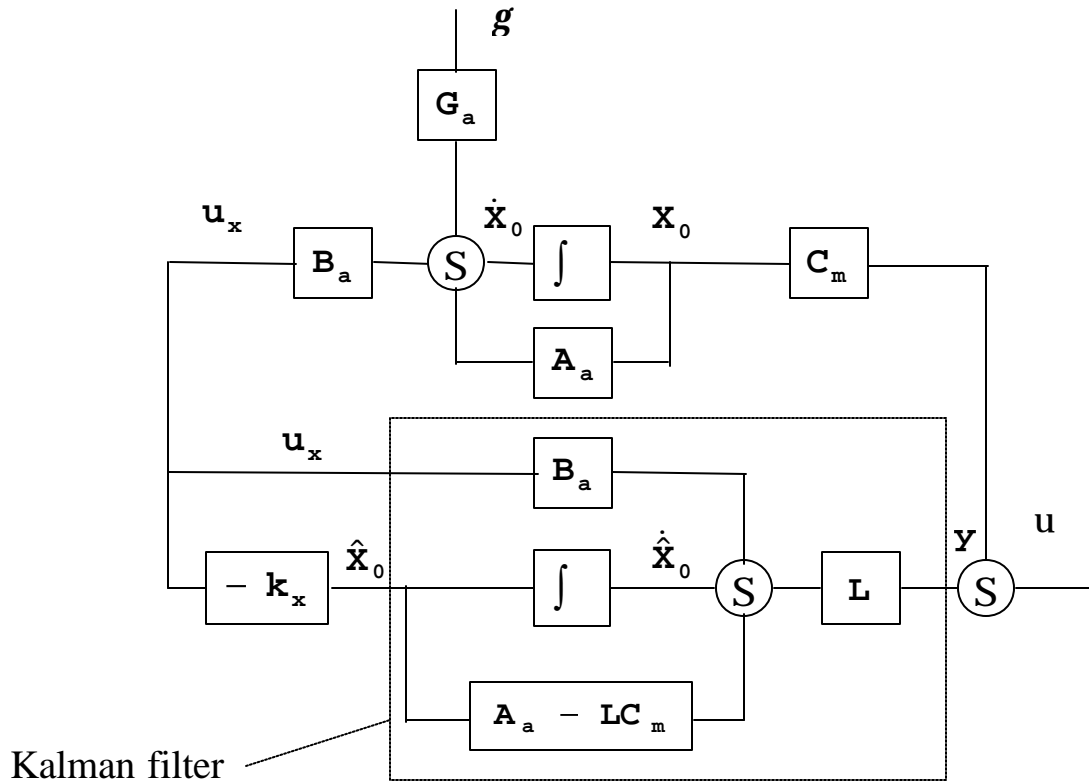


Figure 5-6. Block diagram of the LQE

The LQG system described in *Figure 5-7* is composed of three parts. The top component is the disturbance estimate system expressed by Eq. (5-10), where the input is the unit impulse d and white noise q , while the output is the disturbance state z . The middle component describes the whole dynamic process with the LQG control system expressed by Eq. (4-23). Here it can be observed that the active control force u consists of

5.6 Disturbance Accommodation Control (DAC)

Disturbance Accommodation Control (DAC) theory is a relatively new technique of modern control which enables design feedback controllers to maintain performance specifications in the face of uncertain, persistent acting external disturbances [36].

The DAC theory is a collection of non-statistical modeling and controller design techniques for the class of multi-variable control problems in which it is required to maintain set-point regulation or servo-tracking in the face of a broad range of uncertain, multi-variable, and persistently acting external disturbances. Moreover, the DAC theory permits that control performance to be realized in such a way as to optimally exploit any useful energy or other effects that may be associated with the disturbances.

The first step in any approach to dealing with exogenous disturbances in real time control problems is to mathematically model the anticipated disturbance characteristics. In the DAC method, the anticipated disturbances are always assumed uncertain, but they are not represented by statistical properties such as means, covariances, etc. Rather, they are represented by a basis-function descriptor that may be combined at any one moment of time to create $u_g(t)$. In particular, the class W of anticipated disturbances $u_g(t)$ is represented by [35]

$$W = \left\{ u_g(t) \mid u_g(t) = c_1 f_1(t) + c_2 f_2(t) + \cdots + c_M f_M(t) \right\} \quad (5-30)$$

where $f_i(t)$, $i = 1, \dots, M$, are completely known linearly independent function of time t , and c_i are completely unknown constant weighting coefficients that may jump in value every once-in-a while in a completely unknown manner. Thus, the set of M -functions $\{f_i(t)\}$ form a finite basis-set for the class W of uncertain disturbance functions $u_g(t)$, where at each t the local behavior, waveform geometry, of $u_g(t)$ is

determined by the particular values of the c_i which exist at that moment of time. In other words, the $\{f_i(t)\}$ represent the basic modes of $u_g(t)$ behavior and the weights c_i determine just how those modes are linearly combined at the t .

The exogenous disturbance descriptor Eq. (5-30) is called a wave form model in the DAC theory and represents a time-domain version of the finite-element, or spline-function, technique that has wide applications in engineering problems involving spatially-dependent phenomena (solid mechanics, fluid mechanics, electromagnetic, etc.) [36]. It should be emphasized that in the DAC theory, the values of the arbitrary weighting coefficients c_i in Eq. (5-30) are assumed piecewise constant but otherwise completely unknown. No statistical property or probabilistic structure is assumed about the time behavior of the c_i . Thus, the traditional properties of uncertainty, such as mean, covariance, etc., of $u_g(t)$ are completely unknown and, in fact, are of no concern in the DAC theory. This means that assumptions regarding ergodic behavior, stationary statistics, etc. are not required in the DAC approach.

The waveform model Eq. (5-30) is the key idea behind the DAC approach to disturbance modeling. However, the information reflected in the model Eq. (5-30) must be encoded into another format before it can be used effectively in DAC design recipes. Therefore a disturbance system has to be generated according to the waveform model Eq. (5-30), as mentioned in section 5.2. In Chapter 6 the problem will be discussed in detail.

The strategy of disturbance accommodation control consists of designing the control $\mathbf{u}(t)$ to completely cancel out the effects of the disturbance $u_g(t)$ on the plant behavior. This strategy is prompted by the common attitude that disturbances cause only unwanted disturbance or perturbations in the plant behavior and therefore the best way of accommodating those disturbances is to simply cancel out their effects on the plane. In

terms of the specific plant represented by Eq. (5-9), and disturbance model represented by Eq. (5-10), allocate the control effort expressed by Eq. (5-18) into two parts as follows

$$\mathbf{u} = \mathbf{u}_p + \mathbf{u}_d \quad (5-31)$$

where the first term represented by

$$\mathbf{u}_p = -\mathbf{k}_p \mathbf{X}_0 \quad (5-32)$$

is the control utilized to attenuate transient response, and the second term represented by

$$\mathbf{u}_d = -\mathbf{k}_d \mathbf{z} \quad (5-33)$$

is the control utilized to reduce steady-state response. Substitution of Eqs. (5-32) and (5-33) into Eq. (4-23) and considering Eq. (5-10) yields

$$\begin{aligned} \dot{\mathbf{X}}_0 &= \mathbf{A}_a \mathbf{X}_0 - \mathbf{B}_a \mathbf{k}_p \mathbf{X}_0 - \mathbf{B}_a \mathbf{k}_d \mathbf{z} + \mathbf{F}_a u_g + \mathbf{G}_a \mathbf{g} \\ \mathbf{q} &= \mathbf{C}_a \mathbf{X}_0 \end{aligned} \quad (5-34)$$

In the DAC theory, the task of \mathbf{u}_d is to achieve and maintain the condition of complete absorption

$$\min_{\mathbf{k}_d} \{-\mathbf{B}_a \mathbf{k}_d \mathbf{z} + \mathbf{F}_a u_g\} \quad (5-35)$$

Using the least square method, it is not difficult to obtain the gain matrix \mathbf{k}_d

$$\mathbf{k}_d = (\mathbf{B}_a^T \mathbf{B}_a)^{-1} \mathbf{B}_a^T \mathbf{F}_a \mathbf{C}_z \quad (5-36)$$

In the DAC theory, control component \mathbf{u}_p is responsible for accomplishing the primary control task, such as stabilization, set-point regulation, servo-tracking, etc. One can now proceed to design \mathbf{u}_p by conventional methods. The corresponding gain matrix \mathbf{k}_p can be obtained by [35]

$$\mathbf{k}_p = (\mathbf{B}_a^T \mathbf{B}_a)^{-1} \mathbf{B}_a^T \mathbf{A}_a \quad (5-37)$$

Actually, Eq. (5-31) can be also written in the form of Eq. (5-22), except that the gain matrix \mathbf{K} is expressed by

$$\mathbf{K} = -[\mathbf{k}_p \quad \mathbf{k}_d] \quad (5-38)$$

5.7 The Hybrid LQG/DAC Approach

As stated earlier, that the technique of splitting the total control effort into two task-oriented parts in the DAC design, as shown in Eq. (5-31), is a simple but notable effective design idea which appears to be unique to the DAC theory. In the DAC theory, control component \mathbf{u}_a is responsible for the disturbance reduction task. Its corresponding gain \mathbf{k}_a represented in Eq. (5-36) is convinced. However the choice of the gain matrix \mathbf{k}_p is manifold. In the previous sections, the LQG approach was discussed to seek the optimal control force. Now, the LQG approach is proposed to find \mathbf{k}_p . The technique in which the LQG method is used to design \mathbf{k}_p and the DAC method is used to determine \mathbf{k}_a is referred to as hybrid LQG/DAC control.

The LQG method of developing DAC design starts from the equation of motion

$$\dot{\mathbf{x}}_0 = \mathbf{A}_a \mathbf{x}_0 + \mathbf{B}_a \mathbf{u} \quad (5-39)$$

Following the LQR design procedure developed in the section 5.3, it is not difficult to obtain the gain \mathbf{k}_p by solving the associated algebraic matrix Riccati equation:

$$\mathbf{0} = \mathbf{S}_p \mathbf{A}_a + \mathbf{A}_a^T \mathbf{S}_p + \mathbf{Q}_p - \mathbf{S}_p \mathbf{B}_a \mathbf{R}_p^{-1} \mathbf{B}_a^T \mathbf{S}_p \quad (5-40)$$

Consequently, the optimal feedback gain matrix \mathbf{k}_p can be obtained as following

$$\mathbf{k}_p = \mathbf{R}_p^{-1} \mathbf{B}_a^T \mathbf{S}_p, \quad \mathbf{u}_p = -\mathbf{R}_p^{-1} \mathbf{B}_a^T \mathbf{S}_p \hat{\mathbf{x}}_0 \quad (5-41)$$

Combining \mathbf{k}_p with \mathbf{k}_d

$$\mathbf{k}_d = (\mathbf{B}_a^T \mathbf{B}_a)^{-1} \mathbf{B}_a^T \mathbf{F}_a \mathbf{C}_z \quad (5-36)$$

the hybrid gain matrix can be obtained by

$$\mathbf{K} = -[\mathbf{k}_p \quad \mathbf{k}_d] \quad (5-38)$$

Figure 5-8 describes the dynamic simulation procedure with the hybrid LQG/DAC design. It should be noticed that the estimator developed in the section 5.4 keeps unchanged except for replacing \mathbf{u}_x by \mathbf{u}_p as the input of the estimator in the hybrid LQG/DAC design.

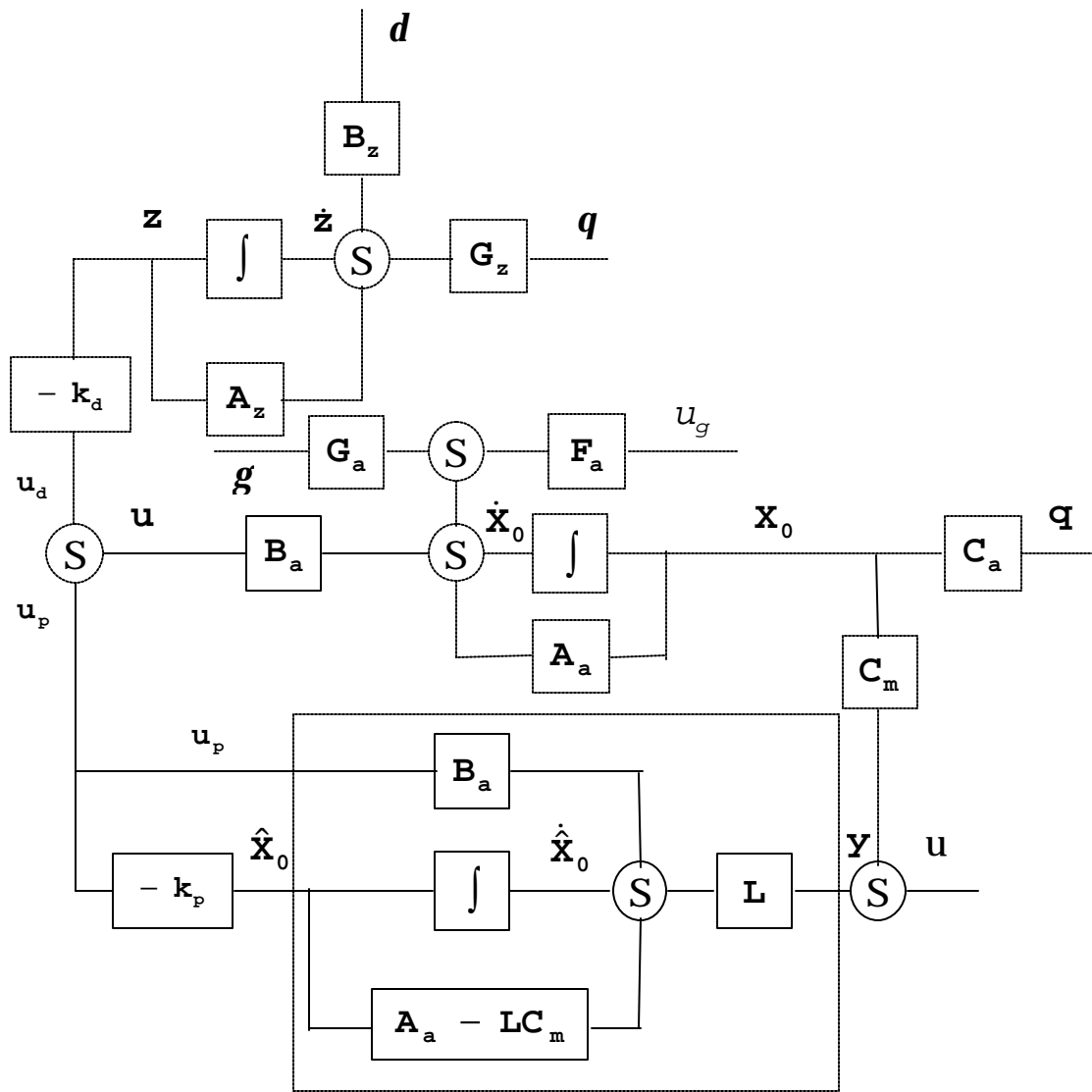


Figure 5-8. Block diagram of the Hybrid LQG/DAC system

CHAPTER SIX

SYSTEM IDENTIFICATION PROBLEM

As per the assumption in the section of Disturbance Rejection Problem that the ground motion can be viewed as the impulse response of a certain system. This is a system identification problem. The system identification problem is to estimate a model of a system based on observed input-output data. In this problem a system impulse function is going to be built, known as disturbance function. Assuming there is an input signal $\mathbf{h}(t)$ and an output signal $\mathbf{z}(t)$, and the signals are related by a linear system, the relationship can be written

$$\mathbf{z}(t) = H(s)\mathbf{h}(t) + \mathbf{n}(t) \quad (6-1)$$

where s is the differential operator and $H(s)\mathbf{h}(t)$ is short for

$$H(s)\mathbf{h}(t) = \int_0^{\infty} \mathbf{h}(t-\tau)\mathbf{h}(\tau) d\tau \quad (6-2)$$

and

$$H(s) = \int_0^{\infty} \mathbf{h}(t) e^{-j\omega t} dt; \quad s^{-1}\mathbf{h}(t) = \int \mathbf{h}(t) dt \quad (6-3)$$

The $\mathbf{h}(t)$ is called the impulse response of the system. Clearly, $\mathbf{h}(t)$ is the output of the system at time t if the input is a single impulse at time zero. The function $H(s)$ is called the transfer function of the system. This function evaluated in the frequency domain gives the frequency function $H(j\omega)$. In Eq. (6-1) $\mathbf{n}(t)$ is an additional, unmeasurable noise. Its properties can be expressed in terms of its autospectrum $F_n(j\omega)$, which is defined by

$$F_n(j\omega) = \int_{-\infty}^{\infty} R_n(t) dt \quad (6-4)$$

where $R_n(\mathbf{t})$ is the autocorrelation function of $r(\mathbf{t})$

$$R_n(\mathbf{t}) = E [r(\mathbf{t})r(\mathbf{t} - \mathbf{t})] \quad (6-5)$$

Alternatively, the noise $r(\mathbf{t})$ can be described as filtered white noise

$$r(\mathbf{t}) = G(s)e(\mathbf{t}) \quad (6-6)$$

where $e(\mathbf{t})$ is white noise with variance \mathbf{s}_e and

$$F_n(j\omega) = \mathbf{s}_e |G(j\omega)|^2 \quad (6-7)$$

Eqs. (6-1) and (6-6) together give a time domain description of the system

$$z(\mathbf{t}) = H(s)\mathbf{h}(\mathbf{t}) + G(s)e(\mathbf{t}) \quad (6-8)$$

while $H(j\omega)$ and Eq. (6-7) constitute a frequency domain description.

A commonly used parametric model is the ARX model that corresponds to

$$H(s) = \frac{s^{-k}B(s)}{A(s)}; \quad G(s) = \frac{1}{A(s)} \quad (6-9)$$

where $B(s)$ and $A(s)$ are polynomials in the integral operator s^{-1}

$$A(s) = 1 + a_1s^{-1} + \dots + a_ns^{-n} \quad (6-10)$$

$$B(s) = b_0 + b_1s^{-1} + \dots + b_ms^{-m} \quad (6-11)$$

Here, the numbers n and m are the orders of the respective polynomials. The model is usually written

$$A(s)\mathbf{z}(s) = B(s)s^{-k}\mathbf{h}(s) + e(s) \quad (6-12)$$

or explicitly

$$\begin{aligned} \mathbf{z}^{(n)}(t) + a_1\mathbf{z}^{(n-1)}(t) + \cdots + a_{n-1}\dot{\mathbf{z}}(t) + a_n\mathbf{z}(t) \\ = b_0\mathbf{h}^{(n-k)}(t) + b_1\mathbf{h}^{(n-k-1)}(t) + \cdots + b_m\mathbf{h}^{(n-m-k)}(t) + e^{(n)}(t) \end{aligned} \quad (6-13)$$

where $\mathbf{z}^{(n)}(t)$ indicates the n th time derivative of $\mathbf{z}(t)$.

In this problem, a system model whose impulse response is the ground motion $u_g(t)$ is established by using AMX. The corresponding relations are expressed by

$$\mathbf{z}(t) = u_g(t), \quad \mathbf{h}(t) = \mathbf{d}(t), \quad n(t) = \mathbf{q}(t) \quad (6-14)$$

The goal is to find $A(s)$ and $B(s)$. The ground motion may be expressed in the following form

$$u_g = \sum_{m=1}^M c_m f_m(t) \quad (6-15)$$

where c_m are arbitrary constant, and $f_m(t)$ are referred to as waveform function. Here the waveform components are assumed to have the form

$$f_m(t) = \begin{cases} \sin(\mathbf{w}_m t) & m = \text{odd} \\ \cos(\mathbf{w}_m t) & m = \text{even} \end{cases} \quad (6-16)$$

Suppose the constants c_m can be written as

$$c_m = \begin{cases} W_m \cos \mathbf{j}_m & m = \text{odd} \\ W_m \sin \mathbf{j}_m & m = \text{even} \end{cases} \quad (6-17)$$

thus, Eq. (6-15) can be rewritten as

$$u_g = \sum_{n=1}^N W_n \sin(\mathbf{w}_n t + \mathbf{j}_n) \quad (6-18)$$

where W_n and \mathbf{j}_n are arbitrary constants. To write the ground motion $u_g(t)$ in the disturbance state model, taking the Laplace's transform of Eq. (6-18), and collecting terms yields:

$$\begin{aligned} u_g(s) &= \sum_{n=1}^N \frac{W_n (\mathbf{w}_n \cos \mathbf{j}_n + s \sin \mathbf{j}_n)}{s^2 + \mathbf{w}_n^2} \\ &= \frac{\mathbf{b}_1 s^{2N-1} + \mathbf{b}_2 s^{2N-2} + \cdots + \mathbf{b}_{2N-1} s + \mathbf{b}_{2N}}{s^{2N} + \mathbf{a}_2 s^{2N-2} + \cdots + \mathbf{a}_{2N-2} s^2 + \mathbf{a}_{2N}} \end{aligned} \quad (6-19)$$

where \mathbf{a}_n and \mathbf{b}_n associated with W_n , \mathbf{w}_n and \mathbf{j}_n are the parameters to be estimated. It is noted that the Laplace's transform of $\mathbf{d}(t)$ is unity, then the right side of Eq. (6-19) is now viewed as the transfer function of a scalar output of a linear stationary system with a unit impulse forcing function, i.e. $\frac{B(s)}{A(s)}$. And the denominator represents the characteristic equation of the linear dynamic system. The information in Eq. (6-19) serves to completely determine a suitable and completely observable model of the form Eq. (5-1). This can be written in the second controller canonical form:

$$u_g(t) = [\mathbf{b}_{2N} \quad \mathbf{b}_{2N-1} \quad \cdots \quad \mathbf{b}_2 \quad \mathbf{b}_1] \cdot \mathbf{z}(t)$$

$$\dot{\mathbf{z}}(t) = \begin{bmatrix} 0 & 1 & 0 & \cdots & 0 & 0 \\ 0 & 0 & 1 & \cdots & 0 & 0 \\ \vdots & & & \cdots & & \\ 0 & 0 & 0 & \cdots & 1 & 0 \\ 0 & 0 & 0 & \cdots & 0 & 1 \\ -\mathbf{a}_{2N} & 0 & -\mathbf{a}_{2N-2} & \cdots & -\mathbf{a}_2 & 0 \end{bmatrix} \cdot \mathbf{z}(t) + \begin{bmatrix} 1 \\ 0 \\ \vdots \\ 0 \\ 0 \\ 0 \end{bmatrix} \mathbf{d}(t) \quad (6-20)$$

Comparing the above equation to Eqs. (4-34), the following equation is immediately obtained

$$\mathbf{A}_z = \begin{bmatrix} 0 & 1 & 0 & \cdots & 0 & 0 \\ 0 & 0 & 1 & \cdots & 0 & 0 \\ \vdots & & & \cdots & & \\ 0 & 0 & 0 & \cdots & 1 & 0 \\ 0 & 0 & 0 & \cdots & 0 & 1 \\ -\mathbf{a}_{2N} & 0 & -\mathbf{a}_{2N-2} & \cdots & -\mathbf{a}_2 & 0 \end{bmatrix}, \quad \mathbf{B}_z = \mathbf{G}_z = \begin{bmatrix} 1 \\ 0 \\ \vdots \\ 0 \\ 0 \\ 0 \end{bmatrix} \quad (6-21)$$

$$\mathbf{C}_z = [\mathbf{b}_{2N} \quad \mathbf{b}_{2N-1} \quad \cdots \quad \mathbf{b}_2 \quad \mathbf{b}_1]$$

CHAPTER SEVEN

NUMERICAL EXAMPLE

7.1 Basic Description and Assumption

As an illustration of the development in the previous chapters, we consider the system similar to that investigated in Chapter 3. The system is a four-story framed building that can be regarded as a flexible structure. The building is claimed to a base in the form of a rigid slab capable of moving horizontally relative to the ground. It is assumed that the base lies on a viscoelastic support, modeled as a viscous damper and an elastic spring connected to the ground in parallel, as shown in *Figure 7-1*.

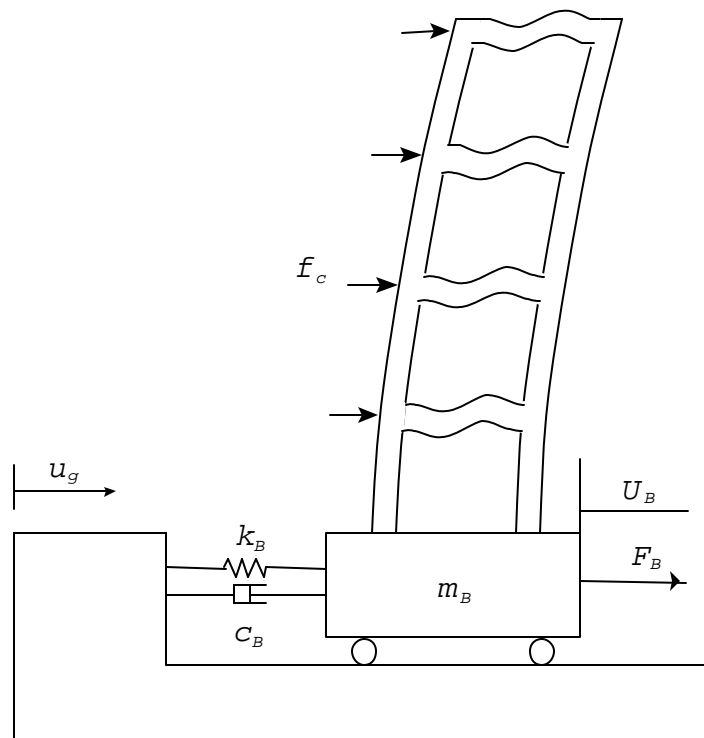


Figure 7-1. Model of a four-storey building system subjected to ground motion

Figure 7-1 shows five horizontal control forces applied on the base and the four floors individually to attenuate the vibration of the building due to the ground motion.

Considering the building is a two-dimensional assemblage of portal frames consisting of rectangular tubes and regarded as distributed-parameter beams and columns, modeled as Euler-Bernoulli beams. All elastic members, whether a beam or column, have the same cross section, which is a hollow rectangle. Each column $l_1^{(i)}$ or $l_2^{(i)}$ is 3 m long and each beam $l_0^{(i)}$ is 7 m long. The mass density ρ_0 is 7800 Kg/m³. The Young's modulus E is 216 GPa. The weight of the base m_B is 8000 Kg. The spring stiffness k_B is 2.63MN/m. The coefficient of viscous damping c_B is 65.7 KNs/m. The parameters of the structure and base are shown in **Table 7-1**.

Table 7-1. The structural parameters used in the example

m_B	k_B	c_B	E	ρ_0	$l_0^{(i)}$	$l_1^{(i)}$	$l_2^{(i)}$
8000 Kg	2.63MN/m	65.7 KNs/m	216 GPa	7800 Kg/m ³	7 m	3 m	3 m

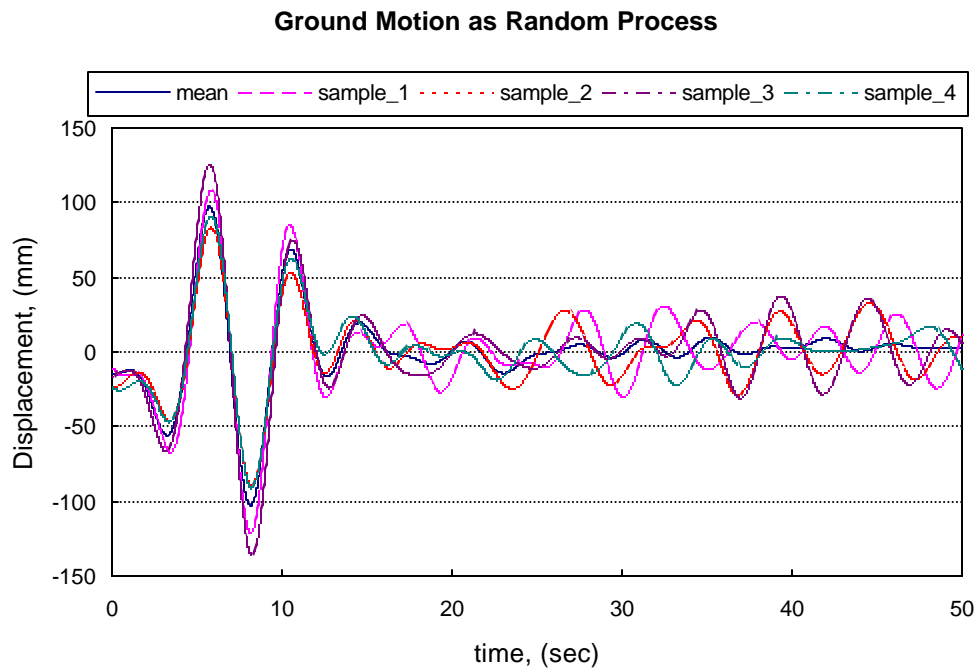
For the sake of simplicity, the motion of the ground and the base are assumed to take place in the horizontal direction of the vertical plane alone. The motion of the ground used in the computer simulation was always assumed uncertain and a random process. As mentioned in Chapter 5, the ground motion was represented by a basis function descriptor that displays the totality of possible waveform components. That may be combined at any one moment of time t to form $u_g(t)$. In particular, it was represented by a combination of a set of sinusoidal functions, as shown in Eq. (7-1)

$$u_g(t) = \sum_{i=1}^{20} A_i \sin(\omega_i t + \mathbf{j}_i) \quad (7-1)$$

Table 7-2. Parameters used in the random motion of ground

i	1	2	3	4	5	6	7	8	9	10
A_i (mm)	7.4	3.6	4.2	4.3	2.3	0.9	2.3	3.9	5.6	8.2
ω_i (rad/s)	0	.0932	.1863	.2795	.3727	.4658	.5590	.6521	.7453	.8385
\mathbf{j}_i (rad)	0	-1.77	-0.935	-1.69	-2.48	-0.459	-1.20	-1.54	-2.04	-2.64
i	11	12	13	14	15	16	17	18	19	20
A_i (mm)	7.9	9.2	10.9	13.8	12.3	10.7	9.7	7.4	6.2	4.8
ω_i (rad/s)	.9317	1.025	1.118	1.211	1.304	1.398	1.491	1.584	1.677	1.770
\mathbf{j}_i (rad)	2.924	2.479	1.914	1.238	.3618	-.304	-.979	-1.80	-2.31	2.932

In **Figure 7-2** is shown some of time histories of the random disturbance $u_g(t)$ for $0 \leq t \leq 50$ s.

**Figure 7-2.** The mean and 4 random samples of the motion of ground

The wind force \mathbf{Q}_w was described as filtered white noise, as seen in Eq. (4-6). The white noise $\mathbf{g}(t)$ has zero mean and variance \mathbf{s}_g . Other noises used in previous development, $\mathbf{q}(t)$ and $\mathbf{u}(t)$, were also to be assumed to be white noise with zero mean. All variances of the white noises are given in **Table 7-3**.

Table 7-3. *The variance of white noise*

\mathbf{s}_g	\mathbf{s}_q	\mathbf{s}_u
0.01	0.1	0.0001

7.2 Modeling of the System by Using the HFEM Technique

As a direct application of the approach developed in Chapter 3, eigenfunctions of a uniform fixed-fixed Euler-Bernoulli beam expressed in Eq. (2-13) were taken as the hierarchical functions. In addition to the structural parameters listed in **Table 7-1**, the other relative parameters were number of stories $N = 4$ and number of hierarchical functions $n_0 = n_1 = 3$. Thus the model of the building system had 49 degrees of freedom before model reduction by using modal truncation approach. To validate advantage of the HFEM, an eigenvalue problem was solved two times using two models, one was HFEM, another was a traditional finite element model as a comparison. The traditional finite element simulation that had 26,800 degrees of freedom was carried out using the commercial software MSC/NASTRAN.

The first 10 natural frequencies of the entire building system from the HFEM is compared with that results from NASTRAN. The comparison is shown in **Table 4**. It shows very good agreement between the two results, with the fact that the analysis carried out by using the HFEM involved less degrees of freedoms, which is a significant improvement. The degrees of freedom were reduced from 26,880 to 49 using HFEM technique, but the accuracy of the

natural frequencies is in reasonable range. The difference between two results was within 2% error.

Considering the highest angular frequency of the disturbance (listed in *Table 7-2*) was only 1.77 rad/s, we took the lowest 5 modes of the building with no the base as the truncated modes in model reduction, as mentioned in Chapter 3. Hence the truncated model had only 12 degrees of freedom.

Table 7-4. Comparison of natural frequencies using HFEM and NASTRAN, (Hz)

Mode	1	2	3	4	5
HFEM	1.497	2.885	5.344	10.49	10.88
NASTRAN	1.480	2.886	5.101	9.924	10.09
Mode	6	7	8	9	10
HFEM	11.53	12.09	12.36	17.6	29.48
NASTRAN	11.25	11.96	12.31	15.46	28.46

7.3 The State Space Implementation of the Control Models

In producing the multiple Channel Control (MCC) model of this example, it is only necessary to adopt five control forces expressed in Eq. (4-10). Following the procedure developed in Chapter 4 it is not difficult to create the MCC model used in the numerical simulation.

As stressed in Chapter 4, it should be noted that the control matrix \mathbf{B}_a in Eqs. (4-30) representing SCC model is different from that in Eqs. (4-22) representing MCC model. When generating the single Channel Control (SCC) model for the example, it was required to find an appropriate weighting matrix \mathbf{U} . It was very tempting to adjust the elements in the weighting

matrix \mathbf{U} so as to minimize the dynamic response of the building to the motion of ground. The weighting matrix \mathbf{U} that we obtained finally was

$$\mathbf{U} = \{2047.5 \quad -0.42 \quad 0.68 \quad 1.02 \quad 1.13\}^T$$

The special single Channel Control (SSCC) model of the example was generated completely following the procedure developed in section 4-3.

7.4 Control Simulation

The three control approaches developed in Chapter 5, the LQG control, the DAC control and the LQG/DAC control, were all simulated and compared in the numerical example in conjunction with the three control models developed in Chapter 4, the MCC model, the SCC model and the SSCC model. Thus, the simulation was carried up in nine cases. The nine cases are as follows:

- Case 1. The MCC model with the LQG control
- Case 2. The MCC model with the DAC control
- Case 3. The MCC model with the LQG/DAC control
- Case 4. The SCC model with the LQG control
- Case 5. The SCC model with the DAC control
- Case 6. The SCC model with the LQG/DAC control
- Case 7. The SSCC model with the LQG control
- Case 8. The SSCC model with the DAC control
- Case 9. The SSCC model with the LQG/DAC control

All nine cases were performed by imitating real experiments. *Figure 7-3* depicts the block diagram of the simulation for the LQG control and the LQG/DAC control. It should be pointed out that the difference among the six simulation cases involved the LQG control or LQG/DAC

control lies in only the values of the gain matrixes \mathbf{K}_x , \mathbf{K}_z and \mathbf{L} . But the simulation processes were completely the same regardless the MCC model, the SCC model or the SSCC model. Similarly, no matter what the control model was the simulation processes for the DAC control were the same. In *Figure 7-4* the block diagram of the simulation for the DAC control is shown.

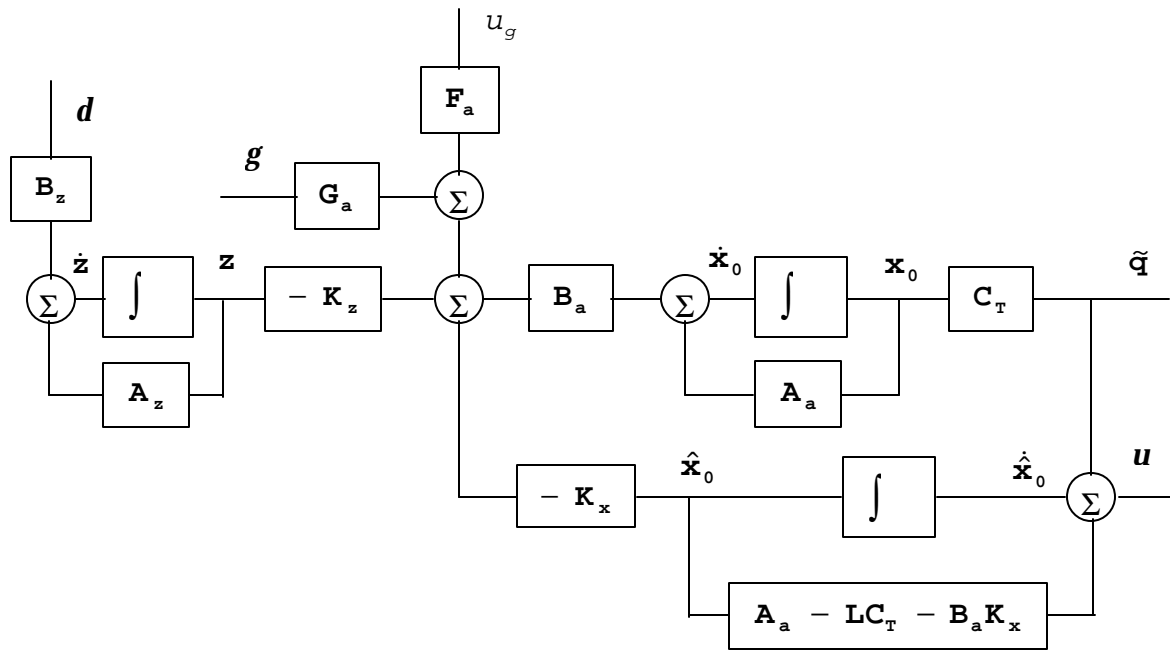


Figure 7-3. Simulation block diagram of the LQG control and the LQG/DAC control

The goal was to minimize the displacement of the top floor relative to the base in the dissertation. Now, when using the LQG control approach to determine the optimal feedback gain matrix, the matrixes \mathbf{Q} and \mathbf{R} were taken individually as mentioned below

$$\mathbf{Q} = \mathbf{C}_T^T \mathbf{C}_T$$

$$\mathbf{R} = \mathbf{I}_{5 \times 5}$$

where $\mathbf{I}_{5 \times 5}$ is a 5x5 unit matrix.

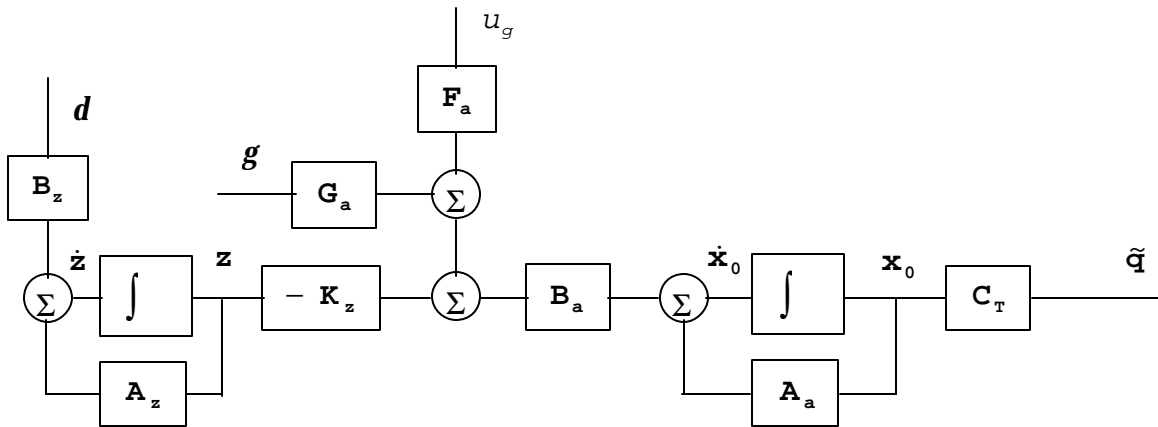


Figure 7-4. Simulation block diagram of the DAC design

7.5 Simulation Results and Discussion

Throughout this work, all computer simulations were transient models and implemented using Matlab. Computer simulation results were described by the displacements, velocities and accelerations, which were depicted as a time history. The displacements, velocities and accelerations are absolute values for the base, but are relative values to the base for the building. It should be noticed that all results are not plotted for the sake of saving space. Only results of the top floor and base are displayed in the plots, while all results are listed in tables. Those in which performance is not obvious are ignored. Besides the time history plots, the root mean square (RMS) values of the displacements, velocities and accelerations are listed. The RMS value is defined by

$$u_{rms} = \sqrt{\frac{1}{T} \int_0^T u^2(t) dt} \quad (7-2)$$

In addition, relative control efficiency is given as an index number, which judges control performance, and is defined by

$$I = \frac{\text{the RMS value without control} - \text{the RMS value with control}}{\text{the RMS value without control}} \times 100\% \quad (7-3)$$

Control forces are given in maximum absolute value, which the actuator is able to provide.

7.5.1 The MCC Model with the LQG Control

Table 7-5 lists the simulation results of the MCC model with the LQG control. It covers the RMS values of the displacements, velocities and accelerations with and without control, the relative control efficiency and the maximum control forces applied on the base and the top floor through the bottom floor.

Figure 7-5 shows the time histories of the displacements of the top floor relative to the base with and without control, in which uncontrolled response is plotted in a blue dashed line and the controlled response in a red solid line.

Figure 7-6 compares the velocities relative to the base on the top floor with and without control.

It is observed that the relative displacement of the top floor was reduced from 20.9 mm to 6.4 mm by using the LQG control in the MCC model, as a result, the relative efficiency corresponding to the displacement I was 69.4%, although the displacement of the base increased by 0.012 mm. Moreover, the velocities and the accelerations of the top floor were also reduced from 0.9793 mm/s and 0.2287 mm/s² to 0.4906 mm/s and 0.1734 mm/s², respectively. Consequently, the corresponding relative efficiencies I were, 49.9% and 24.2% respectively. These preliminary results are quite encouraging.

Table 7-5. Simulation results of the MCC model with the LQG control

	without control	with control	relative efficiency (%)
u_b , (mm)	26.1464	26.1582	-0.045
u_4 , (mm)	20.9302	6.4046	69.4
u_3 , (mm)	15.3743	4.4739	70.9
u_2 , (mm)	9.5583	3.5366	63.0
u_1 , (mm)	3.5917	1.8210	49.3
\dot{u}_b , (mm/s)	0.3611	0.3609	0.06
\dot{u}_4 , (mm/s)	0.9793	0.4906	49.9
\dot{u}_3 , (mm/s)	0.7446	0.3358	54.9
\dot{u}_2 , (mm/s)	0.6154	0.4332	29.6
\dot{u}_1 , (mm/s)	0.5864	0.4328	26.2
\ddot{u}_b , (mm/s ²)	0.054	0.0538	0.45
\ddot{u}_4 , (mm/s ²)	0.2287	0.1734	24.2
\ddot{u}_3 , (mm/s ²)	0.2549	0.1792	29.7
\ddot{u}_2 , (mm/s ²)	0.1452	0.1275	12.2
\ddot{u}_1 , (mm/s ²)	0.2773	0.1994	28.1
F_b , (N)		0.913	
f_4 , (N)		53.666	
f_3 , (N)		51.547	
f_2 , (N)		49.458	
f_1 , (N)		25.870	

Figure 7-7 displays the actuator force acting on the base, where the largest peak value was only 0.913 N. **Figure 7-8** shows the control forces applied on the building from the top floor to the first floor, in which the maximum peak value was 53.7 N acting on the top floor.

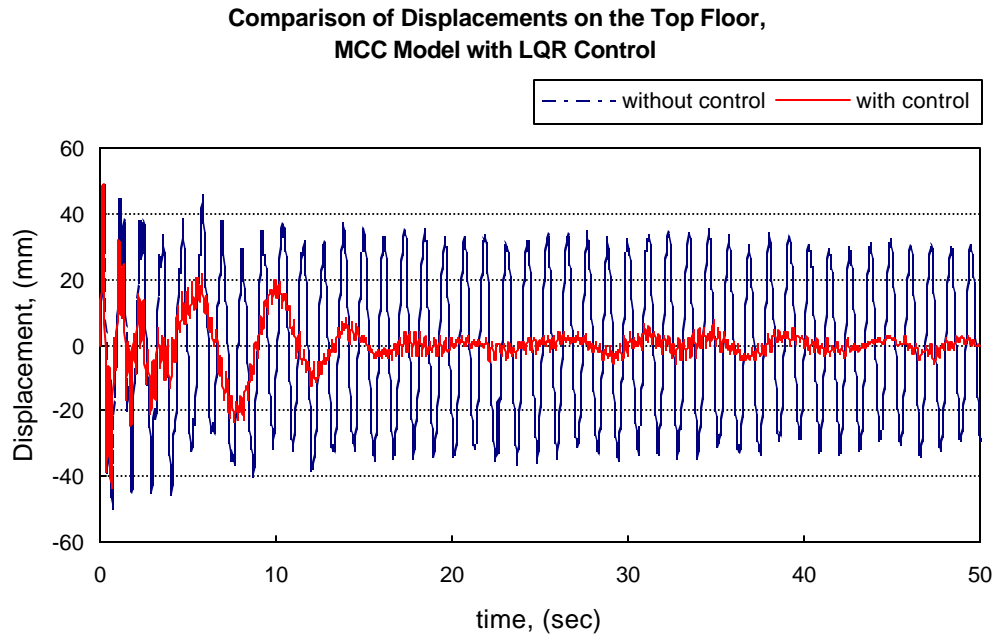


Figure 7-5. Relative displacements of the top floor, (MCC model, LQG control)

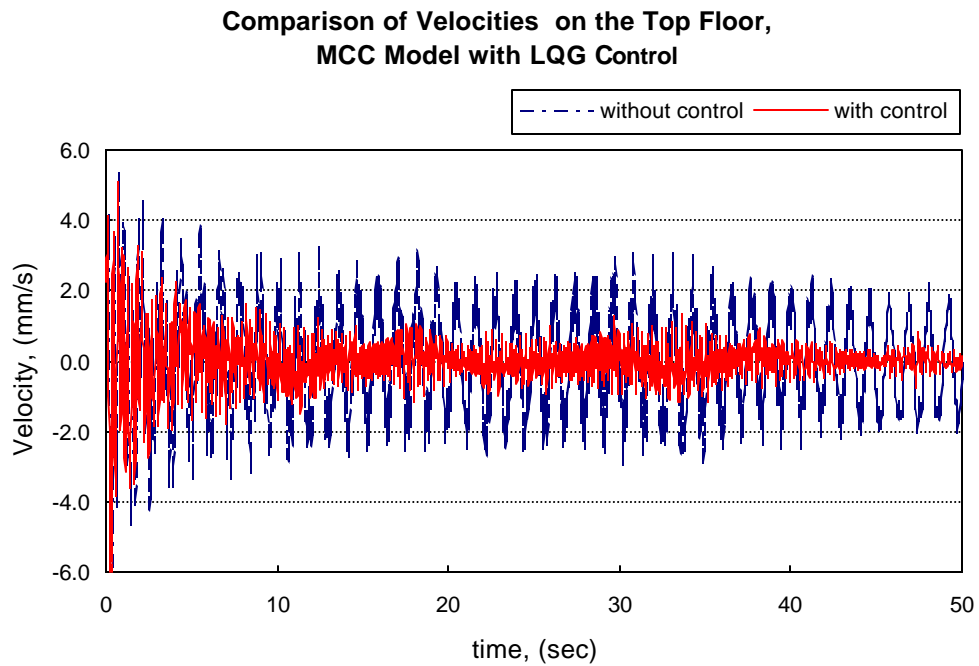


Figure 7-6. Relative velocities of the top floor, (MCC model, LQG control)

Table 7-6. The closed-loop eigenvalues for the MCC model with the LQG control

number	the open-loop eigenvalues	the closed-loop eigenvalues
1	-0.0035+80.9693i	-0.0035+80.9693i
2	-0.0035-80.9693i	-0.0035-80.9693i
3	-0.0035+84.2428i	-0.0035+84.2428i
4	-0.0035-84.2428i	-0.0035-84.2428i
5	-0.0061+5.4653i	-0.0677+54.3117i
6	-0.0061-5.4653i	-0.0677-54.3117i
7	-0.0319+543117i	-0.2587+22.6167i
8	-0.0319-543117i	-0.2587-22.6167i
9	-0.2150+22.6162i	-0.5756+5.4957i
10	-0.2150-22.6162i	-0.5756-5.4957i
11	-3.8387+17.4842i	-3.8390+17.4840i
12	-3.8387-17.4842i	-3.8390-17.4840i

Table 7-6 compares the closed-loop eigenvalues with the open-loop eigenvalues of the MCC model with the LQG control. The results show most closed-loop eigenvalues have greater negative real parts than the open-loop eigenvalues except that first four are the same. This indicates the LQG control increased the damping of the controlled system in essential.

7.5.2 The MCC Model with the DAC Control

In this case, the DAC problem is explored using the same model as in the Case 1, i.e. five independent actuator forces were utilized but the algorithm used to optimize the state feedback gain matrix \mathbf{K}_d was determined by using the DAC approach. Following the procedure mentioned in the previous sections could obtain \mathbf{K}_d easily from Eq. (5-36). The results of the simulation are listed in **Table 7-7**, while the corresponding curves are drawn in **Figure 7-9**

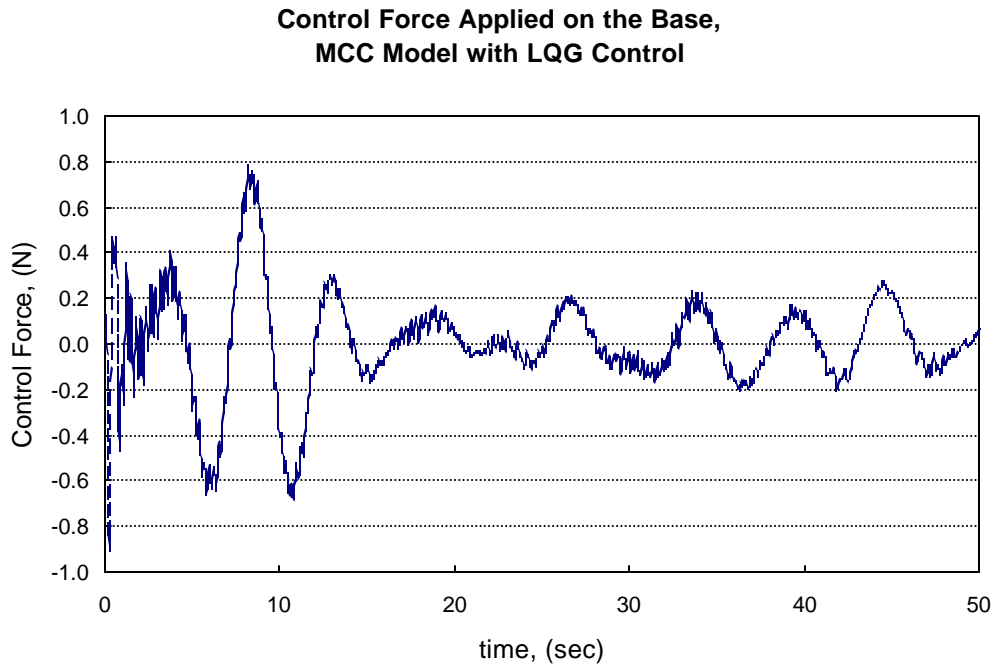


Figure 7-7. Control force applied on the base, (MCC model, LQG control)

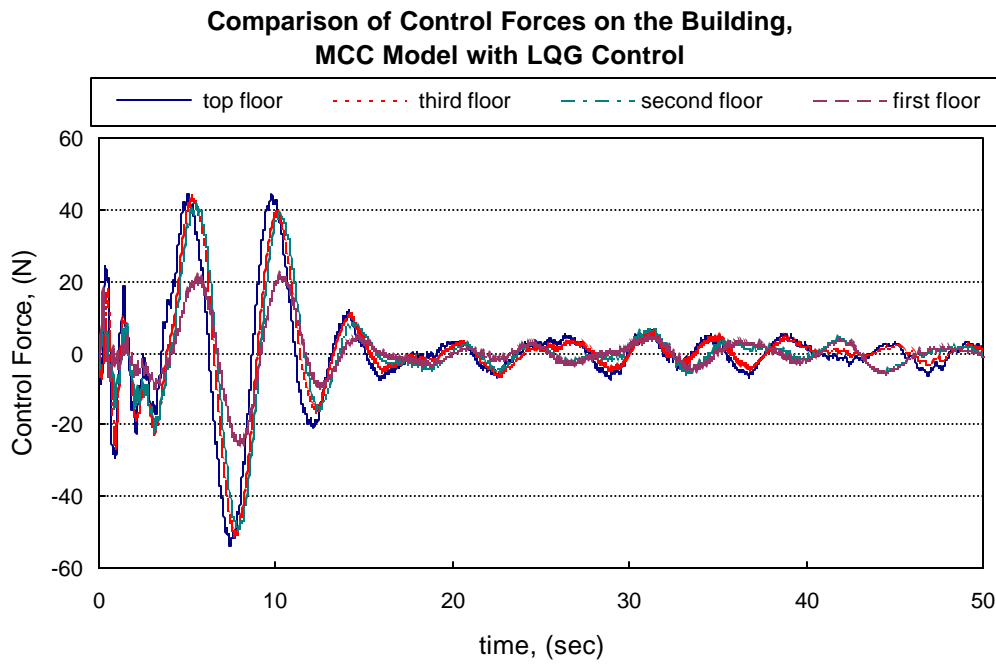


Figure 7-8. Control forces applied on the building, (MCC model, LQG control)

through *Figure 7-12*. *Figure 7-9* illustrates the comparison of the displacements on the base before and after the DAC control based on the MCC model, while *Figure 7-10* displays that on the top floor.

Table 7-7. Simulation results of the MCC model with the DAC control

	without control	with control	relative efficiency (%)
u_b , (mm)	26.1464	0.9413	96.4
u_4 , (mm)	20.9302	6.0698	71.0
u_3 , (mm)	15.3743	4.1818	72.8
u_2 , (mm)	9.5583	3.6513	61.8
u_1 , (mm)	3.5917	2.0976	41.6
\dot{u}_b , (mm/s)	0.3611	0.1141	68.4
\dot{u}_4 , (mm/s)	0.9793	0.5768	41.1
\dot{u}_3 , (mm/s)	0.7446	0.4788	35.7
\dot{u}_2 , (mm/s)	0.6154	0.4696	23.7
\dot{u}_1 , (mm/s)	0.5864	0.5970	-1.8
\ddot{u}_b , (mm/s ²)	0.054	0.0953	-76.4
\ddot{u}_4 , (mm/s ²)	0.2287	0.2491	-8.9
\ddot{u}_3 , (mm/s ²)	0.2549	0.2896	-13.6
\ddot{u}_2 , (mm/s ²)	0.1452	0.1638	-12.8
\ddot{u}_1 , (mm/s ²)	0.2773	0.3164	-14.1
F_b , (kN)		270.2	
f_4 , (N)		0.030	
f_3 , (N)		0.089	
f_2 , (N)		0.175	
f_1 , (N)		0.181	

The most notable characteristics of the DAC control were that the displacement and velocity of the base was significantly decreased. Especially notable, the displacement of the base was reduced by 96% from 26.1 mm to 0.94 mm. The displacement of the top floor was also

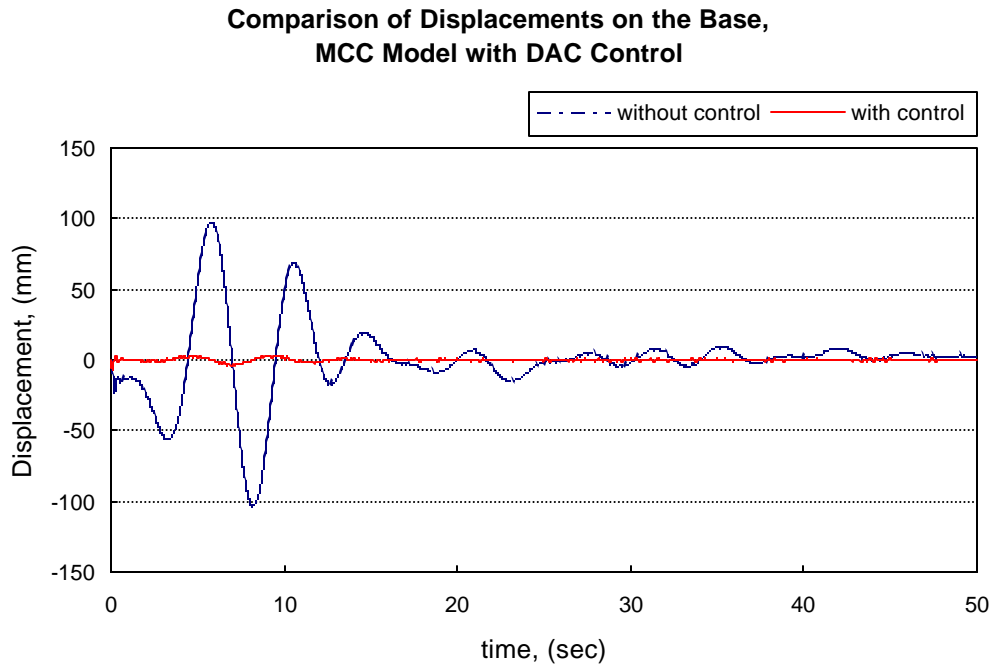


Figure 7-9. Displacements of the base, (MCC model, DAC control)

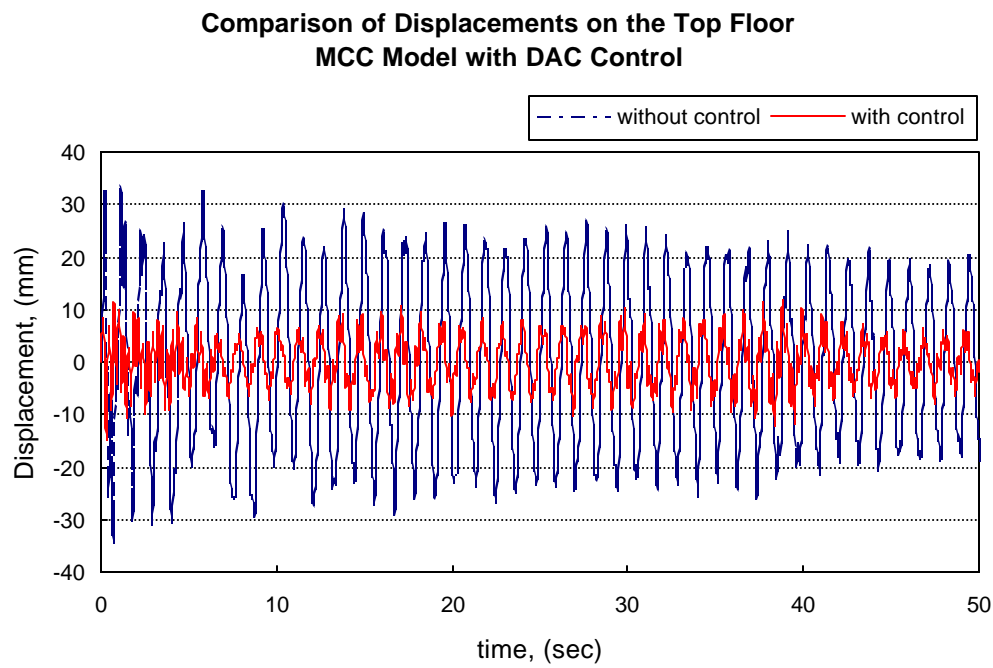


Figure 7-10. Relative displacement of the top floor, (MCC model, DAC control)

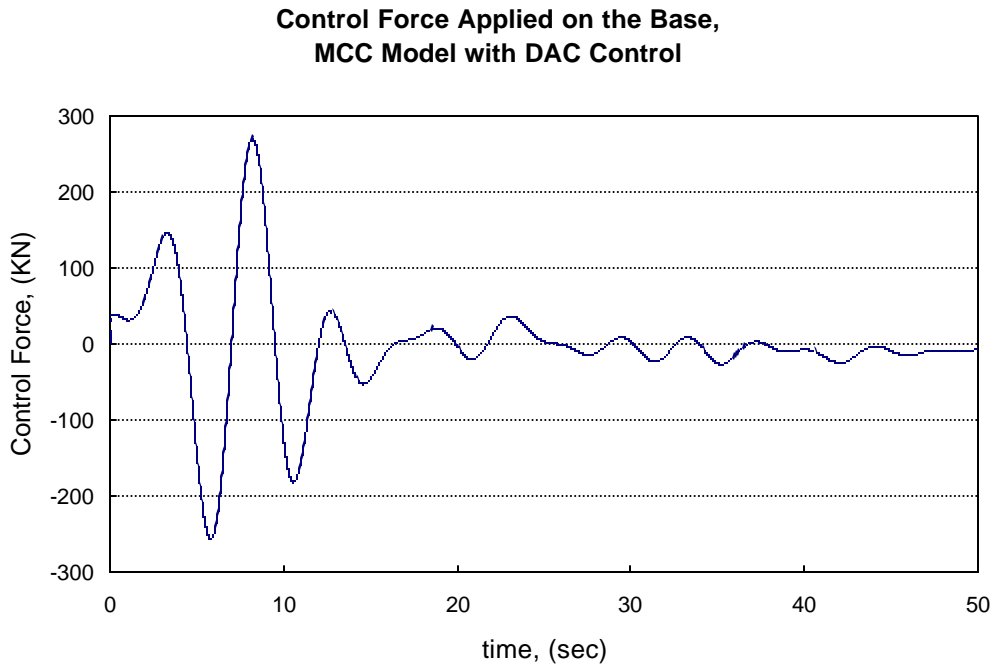


Figure 7-11. Control force applied on the base, (MCC model, DAC control)

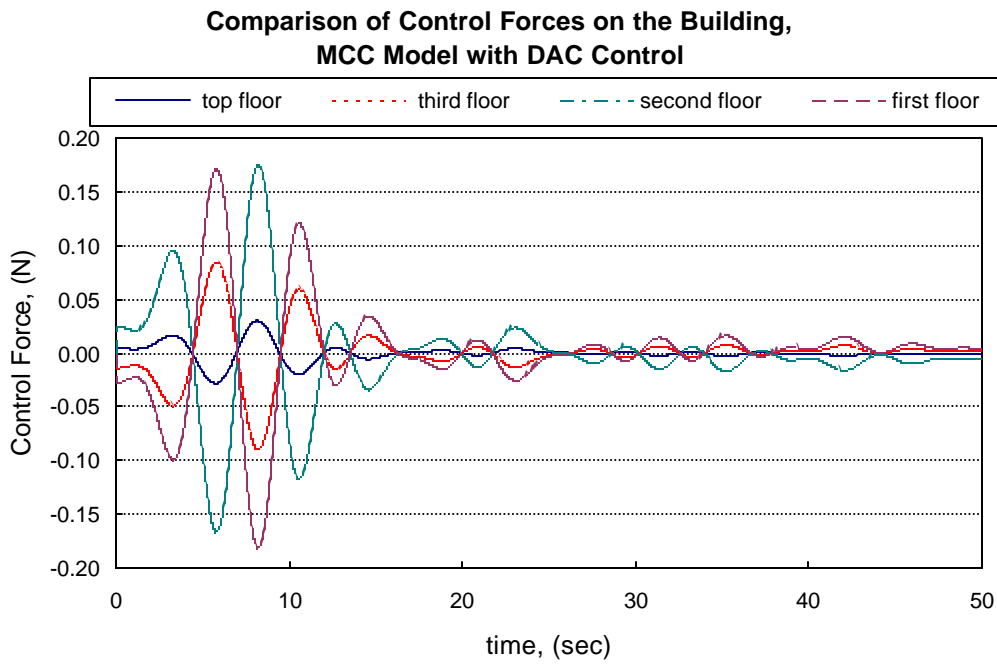


Figure 7-12. Control forces applied on the building, (MCC model, DAC control)

reduced from 20.9 mm to 6 mm. The relative control efficiency was up to 71%.

Figure 7-11 shows the control force acting on the base, the maximum magnitude of which was 270.2 KN. The DAC control force applied on the base was much greater than the LQG control force that was only 0.913 N. *Figure 7-12* depicts the comparison of the control forces applied on the building.

The results illustrate that the performance of the DAC control using the MCC model are good, although the control force acting on the base was huge compared with that in the Case 1 in which the LQG control was utilized.

It should be noted that an interesting phenomenon occurred in that the actuator forces acting on the elastic structure were very small when compared with the forces acting on the base.

The closed-loop eigenvalues of the MCC model with the DAC control were also calculated. The closed-loop eigenvalues are the same as the open-loop eigenvalues. This is because the DAC control only suppresses disturbance other than improves the characteristics of the system.

7.5.3 The MCC Model with the LQG/DAC Control

Table 78 shows the simulation results of the MCC model with the LQG/DAC control. *Figure 7-13* demonstrates the comparison of the displacements of the top floor relative to the base after and before the hybrid LQG/DAC control using the MCC model. It indicates that the RMS value of the relative displacement of the top floor to the base was reduced from 20.9 mm to 2.3 mm. The relative coefficient was 88.9 %, which is the best of three control algorithms in the MCC model.

Figure 7-14 compares the displacements of the base with and without the LQG/DAC control. It can be seen that the displacement of the base was reduced up to 96.7% from 26.1 mm to 0.86 mm by using the hybrid LQG/DAC control.

Table 7-8. Simulation results of the MCC model with the LQG/DAC control

	without control	with control	relative efficiency (%)
u_b , (mm)	26.1464	0.8628	96.7
u_4 , (mm)	20.9302	2.3233	88.9
u_3 , (mm)	15.3743	1.3991	90.9
u_2 , (mm)	9.5583	1.9117	80.0
u_1 , (mm)	3.5917	1.4403	59.9
\dot{u}_b , (mm/s)	0.3611	0.1080	70.1
\dot{u}_4 , (mm/s)	0.9793	0.4054	58.6
\dot{u}_3 , (mm/s)	0.7446	0.3507	52.9
\dot{u}_2 , (mm/s)	0.6154	0.3569	42.0
\dot{u}_1 , (mm/s)	0.5864	0.4052	30.9
\ddot{u}_b , (mm/s ²)	0.054	0.0540	-77.8
\ddot{u}_4 , (mm/s ²)	0.2287	0.2287	21.6
\ddot{u}_3 , (mm/s ²)	0.2549	0.2549	26.8
\ddot{u}_2 , (mm/s ²)	0.1452	0.1452	-7.7
\ddot{u}_1 , (mm/s ²)	0.2773	0.2773	26.4
F_b , (kN)	-	270.0	-
f_4 , (N)	-	5.95	-
f_3 , (N)	-	3.17	-
f_2 , (N)	-	3.34	-
f_1 , (N)	-	3.41	-

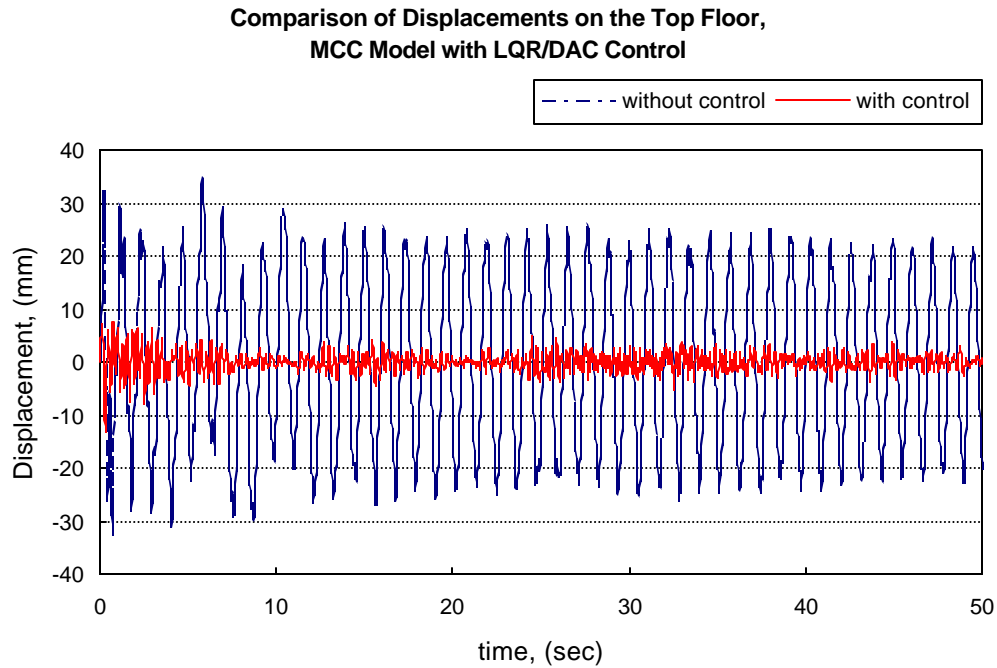


Figure 7-13. Relative displacements of the top floor, (MCC model, LQG/DAC control)

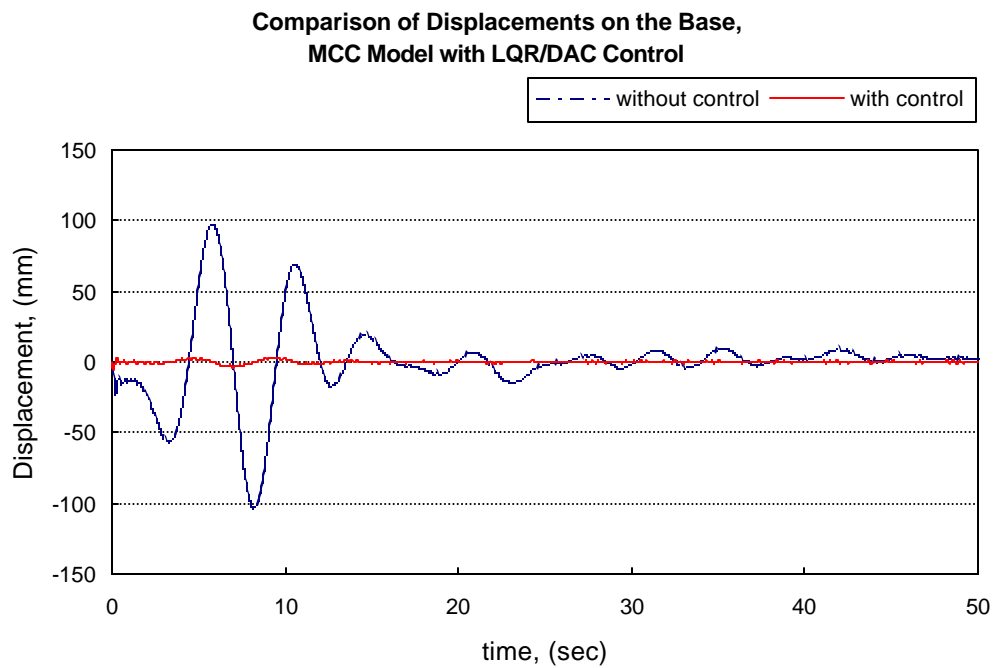


Figure 7-14. Displacements of the base, (MCC model, LQG/DAC control)

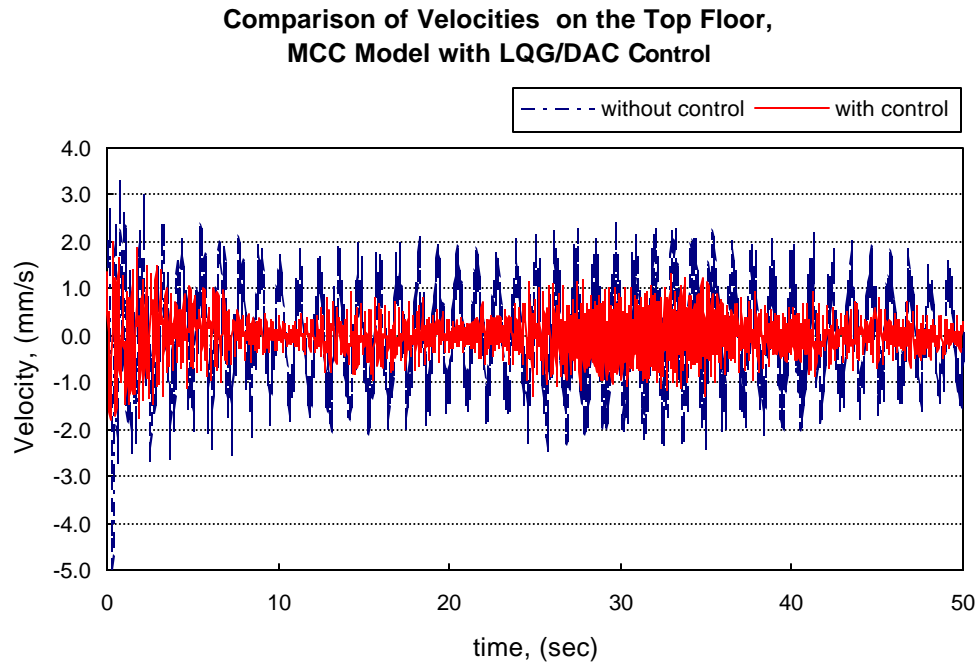


Figure 7-15. Relative velocities on the top floor, (MCC model, LQG/DAC control)

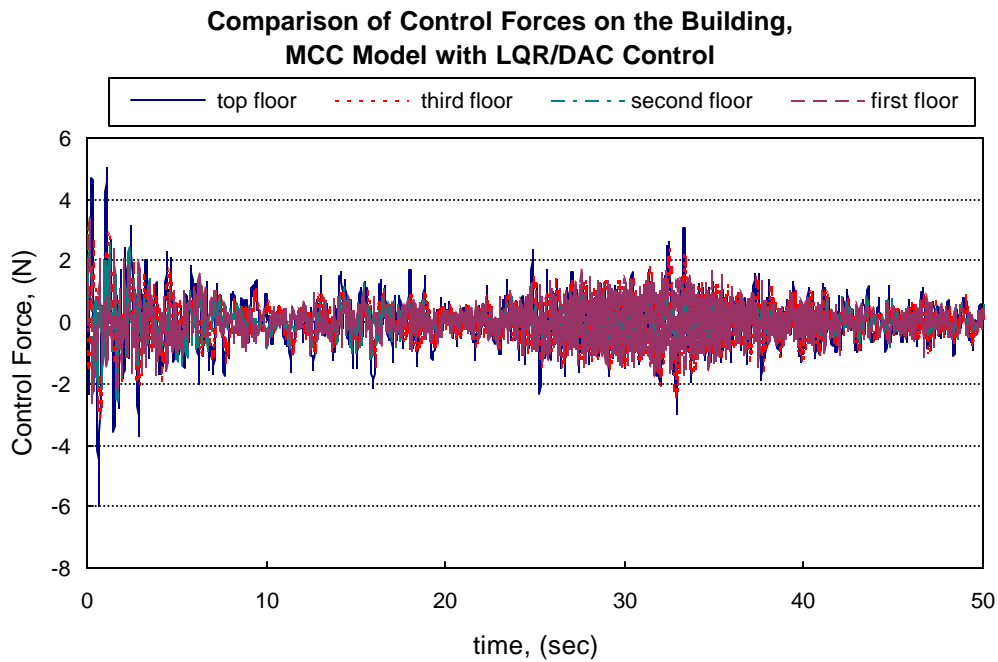


Figure 7-16. Control forces applied on the building, (MCC model, LQG/DAC control)

Figure 7-15 shows the comparison of the relative velocities of the top floor to the base with and without the hybrid LQG/DAC control. The comparison illustrates that the RMS value of the velocity of the top floor relative to the base decreased by 58.6% from 0.9793 mm/s to 0.4054 mm/s.

Figure 7-16 displays the forces acting on the building from the first floor through the top floor. The results indicated that the largest control force that was applied on the top floor was less than 6 N. It was much less than that only using the LQG control, which was 53.7 N. The results are quite encouraging. The reason of enthusiasm is that it is very difficult to apply a large control force on the building even if it is not impossible. However the maximum magnitude of the control force applied on the base still was 270 kN, which had the same order of magnitude as the DAC control. Nevertheless it should not be a tough problem because a number of larger actuators can be adopted simultaneously on the base.

The closed-loop eigenvalues of the MCC model with the hybrid LQG/DAC control were calculated. The same close-loop eigenvalues as the LQG control, shown in **Table 7-6**, were obtained. This is due to the fact that the DAC control does not affect the characteristics of the system.

Summarizing above three cases, it is apparent the most of vibration measures, displacements, velocities and accelerations, were greatly improved by using active controller in the MCC model regardless whether with the LQG, the DAC or the LQG/DAC control law. It is found that the DAC control including the LQG/DAC control mainly suppressed the dynamic response of the base to the earthquake disturbance. As a result the response of the entire building was reduced greatly. This makes sense since the motion of the building structure arose from the motion of the base, instead of the response to the direct input of the ground u_g . In contrast, the LQG control didn't take effect on the motion of base. However the LQG control was able to reduce the vibration of the building effectively. In addition, it was observed that the hybrid LQG/DAC control developed in the dissertation resulted in the most displacement and velocity reduction on

the base and all floors with much less control force applying only on the base, while the LQG control yielded the most acceleration reduction.

7.5.4 The SCC Model with the LQG Control

From the Case 4 through Case 6, simulations where the LQG, DAC and hybrid LQG/DAC controls were used individually to reduce the vibration of the building under seismic excitation were based on the SCC model. The advantage of the SCC model is that, it needs only one channel signal that five actuator forces share. This is economical in real engineering obviously.

Following the procedure developed in the section 4-2 and using the LQG control approach, we obtained the results shown in *Table 7-9*. *Figure 7-17* through *7-19* present the comparison of the displacements, velocities and acceleration of the top floor relative to the base before and after the LQG control. *Figure 7-20* shows the control forces acting on the building.

Figure 7-17 shows the comparison of the displacements of the top floor relative to the base with and without the LQG control in the SCC model. It can be seen that the relative displacement of the top floor was reduced by 88.3%. The RMS value of the relative displacement was reduced from 20.9 mm to 2.4 mm by using the LQG control in the SCC model.

Figure 7-18 displays the comparison of the velocities of the top floor relative to the base with and without the LQG control in the SCC model. It can be seen that the relative velocity of the top floor was reduced by 87.1%. The RMS value of the relative velocity was reduced from 0.98 mm/s to 0.13 mm/s by using the LQG control in the SCC model.

Table 7-9. Simulation results of the SCC model with the LQG control

	without control	with control	relative efficiency (%)
u_b , (mm)	26.1464	21.5969	17.4
u_4 , (mm)	20.9302	2.4488	88.3
u_3 , (mm)	15.3743	1.8449	88.0
u_2 , (mm)	9.5583	1.2139	87.3
u_1 , (mm)	3.5917	0.4849	86.5
\dot{u}_b , (mm/s)	0.3611	0.2882	20.2
\dot{u}_4 , (mm/s)	0.9793	0.1263	87.1
\dot{u}_3 , (mm/s)	0.7446	0.1050	85.9
\dot{u}_2 , (mm/s)	0.6154	0.0972	84.2
\dot{u}_1 , (mm/s)	0.5864	0.0897	84.7
\ddot{u}_b , (mm/s ²)	0.054	0.0497	8.04
\ddot{u}_4 , (mm/s ²)	0.2287	0.0588	74.3
\ddot{u}_3 , (mm/s ²)	0.2549	0.0568	77.7
\ddot{u}_2 , (mm/s ²)	0.1452	0.0553	61.9
\ddot{u}_1 , (mm/s ²)	0.2773	0.0607	78.1
F_b , (kN)		96.58	
f_4 , (N)		19.811	
f_3 , (N)		32.076	
f_2 , (N)		48.113	
f_1 , (N)		53.302	

Figure 7-19 illustrates the comparison of the accelerations of the top floor relative to the base with and without the LQG control in the SCC model. It can be seen that the relative acceleration of the top floor was reduced 74.3%. The RMS value of the relative acceleration was reduced from 0.23 mm/s² to 0.06 mm/s² by using the LQG control in the SCC model. From the results, we observe that the relative acceleration the building was decreased a lot after

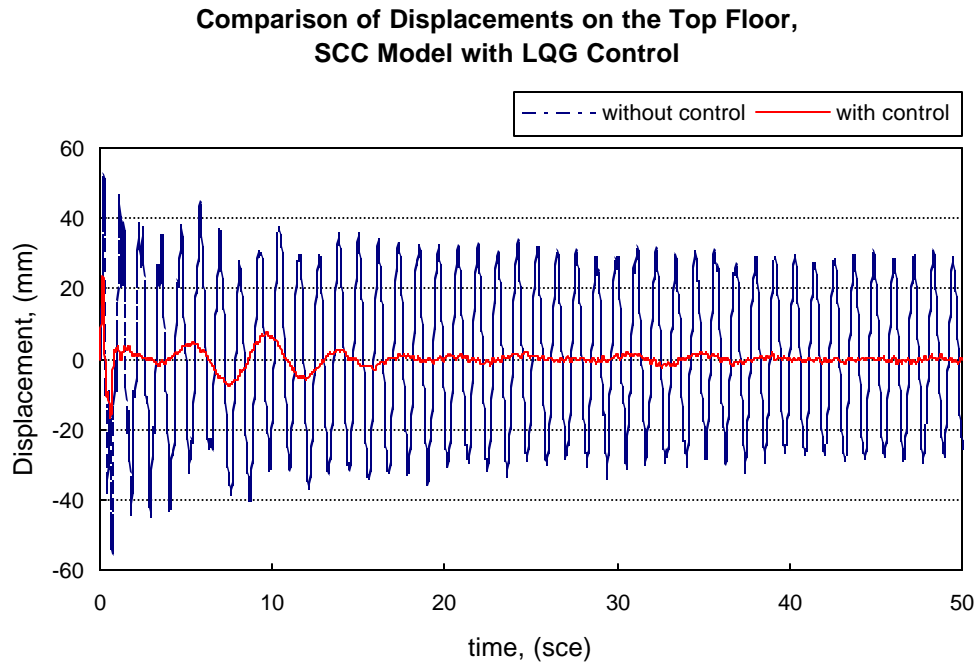


Figure 7-17. Relative displacements of the top floor, (SCC model, LQG control)

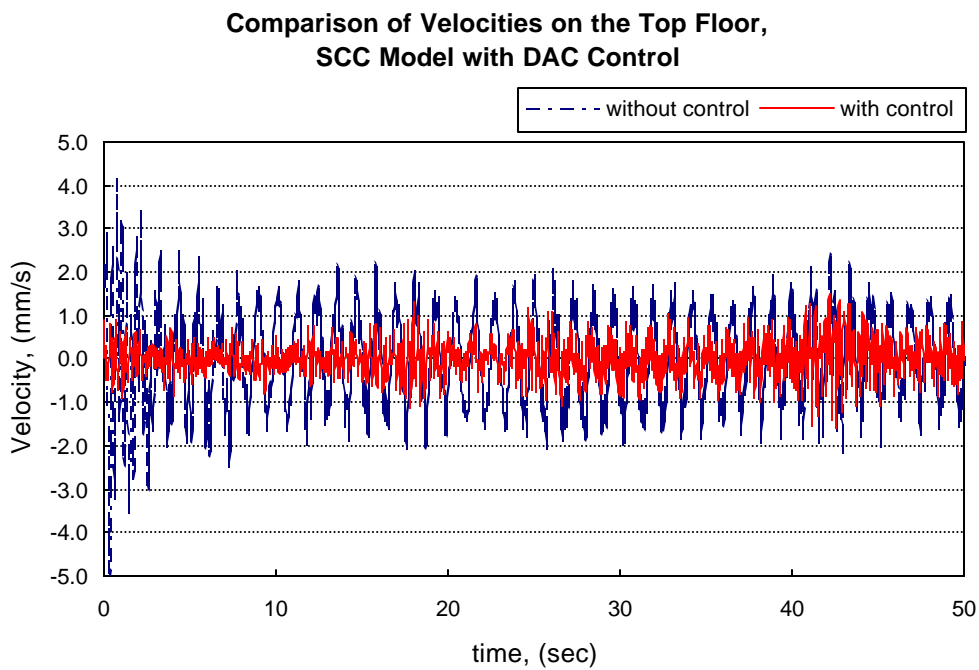


Figure 7-18. Relative velocities of the top floor, (SCC model, LQG control)

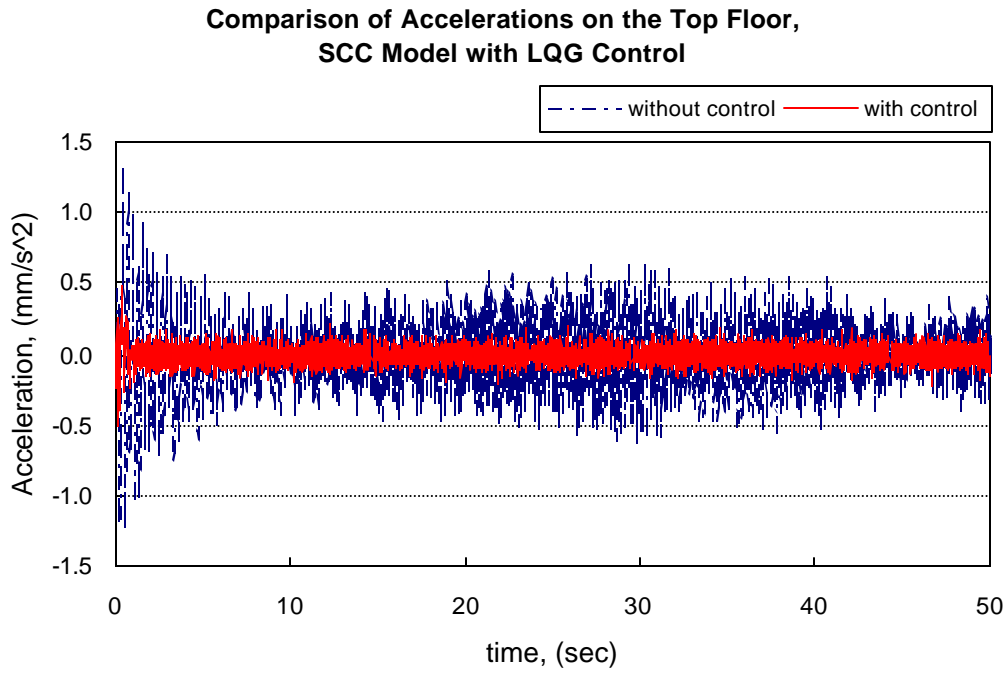


Figure 7-19. Relative accelerations of the top floor, (SCC model, LQG control)

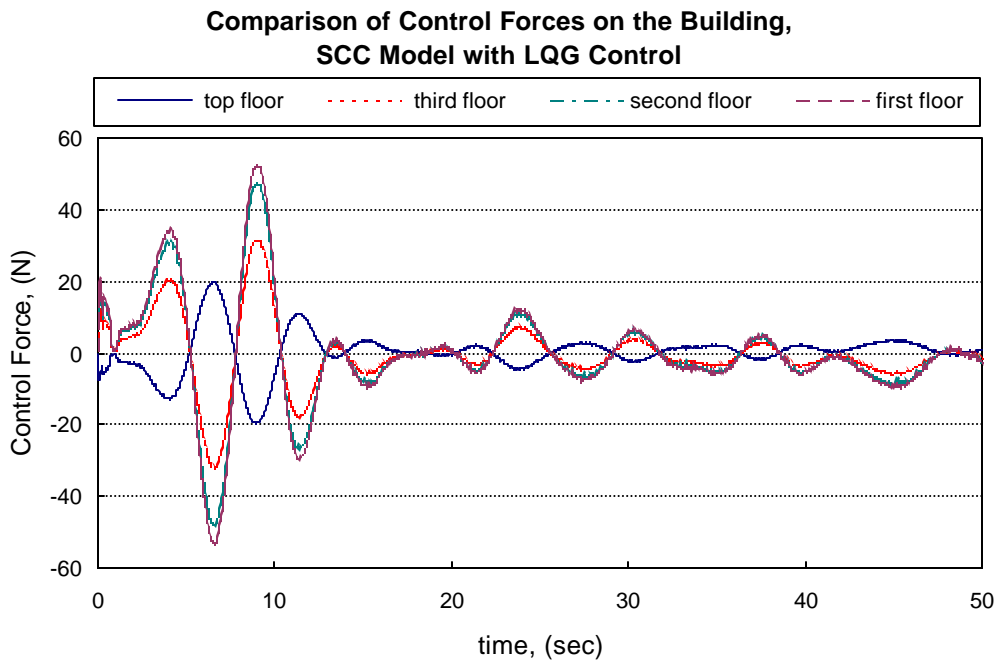


Figure 7-20. Control forces applied on the building, (SCC model, LQG control)

the LQG control in the SCC model compared with that in the MCC model (24.2%). This is one important feature of the LQG control in the SCC model.

Figure 7-20 demonstrates the transient control forces applied on the whole building. It can be seen that the biggest control force that was applied on the first floor were 53.3 N, which was similar to those with the MCC model. However, the LQG control force with the SCC model applied on the base was 96.6 kN, which was greater than that with the MCC model that was only 0.91 N. But the magnitude was acceptable because the control force was applied on the base.

Table 7-10. The closed-loop eigenvalues for the SCC model with the LQG control

number	the open-loop eigenvalues	the closed-loop eigenvalues
1	-0.0035+80.9693i	-0.0035+80.9693i
2	-0.0035-80.9693i	-0.0035-80.9693i
3	-0.0035+84.2428i	-0.0035+84.2428i
4	-0.0035-84.2428i	-0.0035-84.2428i
5	-0.0061+5.4653i	-1.9581+3.9599i
6	-0.0061-5.4653i	-1.9581-3.9599i
7	-0.0319+543117i	-2.2283+54.1581i
8	-0.0319-543117i	-2.2283-54.1581i
9	-0.2150+22.6162i	-4.1477+21.9903i
10	-0.2150-22.6162i	-4.1477-21.9903i
11	-3.8387+17.4842i	-13.6530+21.2443i
12	-3.8387-17.4842i	-13.6530-21.2443i

Table 7-10 compares the closed-loop eigenvalues with the open-loop eigenvalues of the SCC model with the LQG control. The results show most closed-loop eigenvalues have greater

negative real parts than the open-loop eigenvalues except that first four are the same. This indicates the LQG control increased the damping of the controlled system in essential.

7.5.5 The SCC Model with the DAC control

In this case the gain matrix was determined using the DAC control approach based on the SCC model and no estimator was used. The simulation results are shown in *Table 7-11*. *Figures 7-21* and *7-22* present the comparison of the displacements of the top floor and the base before and after the DAC control with the SCC model. *Figure 7-23* shows the comparison of the velocities of the top floor relative to the base with and without the DAC control. *Figure 7-24* shows the control forces acting on the building.

The relative displacement response of the top floor to the base with the DAC control in the SCC model is compared with that without control in *Figure 7-21*. The comparison shows good control performance of the control system with the fact that the relative displacement of the top floor was reduced by 76.3%. The RMS value of the relative displacement was reduced from 20.9 mm to 4.9 mm by using the DAC control in the SCC model.

Figure 7-22 displays the comparison of the displacements of the base with and without the DAC control in the SCC model. It can be seen that the displacement was reduced 58.6 %. The RMS value of the displacement was reduced from 26.1 mm to 10.8 mm by using the DAC control in the SCC model.

Figure 7-23 illustrates the comparison of the velocities of the top floor relative to the base with and without the DAC control in the SCC model. It can be seen that the relative velocity of the top floor was reduced by 63.3 %. The RMS value of the relative velocity was reduced from 0.98 mm/s to 0.36 mm/s by using the DAC control in the SCC model.

Table 7-11. Simulation results of the SCC model with the DAC control

	without control	with control	relative efficiency (%)
u_b , (mm)	26.1464	10.8246	58.6
u_4 , (mm)	20.9302	4.9605	76.3
u_3 , (mm)	15.3743	3.8589	74.9
u_2 , (mm)	9.5583	2.9344	69.3
u_1 , (mm)	3.5917	1.5085	58.0
\dot{u}_b , (mm/s)	0.3611	0.1546	57.2
\dot{u}_4 , (mm/s)	0.9793	0.3594	63.3
\dot{u}_3 , (mm/s)	0.7446	0.3291	55.8
\dot{u}_2 , (mm/s)	0.6154	0.2739	55.5
\dot{u}_1 , (mm/s)	0.5864	0.4662	20.5
\ddot{u}_b , (mm/s ²)	0.054	0.0518	4.07
\ddot{u}_4 , (mm/s ²)	0.2287	0.1834	19.8
\ddot{u}_3 , (mm/s ²)	0.2549	0.2461	3.47
\ddot{u}_2 , (mm/s ²)	0.1452	0.0999	31.2
\ddot{u}_1 , (mm/s ²)	0.2773	0.2702	2.57
F_b , (kN)		271.59	
f_4 , (N)		55.712	
f_3 , (N)		90.2	
f_2 , (N)		135.3	
f_1 , (N)		149.89	

Figure 7-24 demonstrates the time history of the control forces applied on the building. It shows that the biggest control force were 149.9 N, which was exerted on the first floor. From **Table 7-11**, it can be seen that other control forces applying the building, from 55.7 to 149.9 N, were also quite large compared with those in the preceding cases. This implies that it will probably be difficult to implement the control in the real world since these control forces should be exerted on the floor. It is also noted that the DAC control force with the SCC model applied on the base was up to 271.6 kN. It was greater than that with the LQG control, which

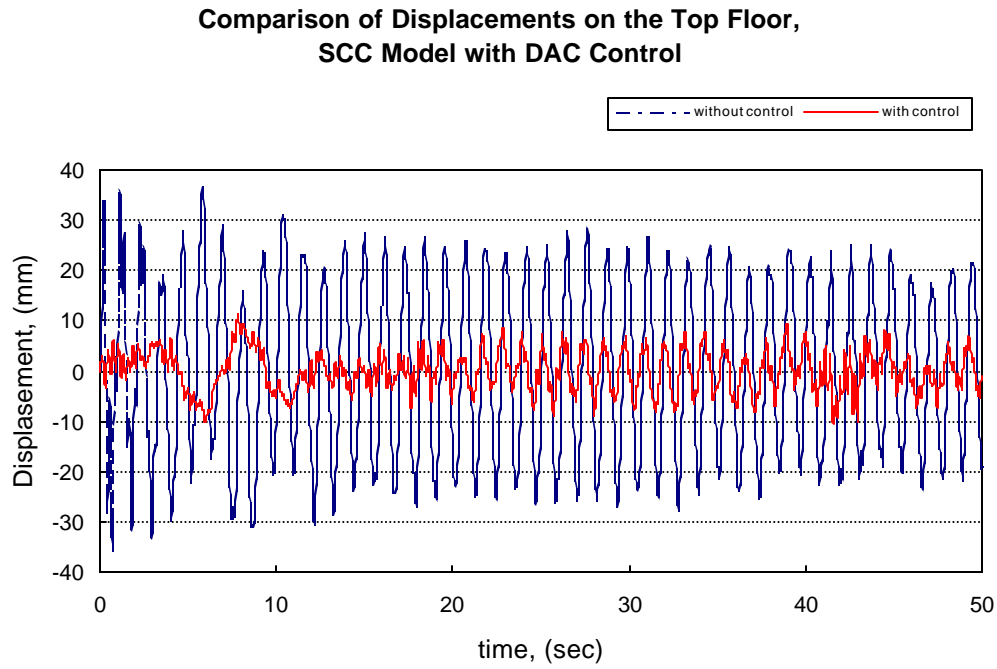


Figure 7-21. Relative displacements of the top floor, (SCC model, DAC control)

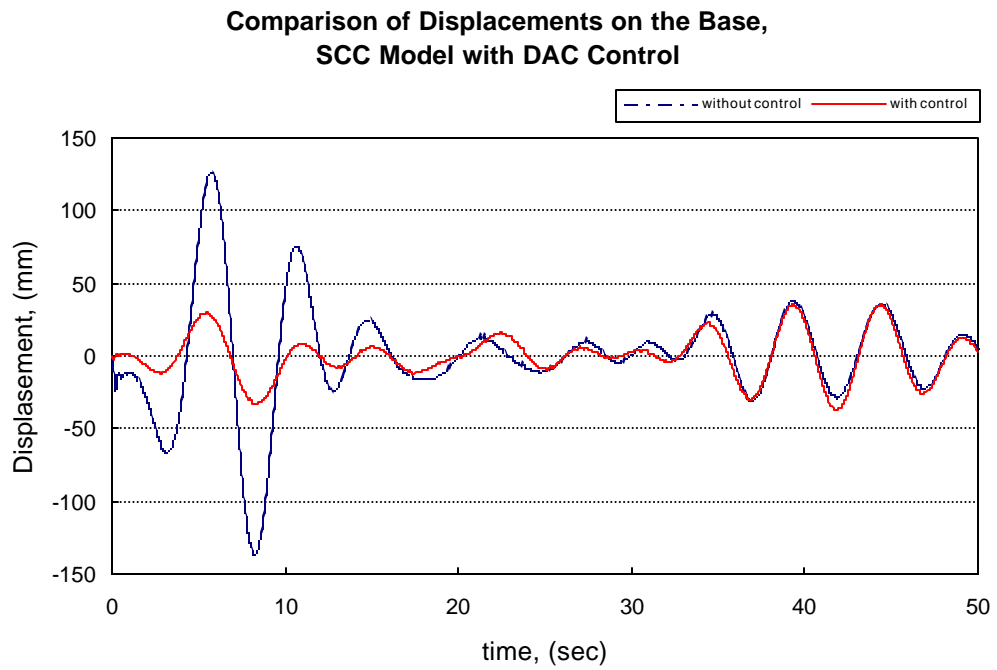


Figure 7-22. Displacements of the base, (SCC model, DAC control)

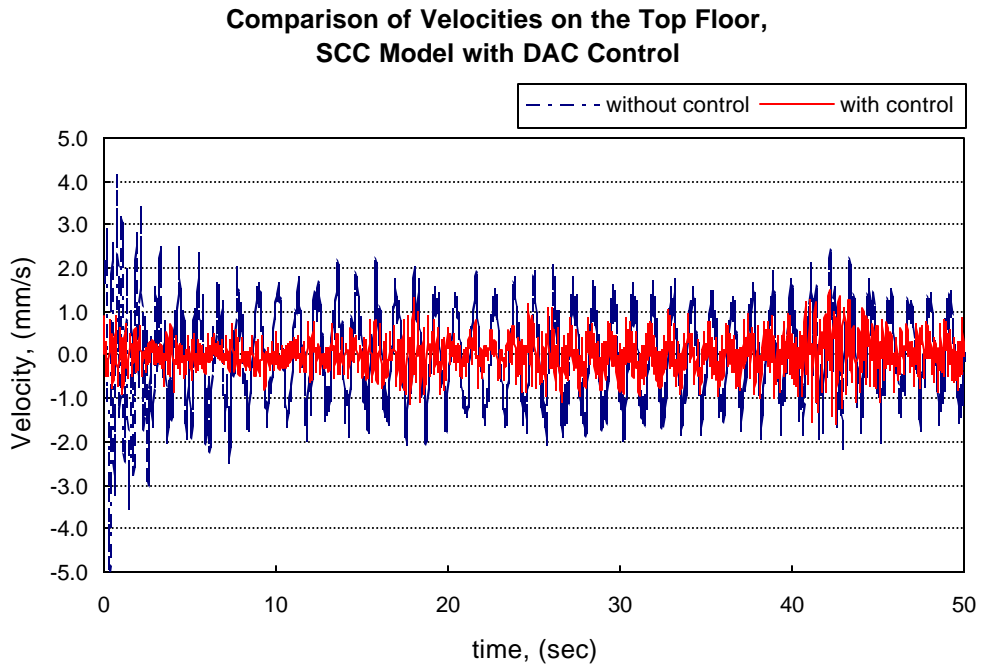


Figure 7-23. Relative velocities on the top floor, (SCC model, DAC control)

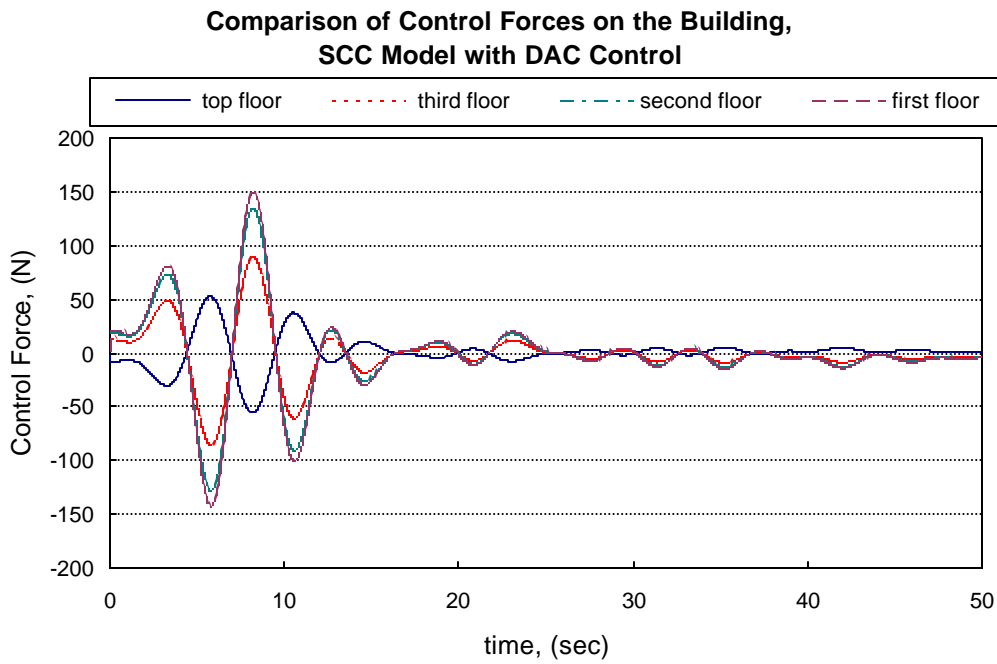


Figure 7-24. Control forces applied on the building, (SCC model, DAC control)

was only 96.6 kN. Luckily, this force is practicable because the control force was applied on the base.

The closed-loop eigenvalues for this case were calculated and are the same as the open-loop eigenvalues. As mentioned in section 7.5.2, the DAC control only suppresses disturbance other than improves the characteristics of the system.

7.5.6 The SCC Model with the hybrid LQG/DAC Control

In this case, we used the hybrid LQG/DAC control approach to optimize the state feedback gain matrix in the SCC model. Then, a computer simulation in which active controllers using the gain was adopted to reduce dynamic response of the building to seismic excitation. *Table 7-12* lists the computer simulation results. *Figures 7-25* to *Figures 7-27* illustrate the corresponding curves of the comparison of the displacements, velocities and acceleration of the top floor relative to the base before and after the hybrid LQG/DAC control. *Figure 7-28* shows the control forces acting on the building.

Figure 7-25 shows the comparison of the displacements of the top floor relative to the base with and without the hybrid LQG/DAC control in the SCC model. It can be seen that the relative displacement of the top floor was reduced 85%. The RMS value of the relative displacement was reduced from 20.9 mm to 3.1 mm by using the hybrid LQG/DAC control in the SCC model.

Figure 7-26 displays the comparison of the velocities of the top floor relative to the base with and without the LQG control in the SCC model. It can be seen that the relative velocity of the top floor was reduced 92.5%. The RMS value of the relative velocity was reduced from 0.98 mm/s to 0.07 mm/s by using the hybrid LQG/DAC control in the SCC model. Comparing the

velocity with those in previous control, we find that the performance of the hybrid LQG/DAC control in the SCC model was the best in reducing vibration velocity of the building.

Table 7-12. Simulation results of the SCC model with the LQG/DAC control

	without control	with control	relative efficiency (%)
u_b , (mm)	26.1464	11.7659	55.0
u_4 , (mm)	20.9302	3.1395	85.0
u_3 , (mm)	15.3743	2.7520	82.1
u_2 , (mm)	9.5583	2.0168	78.9
u_1 , (mm)	3.5917	0.8297	76.9
\dot{u}_b , (mm/s)	0.3611	0.1527	57.7
\dot{u}_4 , (mm/s)	0.9793	0.0734	92.5
\dot{u}_3 , (mm/s)	0.7446	0.0700	90.6
\dot{u}_2 , (mm/s)	0.6154	0.0708	88.5
\dot{u}_1 , (mm/s)	0.5864	0.0780	86.7
\ddot{u}_b , (mm/s ²)	0.054	0.0495	8.34
\ddot{u}_4 , (mm/s ²)	0.2287	0.0583	74.5
\ddot{u}_3 , (mm/s ²)	0.2549	0.0553	78.3
\ddot{u}_2 , (mm/s ²)	0.1452	0.0558	61.6
\ddot{u}_1 , (mm/s ²)	0.2773	0.0627	77.4
F_b , (kN)		309.36	
f_4 , (N)		63.46	
f_3 , (N)		102.74	
f_2 , (N)		154.12	
f_1 , (N)		170.74	

Figure 7-27 illustrates the comparison of the accelerations of the top floor relative to the base with and without the LQG/DAC control in the SCC model. It can be seen that the relative acceleration of the top floor was reduced 74.5%. The RMS value of the relative acceleration

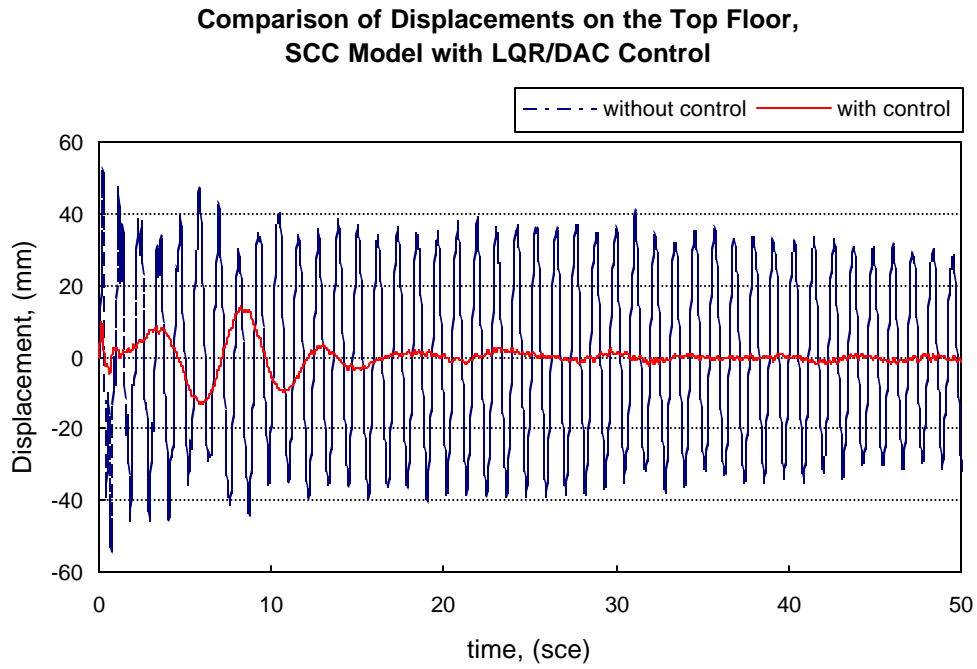


Figure 7-25. Relative displacements of the top floor, (SCC model, LQG/DAC control)

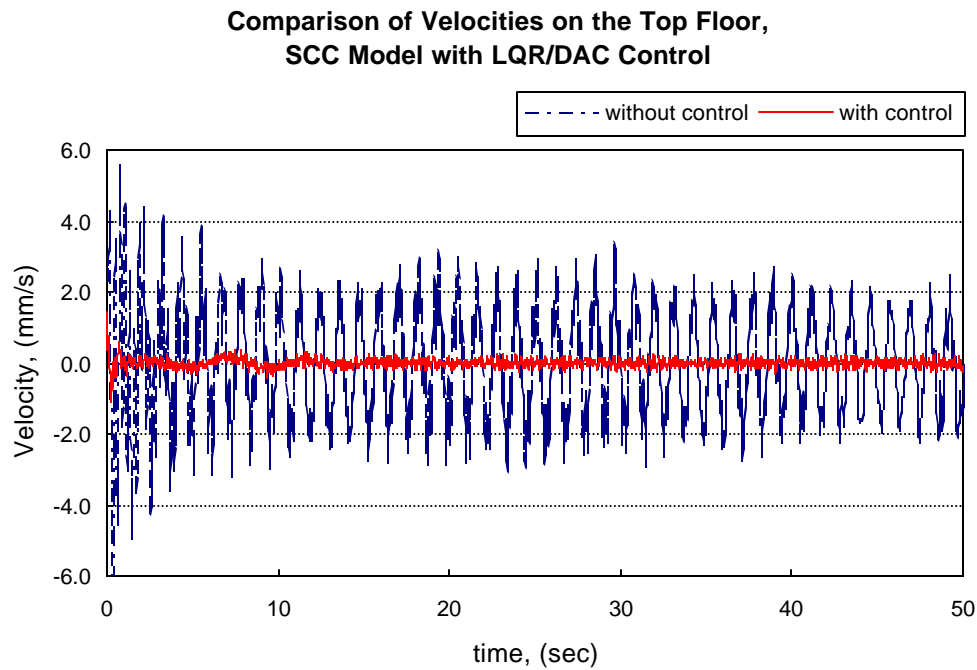


Figure 7-26. Relative velocities of the top floor, (SCC model, LQG/DAC control)

was reduced from 0.23 mm/s^2 to 0.06 mm/s^2 by using the LQG/DAC control in the SCC model. The effect was the same as that with the LQG control.

Figure 7-28 demonstrates the transient control forces applied on the whole building. It can be seen that these control forces were quite large, even larger than those in the LQG control. Similarly, it is not very convenient to realize the control in the physical world. Meanwhile the control force applied on the base was increased to 309.4 kN, which was the biggest value of all nine cases.

The closed-loop eigenvalues of the SCC model with the hybrid LQG/DAC control were calculated. The same close-loop eigenvalues as the LQG control, shown in **Table 7-10**, were obtained. This is due to the fact that the DAC control does not affect the characteristics of the system.

7.5.7 The SSCC Model with the LQG control

From the Case 7 through Case 9, simulations were based on the SSCC model, in which the LQG, DAC and hybrid LQG/DAC controls were used, respectively to reduce the vibration of the building under seismic excitation. As mentioned in Chapter 4, the most remarkable feature of the SSCC model was only one actuator needed to act on the base. In the Case 7, we performed the simulation where the LQG control in the SSCC model was used. **Table 7-13** gives all the simulation results, while **Figure 7-29** through **Figure 7-31** present the comparison of the displacements, velocities and acceleration of the top floor relative to the base before and after the LQG control. In **Figure 7-32** the time history of the LQG control force acting on the base is shown.

Figure 7-29 shows the comparison of the displacements of the top floor relative to the base with and without the LQG control in the SSCC model. It can be seen that the relative

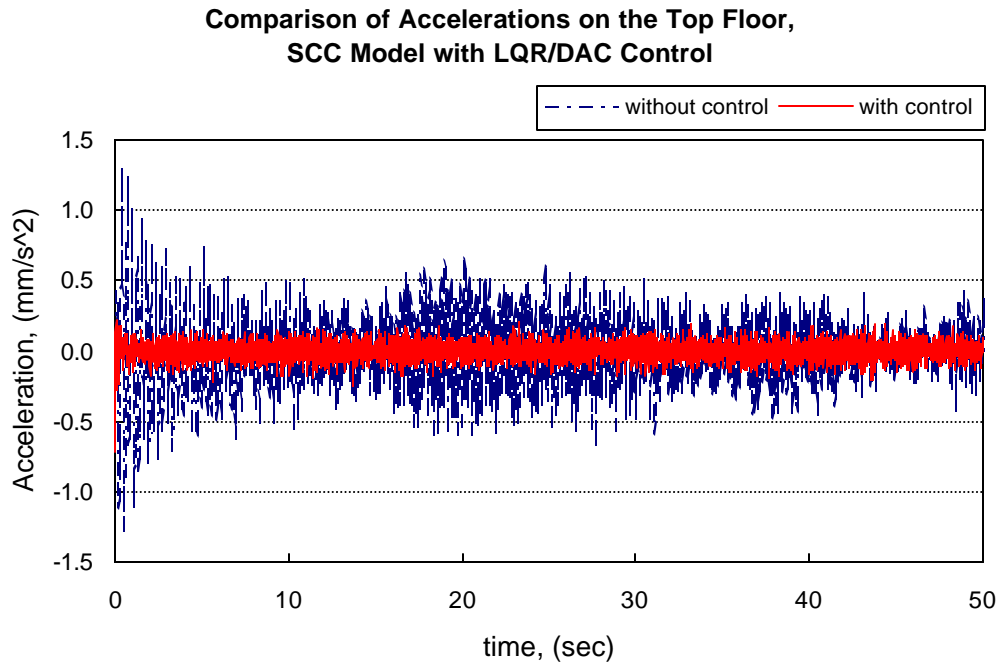


Figure 7-27. Relative accelerations of the top floor, (SCC model, LQG/DAC control)

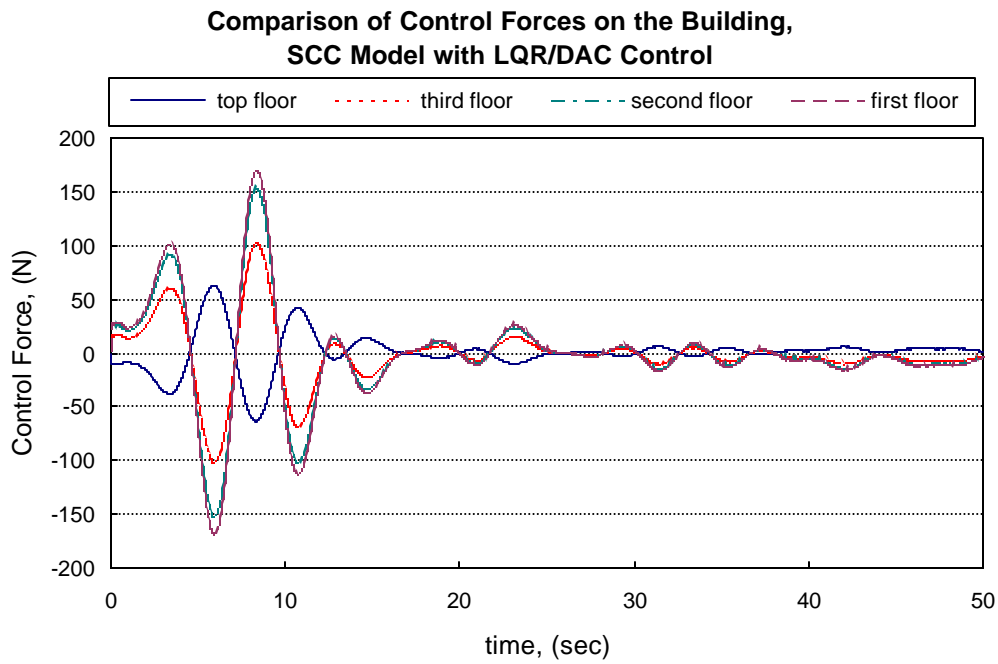


Figure 7-28. Control forces applied on the building, (SCC model, LQG/DAC control)

displacement of the top floor was decreased by 92.7% when using LQG control, while the RMS value of the relative displacement was reduced from 20.9 mm to 1.5 mm.

Table 7-13. Simulation results of the SSCC model with the LQG control

	without control	with control	relative efficiency (%)
u_b , (mm)	26.1464	16.1585	38.2
u_4 , (mm)	20.9302	1.5279	92.7
u_3 , (mm)	15.3743	1.1069	92.8
u_2 , (mm)	9.5583	0.7264	92.4
u_1 , (mm)	3.5917	0.3053	91.5
\dot{u}_b , (mm/s)	0.3611	0.2149	40.5
\dot{u}_4 , (mm/s)	0.9793	0.0911	90.7
\dot{u}_3 , (mm/s)	0.7446	0.0759	89.8
\dot{u}_2 , (mm/s)	0.6154	0.0763	87.6
\dot{u}_1 , (mm/s)	0.5864	0.0774	86.8
\ddot{u}_b , (mm/s ²)	0.054	0.0494	8.59
\ddot{u}_4 , (mm/s ²)	0.2287	0.0567	75.2
\ddot{u}_3 , (mm/s ²)	0.2549	0.0530	79.2
\ddot{u}_2 , (mm/s ²)	0.1452	0.0536	63.1
\ddot{u}_1 , (mm/s ²)	0.2773	0.0588	78.8
F_b , (kN)		134.619	
f_4 , (N)		-	
f_3 , (N)		-	
f_2 , (N)		-	
f_1 , (N)		-	

Figure 7-30 compares the velocities of the top floor relative to the base with and without the LQG control in the SSCC model. By using the LQG control, the relative efficiency corresponding to the velocity was reduced by 90.7% according to **Table 7-13**, and the RMS value of the relative velocity was reduced from 0.98 mm/s to 0.09 mm/s.

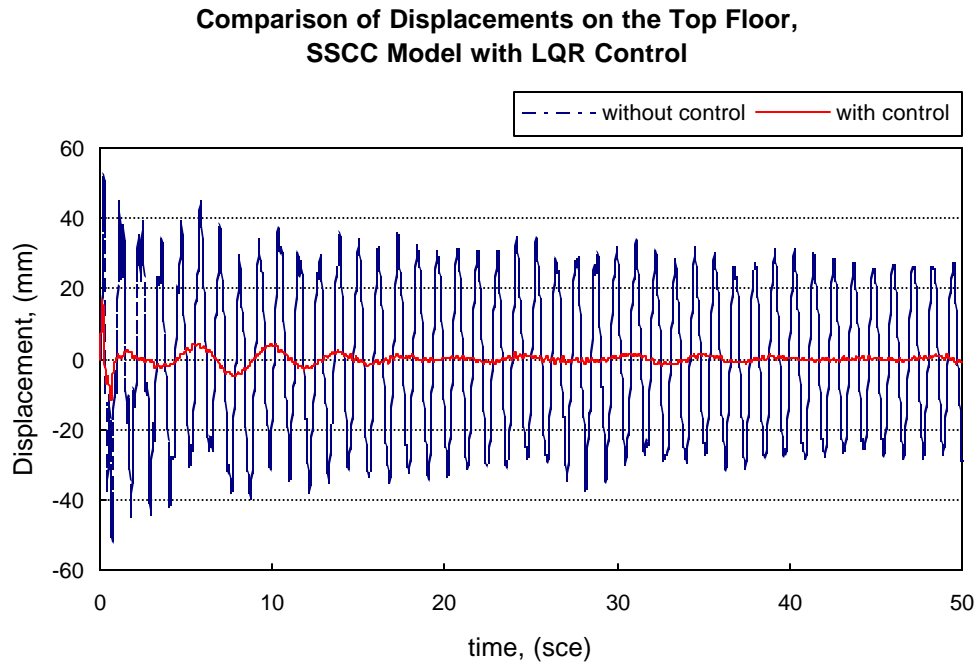


Figure 7-29. Relative displacements of the top floor, (SSCC model, LQG control)

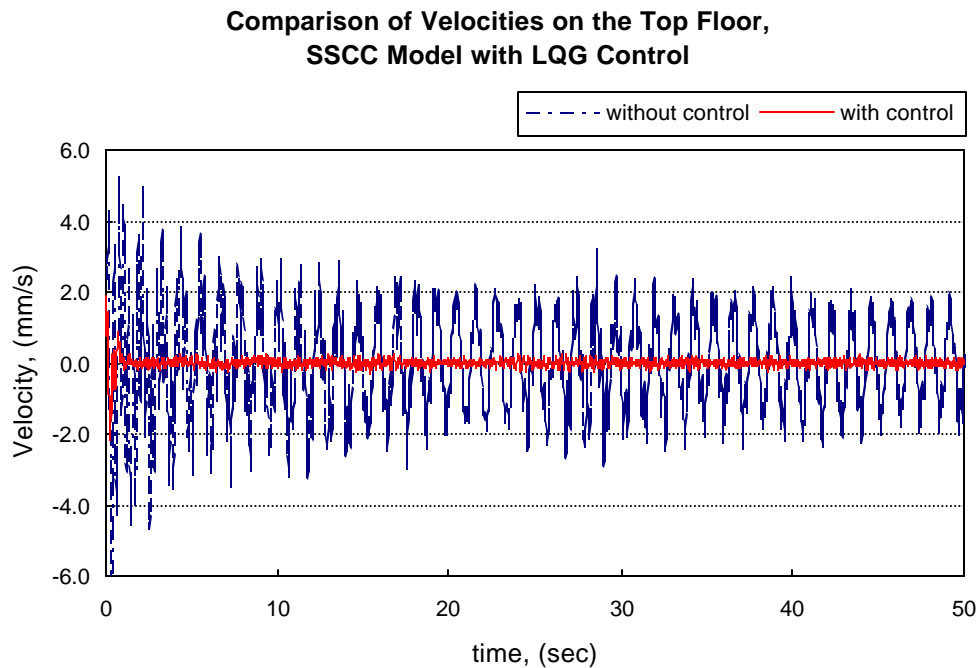


Figure 7-30. Relative velocities of the top floor, (SSCC model, LQG control)

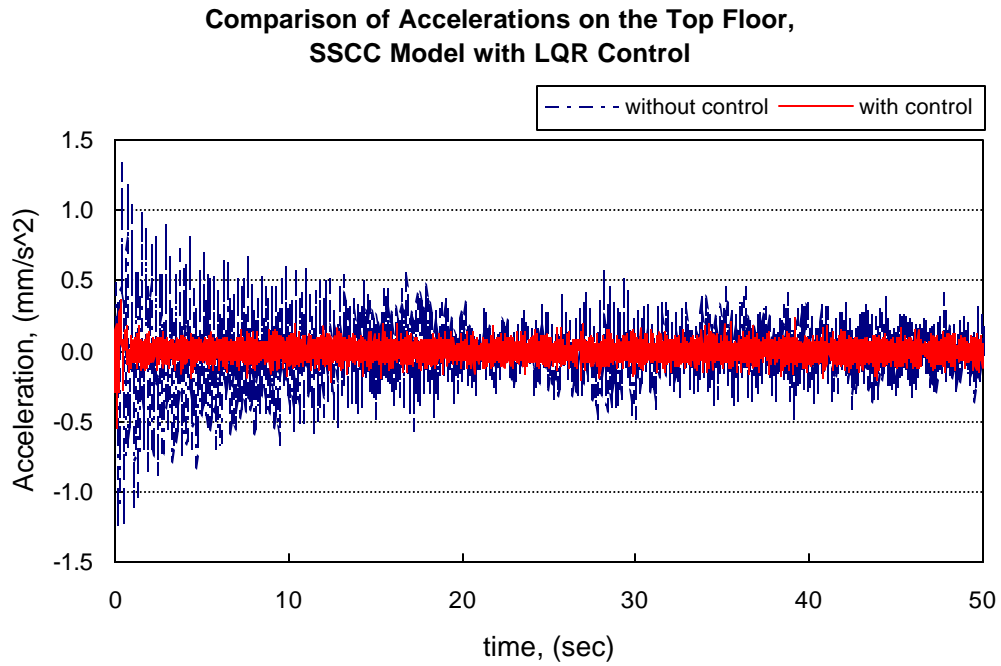


Figure 7-31. Relative accelerations of the top floor, (SSCC model, LQG control)

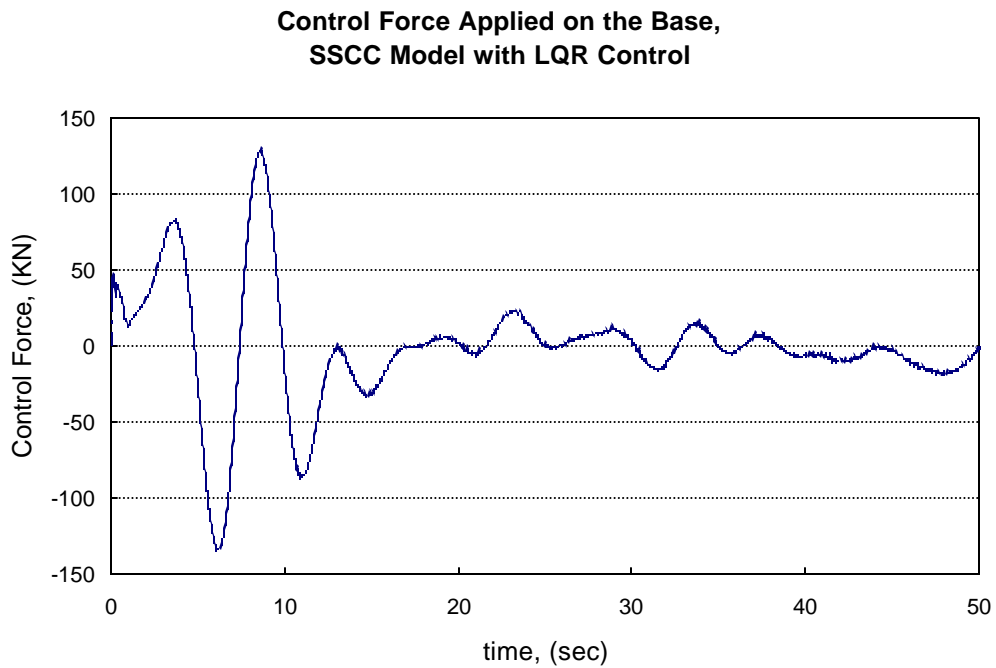


Figure 7-32. Control forces applied on the base, (SSCC model, LQG control)

Figure 7-31 illustrates the accelerations of the top floor relative to the base before and after the LQG control in the SSCC model. By using the LQG control, the RMS value of the relative acceleration was reduced from 0.23 mm/s^2 to 0.05 mm/s^2 , where the relative efficiency of the acceleration was reduced by 75.2%.

Figure 7-32 demonstrates the transient control forces applied on the base. It can be observed that the maximum peak value of the control force was only 134.6 kN, which was quite larger compared with those LQG control forces acting on the base in the previous cases. But the cost was still the most economy because this control force was only one used to reduce vibration of the building.

Table 7-14. The closed-loop eigenvalues for the SCC model with the LQG control

number	the open-loop eigenvalues	the closed-loop eigenvalues
1	-0.0035+80.9693i	-0.0035+80.9693i
2	-0.0035-80.9693i	-0.0035-80.9693i
3	-0.0035+84.2428i	-0.0035+84.2428i
4	-0.0035-84.2428i	-0.0035-84.2428i
5	-0.0061+5.4653i	-1.8525+3.8168i
6	-0.0061-5.4653i	-1.8525-3.8168
7	-0.0319+543117i	-2.7876+54.2144i
8	-0.0319-543117i	-2.7876-54.2144i
9	-0.2150+22.6162i	-4.1959+21.7732i
10	-0.2150-22.6162i	-4.1959-21.7732i
11	-3.8387+17.4842i	-16.8531+22.3393i
12	-3.8387-17.4842i	-16.8531-22.3393i

Table 7-14 compares the closed-loop eigenvalues with the open-loop eigenvalues of the SCC model with the LQG control. The results show most closed-loop eigenvalues have greater

negative real parts than the open-loop eigenvalues except that first four are the same. This indicates the LQG control increased the damping of the controlled system in essential.

Comparing the results with those from the previous simulations, it is observed that the performance of the LQG control in the SSCC model was the best one. Not only was the reduction of the vibration including all the measurements of displacement, velocity and acceleration at the top of the building largest, but that at other floors were largest. Moreover, the control force only exerted on the base was still relatively small among all the previous control cases except the LQG control cases.

7.5.8 The SSCC Model with the DAC control

In this case, the DAC technique was used to seek the optimal state feedback gain in the SSCC model. Similar to the Case 7 only one actuator force was also needed since the SSCC model was used. *Table 7-15* lists the numerical results, while *Figures 7-33 to 7-36* demonstrate the performance curves.

Figure 7-33 presents the comparison of the displacements of the top floor relative to the base with and without the DAC control. It can be found that the relative displacement of the top floor was reduced by 82.5% and the RMS value of the displacement was reduced from 20.9 mm to 3.7 mm by using the DAC control based on the SSCC model.

Figure 7-34 compares the absolute displacements of the base with and without the DAC control in the SSCC model. After using the DAC control based on the SSCC model, the displacement was decreased by 98.4%, and the RMS value was reduced from 26.1 mm to 0.42 mm.

Table 7-15. Simulation results of the SSCC model with the DAC control

	without control	with control	relative efficiency (%)
u_b , (mm)	26.1464	0.4189	98.4
u_4 , (mm)	20.9302	3.6628	82.5
u_3 , (mm)	15.3743	2.1832	85.8
u_2 , (mm)	9.5583	2.9440	69.2
u_1 , (mm)	3.5917	1.8030	49.8
\dot{u}_b , (mm/s)	0.3611	0.0979	72.9
\dot{u}_4 , (mm/s)	0.9793	0.4916	49.8
\dot{u}_3 , (mm/s)	0.7446	0.4155	44.2
\dot{u}_2 , (mm/s)	0.6154	0.3840	37.6
\dot{u}_1 , (mm/s)	0.5864	0.4586	21.8
\ddot{u}_b , (mm/s ²)	0.054	0.0957	-77.3
\ddot{u}_4 , (mm/s ²)	0.2287	0.1965	14.1
\ddot{u}_3 , (mm/s ²)	0.2549	0.2243	12.0
\ddot{u}_2 , (mm/s ²)	0.1452	0.1353	6.8
\ddot{u}_1 , (mm/s ²)	0.2773	0.2429	12.4
F_b , (kN)	-	270.161	-
f_4 , (N)	-	-	-
f_3 , (N)	-	-	-
f_2 , (N)	-	-	-
f_1 , (N)	-	-	-

Figure 7-35 displays the comparison of the velocities of the top floor relative to the base before and after the DAC control in the SSCC model. It can be observed that by using the DAC control the relative velocity of the top floor was decreased by 49.8% and the RMS value of the relative velocity was reduced from 0.98 mm/s to 0.49 mm/s.

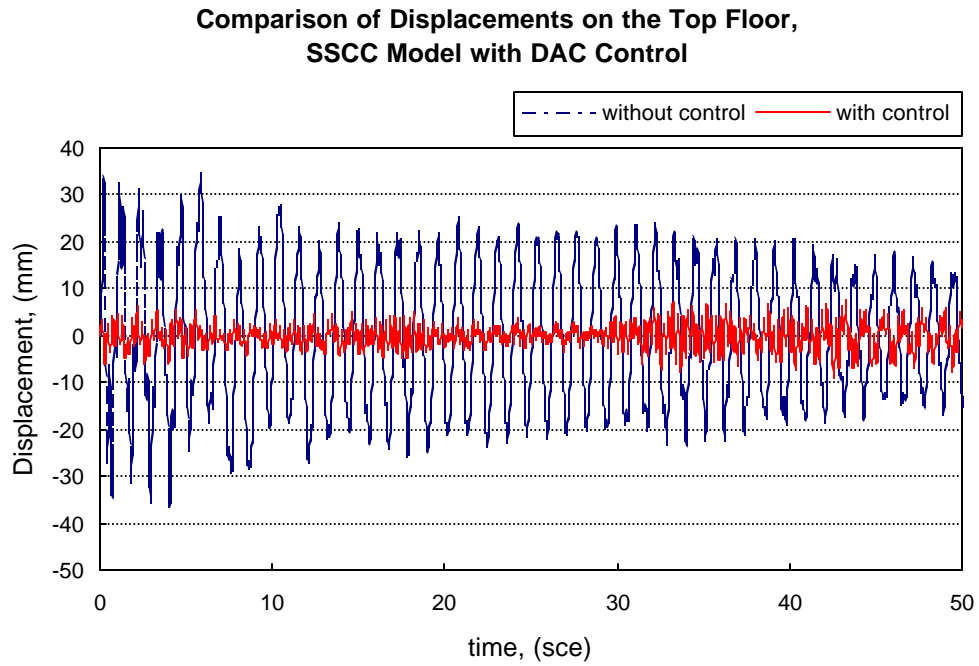


Figure 7-33. Relative displacements of the top floor, (SSCC model, DAC control)

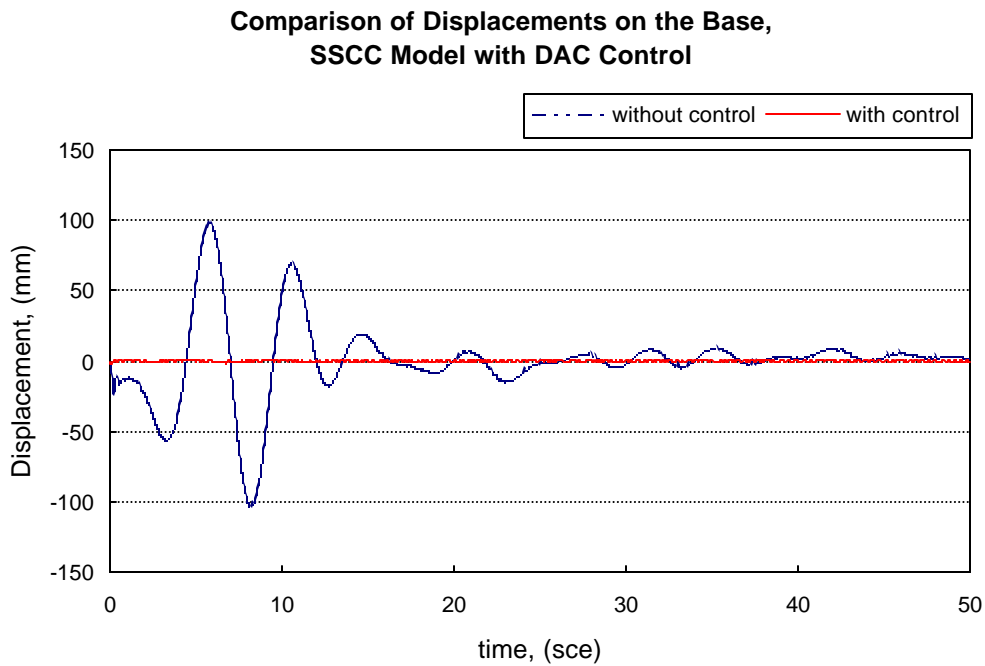


Figure 7-34. Displacements of the base, (SSCC model, DAC control)

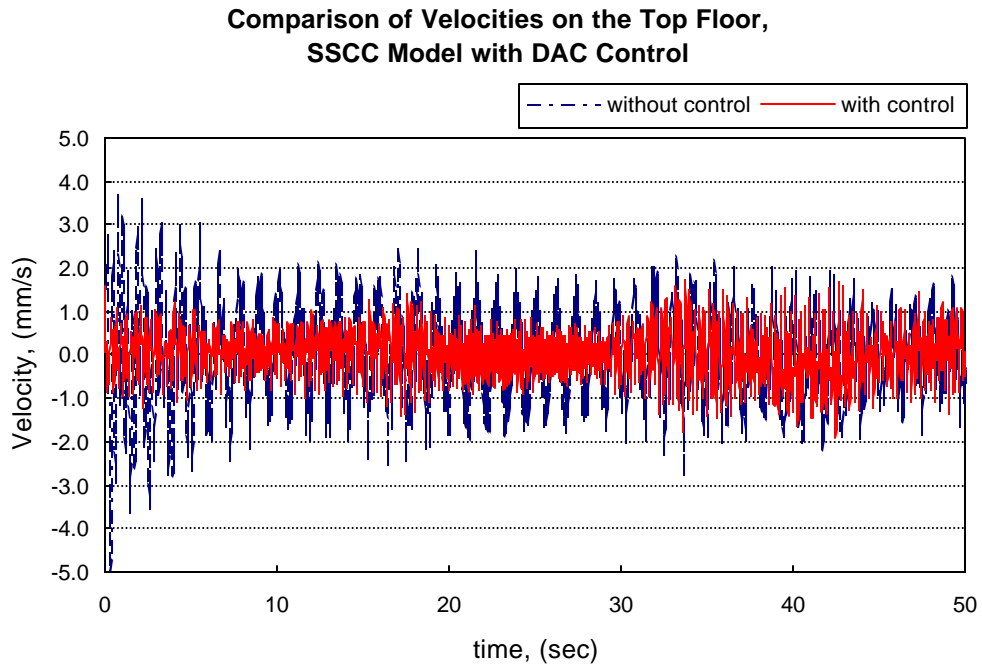


Figure 7-35. Relative velocities of the top floor, (SSCC model, DAC control)

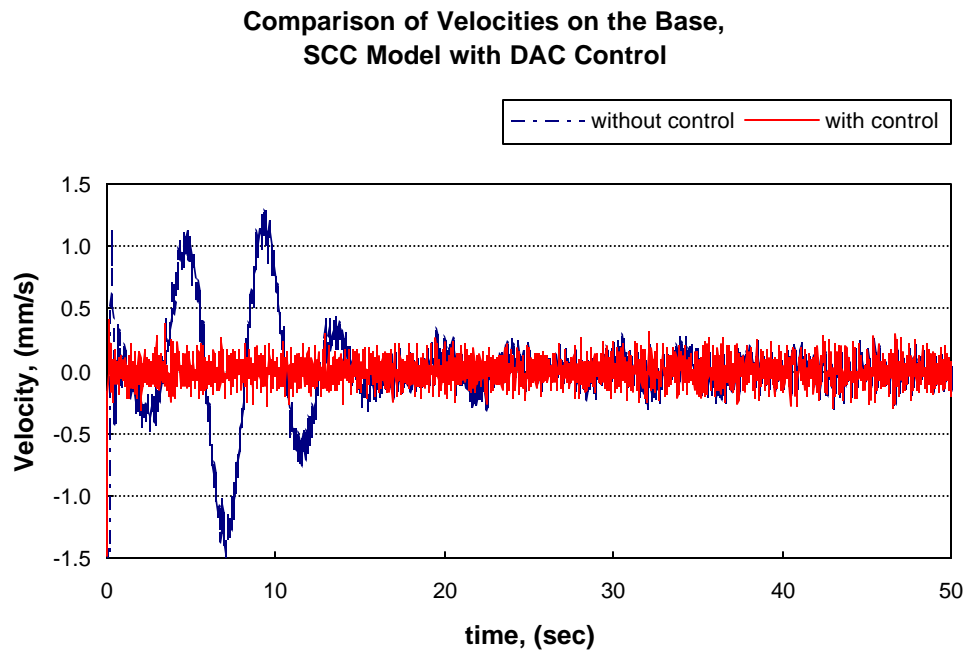


Figure 7-36. Velocities of the base, (SSCC model, DAC control)

Figure 7-36 demonstrates the comparison of the absolute velocities of the base with and without the DAC control in the SSCC model. The relative efficiency of the velocity was reduced 72.9% and the RMS value of the velocity was reduced from 0.36 mm/s to about 0.1 mm/s by using the DAC control in the SSCC model.

In **Table 7-15**, note that the control force applied on the base was 270.16 kN, which had the same order of magnitude as most of control forces applied on the base. Comparing the results with those from the previous simulations observes that the DAC control in the SSCC model had the best effect on reducing vibrations of the base.

Similar to previous cases using the DAC control, the closed-loop eigenvalues calculated are the same the open-loop eigenvalues since the DAC control does not affect the characteristics of the controlled system.

7.5.9 The SSCC Model with the LQG/DAC control

Finally we conducted the computer simulation of the dynamic response of the building under seismic excitation with and without the LQG/DAC control in the SSCC model. The results obtained are shown in **Table 7-16**. **Figure 7-37** through **7-40** present the comparison of the displacements and the velocities of the top floor and the base.

Figure 7-37 shows the comparison of the displacements of the top floor relative to the base with and without the LQG/DAC control in the SSCC model. It can be seen that the relative efficiency of the displacement of the top floor was reduced 97.5% and the RMS value of the relative displacement was reduced from 20.9 mm to 0.52 mm by using the LQG/DAC control in the SSCC model.

In **Figure 7-38**, the absolute displacements of the base with and without the LQG/DAC control in the SSCC model are compared. There, the relative efficiency of the displacement was reduced by 99.1% and the RMS value of the displacement was reduced from 26.1 mm to 0.24 mm by using the LQG/DAC control based on the SSCC model.

Table 7-16. Simulation results of the SSCC model with the LQG/DAC control

	without control	with control	relative efficiency (%)
u_b , (mm)	26.1464	0.2353	99.1
u_4 , (mm)	20.9302	0.5233	97.5
u_3 , (mm)	15.3743	0.3690	97.6
u_2 , (mm)	9.5583	0.3537	96.3
u_1 , (mm)	3.5917	0.2155	94.0
\dot{u}_b , (mm/s)	0.3611	0.0766	78.8
\dot{u}_4 , (mm/s)	0.9793	0.0921	90.6
\dot{u}_3 , (mm/s)	0.7446	0.0879	88.2
\dot{u}_2 , (mm/s)	0.6154	0.0911	85.2
\dot{u}_1 , (mm/s)	0.5864	0.0897	84.7
\ddot{u}_b , (mm/s ²)	0.054	0.0992	-83.7
\ddot{u}_4 , (mm/s ²)	0.2287	0.1141	50.1
\ddot{u}_3 , (mm/s ²)	0.2549	0.0981	61.5
\ddot{u}_2 , (mm/s ²)	0.1452	0.1127	22.4
\ddot{u}_1 , (mm/s ²)	0.2773	0.1048	62.2
F_b , (kN)		270.562	
f_4 , (N)		-	
f_3 , (N)		-	
f_2 , (N)		-	
f_1 , (N)		-	

Figure 7-39 displays the comparison of the velocities of the top floor relative to the base with and without the LQG/DAC control in the SSCC model. It can be seen that the

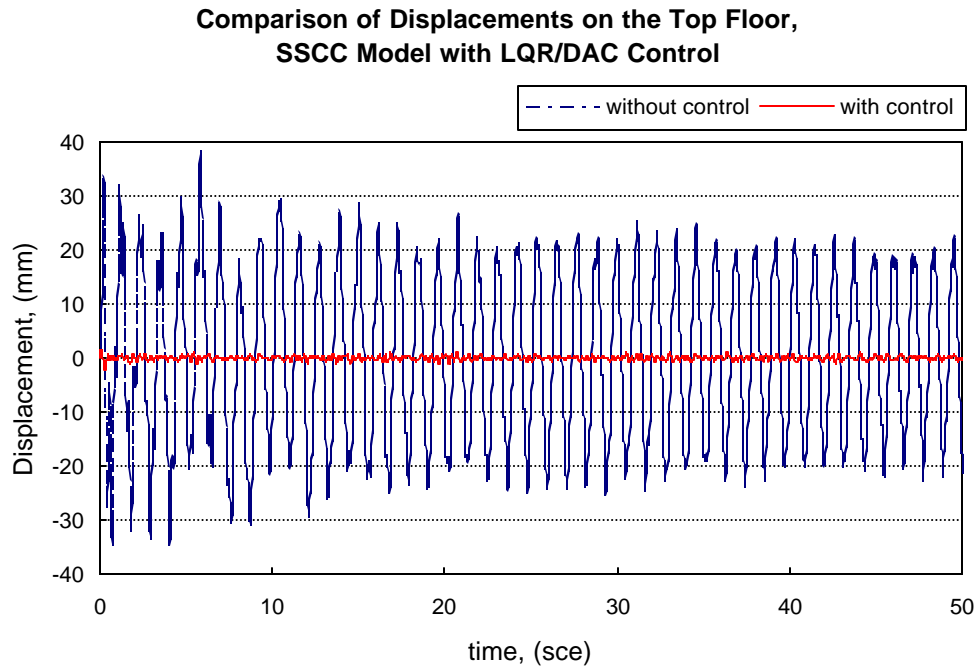


Figure 7-37. Relative displacements of the top floor, (SSCC model, LQG/DAC control)

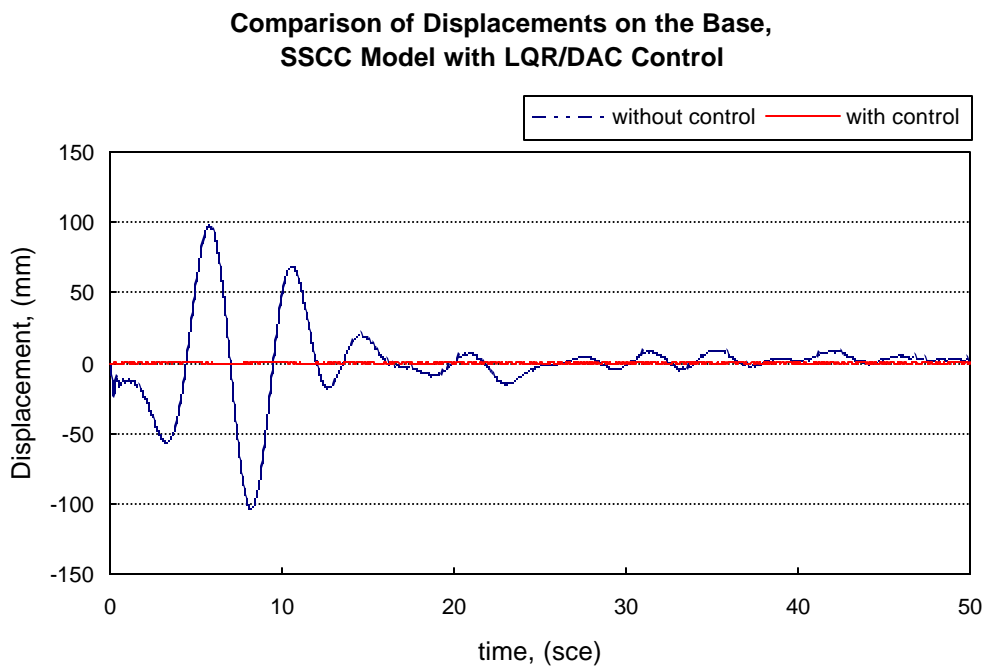


Figure 7-38. Displacements of the base, (SSCC model, LQG/DAC control)

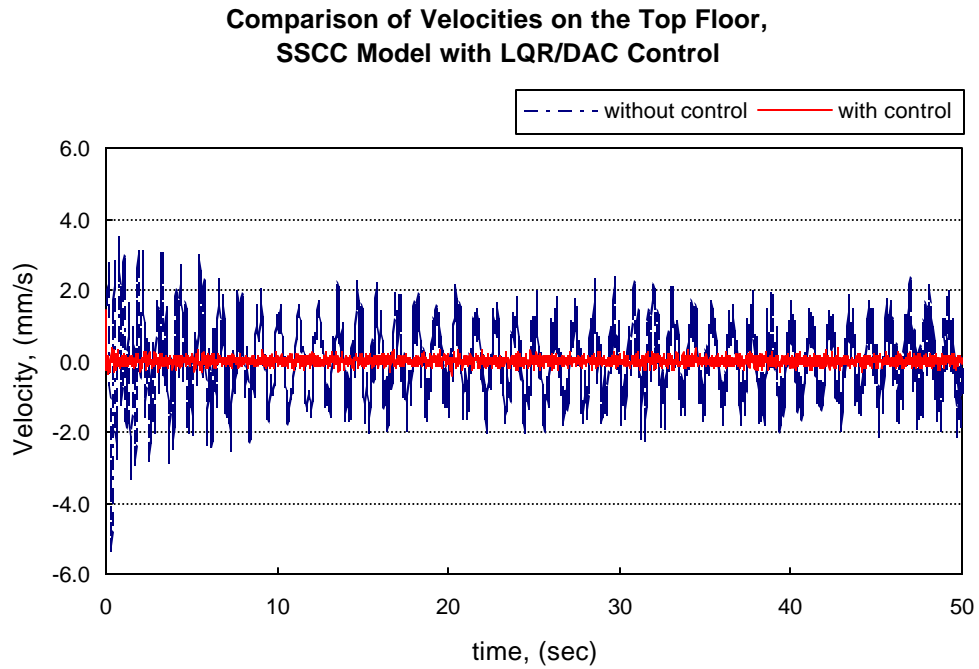


Figure 7-39. Relative velocities on the top floor, (SSCC model, LQG/DAC control)

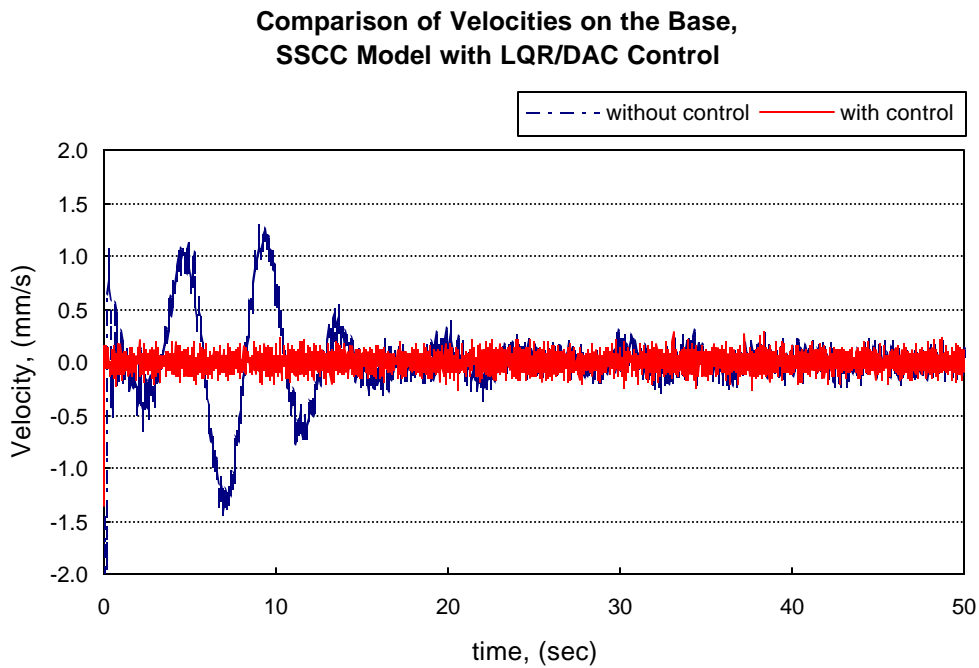


Figure 7-40. Velocities on the base, (SSCC model, LQG/DAC control)

relative efficiency of the velocity of the top floor was reduced by 90.6% and the RMS value of the relative velocity was reduced from 0.98 mm/s to 0.09 mm/s by using the LQG/DAC control in the SSCC model.

Figure 7-40 demonstrates the comparison of the velocities of the base with and without the LQG/DAC control in the SSCC model. After using the hybrid control the relative efficiency of the velocity was reduced by 78.8%, while the RMS value of the absolute velocity was reduced from 0.36 mm/s to about 0.08 mm/s.

From *Table 7-16* it is observed that the largest control force exerted on the base was 270.6 kN, which had the same order of magnitude as much of the control force exerted on the base.

The closed-loop eigenvalues of the SSCC model with the hybrid LQG/DAC control were calculated. The same close-loop eigenvalues as the LQG control, shown in *Table 7-14*, were obtained. This is due to the fact that the DAC control does not affect the characteristics of the system.

7.6 Summary

Synthesizing the simulation results above, it can be observed:

1. The hybrid LQG/DAC design in conjunction with the SSCC model is the best suitable, when the primary objective is the displacement reduction of the top floor relative to the base. 97.5% displacement reduction can be achieved.
2. The hybrid LQG/DAC design based on the SCC model is the most favorable option when the velocity reduction of the top floor relative to the base is desired. This allows us to reduce the relative velocity by 92.5%;
3. The LQG control with the SSCC model is the first choice in the instance that the acceleration reduction of the top floor relative to the base is priority. In the example, the acceleration is decreased up to 75.2% by using the LQG control with the SSCC model.
4. If the number and magnitude of the control forces is limited, the LQG control with the SSCC model is better, where one control force of 134.6 kN applied in the base can results in the effectiveness of 92.7% displacement reduction, 90.7% velocity reduction and 75.2% acceleration reduction of the top floor relative to the base.
5. Single Channel Control model including the SCC and SSCC model not only saves resource but also results in significant vibration reduction in conjunction with the hybrid LQG/DAC design.

CONCLUSIONS

This dissertation has investigated the two most important problems of active vibration control, modeling and control design. Three state variable models of building structures with feedback control system under seismic excitation have been developed. The modeling process contains two parts, the derivation of discrete differential equations of motion based on the extended Hamilton principle by using HFEM and the state space realization of the discrete equation. In the state space realization, three models namely the MCC, the SCC and the SSCC model have been proposed. The control system design primarily adopts two differential control methodologies, the LQG and the DAC approaches. Also, a hybrid LQG/DAC design has been proposed.

All the three models include a passive control system consisting of a viscous damper and an elastic spring used to isolate vibrations transmitted from ground motion. The MCC model is a general multiple input/multiple output (MIMO) dynamic system. The SSCC model, where only one actuator acting on the base is needed, is a single input/multiple output (SIMO) dynamic system. However the SCC model has duality. On one hand, it is a MIMO system when control actuators are regarded as the input. On the other hand, it can be regarded as a SIMO system when a control signal acts as the input. Moreover, three different types of control methodologies, the LQG, the DAC and the hybrid LQG/DAC control approaches, have been successfully developed to actively suppress the vibration of the building structures due to seismic disturbance. The distinction of the three control designs lies in the application of different algorithms for optimizing the state feedback gain matrix. Additionally, the Kalman filter is used as an optimal observer to estimate the state of the system in the LQG and the LQG/DAC design. At the same time, a system identification technique was adopted to model the disturbance state equation, which proved to be indispensable for the feedback control in the state space.

A numerical simulation of a four-story building has been carried out under nine cases considering various combinations of the three models and the three control designs. The

number of cases was necessary to verify the effectiveness of control technique developed in this study. The simulation results are quite encouraging. In general, the hybrid LQG/DAC control in conjunction with the SSCC model is the best choice.

Although the proposed methods utilize many well-known concepts and methodologies, some significant contributions of the dissertation are:

- A development of the HFEM for modeling building structures with feedback control system with fewer than average degrees of freedom without losing accuracy.
- Three control models, the MCC, the SCC and the SSCC models, are proposed. It has been shown that the standard state-space control design techniques, such as the LQG control techniques, can be straightforwardly used in these models. The main advantage of the SCC model is that only one control signal is necessary. Evermore attractively, only one actuator is need in the SSCC model.
- The DAC technique is developed to actively reduce vibration of buildings subjected to seismic excitation. The hybrid LQG/DAC approach proposed in the study has especially illustrated significant potential compared with other control designs. The simulation results have shown excellent performance of the hybrid LQG/DAC approach.

BIBLIOGRAPHY

(Listed alphabetically according to author's last name)

- [1] Abdel-Mooty, M. and Roorda, J., "Time-Delay Compensation in Active Damping Structures," *JOURNAL OF ENGINEERING MECHANICS*, Vol. 117, No. 11, 1991, pp. 2549-2470.
- [2] Aldemir, U. and Bakioglu, M., "Active Structural Control Based on the Prediction and Degree of Stability," *JOURNAL OF SOUND AND VIBRATION*, Vol. 247, No. 4, 2001, pp. 561-576.
- [3] Aldemir, U., Bakioglu, M., and Akhiev, J., "Optimal Control of Linear Buildings under Seismic Excitations," *EARTHQUAKE ENGINEERING AND STRUCTURAL DYNAMICS*, Vol. 30, Issue 6, 2001, pp. 835-851.
- [4] Ankireddi, S. and Yang, H. T. Y., "Sampled-Data H_2 Optimal Output Feedback Control for Civil Structures," *EARTHQUAKE ENGINEERING AND STRUCTURAL DYNAMICS*, Vol. 28, 1999, pp. 921-940.
- [5] Arfiadi, Y. and Hadi, N. S., "Passive and Active Control of Three-Dimensional Buildings," *EARTHQUAKE ENGINEERING AND STRUCTURAL DYNAMICS*, Vol. 29, 2000, pp. 388-396.
- [6] Babuska, I., Szabo, B. A. and Katz, I. N., "The p -Version of the Finite element Method," *SIAM JOURNAL OF NUMERICAL ANALYSIS*, Vol. 18, No. 3, 1981, pp. 515-545.
- [7] Babuska, I. and Dorr, B. M. "Error Estimates for the Combined h and p Version of the Finite element Method," *NUMERICAL MATHEMATICS*, Vol. 37, 1981, pp. 257-277.
- [8] Balendra, T. *VIBRATION OF BUILDINGS TO WIND AND EARTHQUAKE LOADS*, Springer-Verlag London Limited, 1993.

-
- [9] Bani-Han, K., Ghaboussi, J. and Schneider, S. P., "Experimental Study of Neural Network Based Structural Control," *6TH U.S. NATIONAL CONFERENCE ON EARTHQUAKE ENGINEERING*, Seattle, WA, 1998
- [10] Bardell, N. S., "Free Vibration Analysis of a Flat Plate Using the Hierarchical Finite Element Method," *JOURNAL OF SOUND AND VIBRATION*, Vol. 151, 1991, pp. 263-289.
- [11] Bardell, N. S., "The Free Vibration of Skew Plates Using the Hierarchical Finite Element Method," *COMPUTERS AND STRUCTURES*, Vol. 45(5/6), 1992, pp. 841-874.
- [12] Beslin, O. and Nicolas, J., "A Hierarchical Functions for Predicting Very High Order Plate Bending Modes with Any Boundary Conditions," *JOURNAL OF SOUND AND VIBRATION*, Vol. 202, No. 5, 1997, pp. 633-655.
- [13] Brogan, W. L., *MODERN CONTROL THEORY*, Prentice Hall, New Jersey, 1991.
- [14] Brown, A. S. and Yang, T. Y., "Neural Networks for Multiobjective Adaptive Structural Control," *JOURNAL OF STRUCTURAL ENGINEERING*, Vol. 127, Issue 2, 2001, pp.203-210
- [15] Burke, S. E. and Hubbard, J. E. Jr., "Active Vibration Control of a Simply Supported Beam Using a Spatially Distributed Actuator," *IEEE CONTROL SYSTEMS MAGAZINE*, August 1987, pp. 25-30.
- [16] Chen, H. M., Tsai, K. H., Qi, G. Z., Yang, J. C. S. and Amini, F., "Neural Network Based Structural Control," *JOURNAL OF COMPUTATIONAL CIVIL ENGINEERING*, Vol. 9, No. 2, 1995, pp. 168-176.
- [17] Chopra, A. K., *DYNAMICS OF STRUCTURES*, Prentice Hall, 1995.
- [18] Cook, R. D., *FINITE ELEMENT MODELING FOR STRESS ANALYSIS*, John Wiley & Sons, Inc., 1995.
- [19] Dai, Y. and Fuller, C. R., "Numerical Simulation of Active Control of Interior Noise in a Business Jet with Point Force Actuators," *PROCEEDINGS OF INTER-NOISE 95*, Newport Beach, CA, USA, 1995, pp.533-536.

-
- [20] Dorato, P., Abdallah, C. and Cerone V., *LINEAR-QUADRATIC CONTROL: AN INTRODUCTION*, Prentice-Hall, In., New Jersey, 1995.
- [21] Faravelli, L. and Venini, P., "Active Structural Control by Neural Networks," *JOURNAL OF STRUCTURAL CONTROL*, Vol. 1, 1994, pp. 79-101.
- [22] Friedland, B., *CONTROL SYSTEM DESIGN, AN INTRODUCTION TO STATE-SPACE METHODS*, McGraw-Hill Book Company, 1986
- [23] Fuller, C. R., Elliott, S. J. and Nelson, P. A., *ACTIVE CONTROL OF VIBRATION*, Academic Press Limited, London, Great Britain, 1996.
- [24] Fur, L.-S., Yang, H. T. Y. and Ankireddi, S., "Vibration Control of Tall Buildings under Seismic and Wind Loads," *JOURNAL OF STRUCTURAL ENGINEERING*, Vol. 122, No. 8, 1994, pp. 948-957.
- [25] Guenfaf, L. Djebiri, M. Boucherit, M. S. and Boudjema, F., "Generalized Minimum Variance Control for Buildings under Seismic Ground Motion," *EARTHQUAKE ENGINEERING AND STRUCTURAL DYNAMICS*, Vol. 30, Issue 7, 2 001, pp. 945-960.
- [26] Habib, M. S. and Radcliffe, C. J., "Active Parametric Damping of Distributed Parameter Beam Trans verse Vibration," *JOURNAL OF DYNAMIC SYSTEMS, MEASUREMENT, AND CONTROL*, Vol. 113, June 1991, pp. 295-299.
- [27] Hanagan, L. M., Kulasekere, E. C., Walgama, K. S. and Premaratne, K., "Optimal Placement of Actuators and Sensors for Floor Vibration Control," *JOURNAL OF STRUCTURAL ENGINEERING*, Vol. 126, Issue 12, 2000, pp.1380-1387.
- [28] Houmat, A., "An Alternative Hierarchical Finite Element Formulation Applied to Plate Vibrations," *JOURNAL OF SOUND AND VIBRATION*, Vol. 206, No. 2, 2001, pp. 201-215
- [29] Huang, C. S. and Lin, H. L., "Modal Identification of Structures from ambient Vibration, Free Vibration, and Seismic Response Data via a Subspace Approach," *EARTHQUAKE ENGINEERING AND STRUCTURAL DYNAMICS*, Vol. 30, Issue 12, 2001, pp. 1857-1878.

- [30] Hyland, D. C., Junkins, J. L. and Longman, R. W., "Active Control Technology for Large Space Structures," *JOURNAL OF GUIDANCE, CONTROL, AND DYNAMICS*, Vol. 16, No. 5, 1993, pp. 801-821.
- [31] Inman, D. J., *VIBRATION, WITH CONTROL, MEASUREMENT, AND STABILITY*, Prentice Hall, New Jersey, 1989.
- [32] Inman, D. J. and Leo, D. J., Controllability issues in Smart Structural Control Systems," *SOCIETY OF ENGINEERING SCIENCE 29TH ANNUAL MEETING*, 1992.
- [33] Jalihal, P., Utku, S. and Wada, B. K., "Active Base Isolation in Buildings Subjected to Earthquake Excitation," *PROCEEDINGS OF THE 1994 INTERNATIONAL MECHANICAL ENGINEERING CONGRESS AND EXPOSITION*, Ad-Vol. 45/MD-Vol. 54, Chicago, IL, 1994, pp. 381-388.
- [34] Joghataie, A. And Ghaboussi, J., "A Comparative Study of Learning Methods and Mathematical Algorithms in Structural Control," *11TH WORLD CONFERENCE ON EARTHQUAKE ENGINEERING*, Paper No. 1432, 1996.
- [35] Johnson, C. D. "Theory of Disturbance-Accommodating Controllers," *CONTROL AND DYNAMICS*, Vol. 12, 1976, pp387-489.
- [36] Johnson, C. D. "Disturbance-Accommodating Control; An Overview of the Subject," *JOURNAL OF INTERDISCIPLINARY MODELING AND SIMULATION*, Vol. 3, No. 1, 1980, pp. 1-29.
- [37] Johnson, C. D. "A Discrete-Time Disturbance-Accommodating Control Theory for Digital Control of Dynamical Systems," *CONTROL AND DYNAMIC SYSTEM*, Vol. 18, 1982, pp. 223-315.
- [38] Johnson, E. A., Voulgris, P. G. and Bergman, L. A., "Multiobjective Optimal Structural Control of the Notre Dame Building Model Benchmark," *EARTHQUAKE ENGINEERING AND STRUCTURAL DYNAMICS*, Vol. 27, 1998, pp. 1165-1187.
- [39] Juang, J. N. Sae-Ung, S. and Yang, J. N., "Active Control of Large Building Structures," *STRUCTURAL CONTROL*, Edited by Leipholz, H. H. E., ed., North-Holland Publishing Co., Amsterdam, The Netherlands, 1979, pp. 663-676.

- [40] Kelly, J. M., Leitmann, G. and Soldatos, A. G., "Robust Control of Based Isolated Structures under Earthquake Excitation," *JOURNAL OF OPTIMIZATION THEORY AND APPLICATIONS*, Vol. 53, No. 2, 1987, pp. 159-180.
- [41] Kim, D. and Lee, I., "Neuro-Control of Seismically Excited Steel Structure through Sensitivity Evaluation Scheme," *EARTHQUAKE ENGINEERING AND STRUCTURAL DYNAMICS*, Vol. 30, Issue 9, 2001, pp. 1361-1377.
- [42] Kim, Y. and Ghaboussi, J., "A New Method of Reduced Order Feedback Control Using Genetic Algorithms," *EARTHQUAKE ENGINEERING AND STRUCTURAL DYNAMICS*, Vol. 28, 1999, pp. 193-212.
- [43] Librescu, L., Song, O. and Rogers, C.A. "Adaptive Vibrational Behavior of Cantilevered Structures Modelled as Composite Thin-Walled Beams," *INTERNATIONAL JOURNAL OF ENGINEERING SCIENCE*, Vol. 31, No. 5, 1993, pp. 775-792.
- [44] Librescu, L., Meirovitch, L. and Song, O., "Integrated Structural Tailoring and Control Using Adaptive Materials for Advanced Aircraft Wings," *JOURNAL OF AIRCRAFT*, Vol. 33, No. 1, 1996, pp. 203-213.
- [45] Librescu, L., Meirovitch, L. and Na, S. S., "Control of Cantilevers Vibration Via Structural Tailoring and Adaptive Materials," *AIAA JOURNAL*, Vol. 35, No. 8, 1997, 1309-1315.
- [46] Liut, D. A., Matheu, E. E., Singh, M. P. and Mook, D. T., "Neural-Network Control of Building Structures," *9TH INTERNATIONAL CONFERENCE ON ADAPTIVE STRUCTURES AND TECHNOLOGIES*, Cambridge, MA, 1998, pp. 465-475.
- [47] Liut, D. A., Matheu, E. E., Singh, M. P. and Mook, D. T., "Neural-Network Control of Building Structures by a Force-Matching Training Scheme," *EARTHQUAKE ENGINEERING AND STRUCTURAL DYNAMICS*, Vol. 28, Issue 12, 1999, pp. 1601-1620.
- [48] Loh, C.-H. and Chao, C.-H., "Effectiveness of Active Tuned Mass Damper and Seismic Isolation on Vibration Control of Multi-Story Building," *JOURNAL OF SOUND AND VIBRATION*, Vol. 193, No. 4, 1996, pp. 773-792.

- [49] Luco, J. E., Wong, H. L. and Mita, A., "Active Control of the Seismic Response of Structures by Combined Use of Base Isolation and Absorbing Boundaries," *EARTHQUAKE ENGINEERING AND STRUCTURAL DYNAMICS*, Vol. 21, No. 6, 1992, pp. 525-541.
- [50] Marsden, J. E. and Hughes, T. R., *MATHEMATICAL FOUNDATIONS OF ELASTICITY*, Prentice-Hall, Inc., Englewood Cliffs, NJ, 1983.
- [51] Martin, C. R. and Soong, T. T., "Modal Control of Multistory Buildings," *JOURNAL OF ENGINEERING MECHANICS*, Vol. 102, No. 4, 1976, pp. 613-623.
- [52] Mei, G., Kareem, A., and Kantor, J. C., "Real-Time Model Predictive Control of Structures under Earthquakes," *EARTHQUAKE ENGINEERING AND STRUCTURAL DYNAMICS*, Vol. 30, Issue 7, 2001, pp. 995-1019.
- [53] Meirovitch, L., *METHODS OF ANALYTICAL DYNAMICS*, McGraw-Hill Book Co., New York, 1970.
- [54] Meirovitch, L. and Öz, H., "Active Control of Structures by Modal Synthesis," *STRUCTURAL CONTROL*, Edited by H. H. Leioholz, North Holland Publishing, The Netherlands, 1979, pp. 505-521.
- [55] Meirovitch, L., *COMPUTATIONAL METHODS IN STRUCTURAL DYNAMICS*, Sijthoff and Noordhoff, Alphen aan den Rijn, The Netherlands, 1980.
- [56] Meirovitch, L. and Baruh, H., "On the inclusion Principle for the Hierarchical Finite Element Method," *INTERNATIONAL JOURNAL FOR NUMERICAL METHODS IN ENGINEERING*, Vol. 19, 1983, pp. 281-291.
- [57] Meirovitch, L. and Silverberg, L. M., "Control of Structures Subjected to Seismic Excitation," *JOURNAL OF ENGINEERING MECHANICS*, Vol. Vol. 109, No. 2, 1983, pp. 604-618.
- [58] Meirovitch, L. and Kwak, M. K., "Convergence of the Classical Rayleigh-Ritz Method and the Finite Element Method," *AIAA JOURNAL*, Vol. 28, No. 8, 1990, pp. 1509-1516.
- [59] Meirovitch, L., *DYNAMICS AND CONTROL OF STRUCTURES*, Wiley-Interscience, New York, 1990.

- [60] Meirovitch, L. and Kwak, M. K., "Rayleigh-Ritz Based Substructure Synthesis for Flexible Multibody Systems," *AIAA JOURNAL*, Vol. 29, No. 10, 1991, pp. 1709-1719.
- [61] Meirovitch, L. and Stemple, T. J., "Dynamics and Control of Flexible Multibody Systems," *SWITZERLAND CONFERENCE*, August, 1994.
- [62] Meirovitch, L. and Stemple, T. J., "Base-isolation Control of Structures in Earthquakes," *PROCEEDINGS OF THE 10TH VPI&SU STRUCTURAL DYNAMICS AND CONTROL SYMPOSIUM*, 1995, pp. 263-274.
- [63] Meirovitch, L. and Stemple, T. J., "Nonlinear Control of Structures in Earthquakes," *JOURNAL OF ENGINEERING MECHANICS*,
- [64] Meirovitch, L., *PRINCIPLES AND TECHNIQUES OF VIBRATIONS*, Prentice Hall, New Jersey, 1997.
- [65] Meirovitch, L. and Stemple, T. J., "A New Approach to the Modeling of Distributed Structures for Control,"
- [66] Miller, R. K., Masri, S. F., Dehghanyar, T. J. and Caughey, T. K., "Active Vibration Control of Large Civil Structures," *JOURNAL OF ENGINEERING MECHANICS*, Vol. 114, No. 9, 1988, pp. 1542-1570.
- [67] Nagashima, I., "Optimal Displacement Feedback Control Law for Active Tuned Mass Damper," *EARTHQUAKE ENGINEERING AND STRUCTURAL DYNAMICS*, Vol. 30, Issue 8, 2001, pp. 1221-1242.
- [68] Ni, Y. Q. And Ko, J. M., "Random Seismic Response Analysis of Adjacent Buildings Coupled with Non-Linear Hysteretic Dampers," *JOURNAL OF SOUND AND VIBRATION*, Vol. 246, No. 3, 2001, pp. 403-417.
- [69] Nishitani, A. and Inoue, Y., "Overview of the Application of Active/Semiactive Control to Building Structures in Japan," *EARTHQUAKE ENGINEERING AND STRUCTURAL DYNAMICS*, Vol. 30, Issue 11, 2001, pp. 1565-1574.
- [70] Peano, A., "Hierarchies of Conforming Finite Elements for Plane elasticity and Plate Bending," *Computers and Mathematics with Applications*, Vol. 2, 1976, pp. 211-224.

-
- [71] Preumont, A., Dufour, J. P. and Malekian, C., "Active Damping by a Local Force Feedback with Piezoelectric Actuators," *JOURNAL OF GUIDANCE, CONTROL, AND DYNAMICS*, Vol. 15, No. 2, 1992, pp. 390-395.
- [72] Pu, J-P. and Hsu, D.-S., "Optimal Control of Tall Building," *JOURNAL OF ENGINEERING MECHANICS*, Vol. 114, No. 6, 1988, pp. 973-989.
- [73] Pu, J-P. and Kelly, M., "Active Control and Seismic Isolation," *JOURNAL OF ENGINEERING MECHANICS*, Vol. 117, No. 10, 1991, pp. 2221-2236.
- [74] Reinhorn, A. M., Soong, T. T. and Wen, C. Y., "Base Isolated Structures with Active Control," *RECENT ADVANCES IN DESIGN, ANALYSIS, TESTING AND QUALIFICATION METHODS*, ASME PVP-Vol. 127, 1987, pp. 413-419.
- [75] Reinhorn, A. M., Manolis, G. D. and Wen, C. Y., "Active Control of Inelastic Structures," *JOURNAL OF ENGINEERING MECHANICS*, Vol. 113, No. 3, 1987, pp. 315-333.
- [76] Rfooei, F. R. and Tadjbakksh, I. G., "Optimal control of Structures with Acceleration, Velocity, and Displacement Feedback," *JOURNAL OF ENGINEERING MECHANICS*, Vol. 119, No. 10, 1993, pp. 1993-2010.
- [77] Ribakov, Y. and Gluck, J., "Active Control of MDOF Structures with Supplemental Electrorheological Fluid Dampers," *EARTHQUAKE ENGINEERING AND STRUCTURAL DYNAMICS*, Vol. 28, 1999, pp. 143-156.
- [78] Ribeiro, P. and Petyt, M., "Non-Linear Vibration of Beams with Internal Resonance by the Hierarchical Finite-Element Method," *JOURNAL OF SOUND AND VIBRATION*, Vol. 224, No. 4, 1999, pp. 591-624
- [79] Ribeiro, P., "Hierarchical Finite Element Analysis of Geometrically Non-Linear Vibration of Beams and Plane Frames," *JOURNAL OF SOUND AND VIBRATION*, Vol. 246, No. 2, 2001, pp. 225-244
- [80] Sener, M. and Utku, S., "Active-Passive Base Isolation System for Seismic Response Controlled Structures," *PROCEEDINGS OF THE 36TH AIAA/ASME/ASCE/AHS/ASC STRUCTURES, STRUCTURAL DYNAMICS, AND MATERIALS*

-
- CONFERENCE AND AIAA/ASME ADAPTIVE STRUCTURES FORUM*, Part 4 (of 5), New Orleans, LA, April 4–April 13, 1995, pp. 2350-2359.
- [81] Song, O., Librescu, L. and Rogers, C.A., “Adaptive Response Control of Cantilevered Thin-Walled Beams Carrying Heavy Concentrated Masses,” *JOURNAL OF INTELLIGENT MATERIAL SYSTEMS AND STRUCTURES*, Vol. 5, No. 1, 1994, pp. 42-48.
- [82] Soong, T. T., *ACTIVE STRUCTURAL CONTROL: THEORY AND PRACTICE*, Longman Scientific and Technical, Essex, England, 1990.
- [83] Spencer, B. F., Dyke, S. J. and Deoskar, H. S., “Benchmark Problems in Structural Control: Part I-Active Mass Driver System,” *EARTHQUAKE ENGINEERING AND STRUCTURAL DYNAMICS*, Vol. 27, 1998, pp. 1127-1139.
- [84] Spencer, B. F., Dyke, S. J. and Deoskar, H. S., “Benchmark Problems in Structural Control: Part II-Active Tendon System,” *EARTHQUAKE ENGINEERING AND STRUCTURAL DYNAMICS*, Vol. 27, 1998, pp. 1141-1157.
- [85] Sun, Z., Sun, J. C., Wang, C. and Dai, Y., “Dynamic Vibration Absorbers Used for Increasing the Noise Transmission Loss of Aircraft Panels,” *APPLIED ACOUSTICS*, Vol. 48, No. 4, 1996, pp. 311-321.
- [86] Szabo, B. A., “Some Recent Developments in the Finite Element Method,” *COMPUTERS AND MATHEMATICS WITH APPLICATIONS*, Vol. 5, 1979, pp. 99-115.
- [87] Tadjbakhsh, I. G. and Rofooei, F., “Optimal Hybrid Control of Structures under Earthquake Excitation,” *EARTHQUAKE ENGINEERING AND STRUCTURAL DYNAMICS*, Vol. 21, 1992, pp. 233-252.
- [88] Wang, Y., Lee, C. and Chen, K., “Seismic Structural Control Using a Novel High-Performance Active Mass Driver System,” *EARTHQUAKE ENGINEERING AND STRUCTURAL DYNAMICS*, Vol. 29, 2000, pp. 1629-1646.
- [89] Wie, B. and Gonzalez, M., “Control Synthesis for Flexible Space Structures Excited by Persistent Disturbances,” *JOURNAL OF GUIDANCE*, Vol. 15, No. 1, 1992, pp. 73-80.
-

- [90] Wong, K. K. F. and Yang, R., "Evaluation of Response and Energy in Actively Controlled Structures," *EARTHQUAKE ENGINEERING AND STRUCTURAL DYNAMICS*, Vol. 30, Issue 12, 2001, pp. 1495-1510.
- [91] Wong, K. K. F. and Yang, R., "Effectiveness of Structural Control Based on Control Energy Perspectives," *EARTHQUAKE ENGINEERING AND STRUCTURAL DYNAMICS*, Vol. 30, Issue 12, 2001, pp. 1747-1768.
- [92] Wu, J. and Yang, J. N., "LQG Control of Lateral-Torsional Motion of Nanjing TV Transmission Tower," *EARTHQUAKE ENGINEERING AND STRUCTURAL DYNAMICS*, Vol. 29, 2000, pp. 1111-1130.
- [93] Yang, J. N., "Application of Optimal Control Theory to Civil Engineering Structures," *JOURNAL OF ENGINEERING MECHANICS*, Vol. 101, No. 6, 1975, pp. 819-836.
- [94] Yang, J. N., Danielians A. and Liu, S. C., "Aseismic Hybrid Control Systems for Building Structures," *JOURNAL OF ENGINEERING MECHANICS*, Vol. 117, No. 4, 1991, pp. 836-853.
- [95] Yang, J. N., Li, Z., Danielians and Liu, S. C., "Aseismic Hybrid Control of Nonlinear and Hysteretic Structures, I," *JOURNAL OF ENGINEERING MECHANICS*, Vol. 118, No. 7, 1992, pp. 1423-1440.
- [96] Yang, J. N., Li, Z., Danielians and Liu, S. C., "Aseismic Hybrid Control of Nonlinear and Hysteretic Structures, II," *JOURNAL OF ENGINEERING MECHANICS*, Vol. 118, No. 7, 1992, pp. 1441-1456.
- [97] Yao, J. T. P., "Concept of Structural Control," *ASCE JOURNAL OF STRUCTURAL DIVISION*, Vol. 98, 1972, pp. 1567-1574.
- [98] Young, P. M. and Bienkiewicz, B., "Robust Controller Design for the Active Mass Driver Benchmark Problem," *EARTHQUAKE ENGINEERING AND STRUCTURAL DYNAMICS*, Vol. 27, 1998, pp. 1149-1164.
- [99] Zhu, D. C., "Development of Hierarchical Finite Element Methods at BIAA," *PROCEEDINGS OF THE INTERNATIONAL CONFERENCE ON COMPUTATIONAL MECHANICS*, Tokyo I, 1986, pp.123-128.

- [100] Zienkiewicz, O. C., Irons, B. M., Scott, F. E. and Campbell, J. S., "Three Dimensional Stress Analysis," *Proceedings of the IUTAM Symposium on High Speed Computing of Elastic Structures*, Liege, Belgium, 1970.
- [101] Zienkiewicz, O. C., Kelly, D. W., Gago, J. and Babuska, I., "Hierarchical Finite Element Approaches, Error Estimates and Adaptive Refinement," Report C/R/382/81, Institute for Numerical Methods in Engineering, University College of Swansea, UK, 1981.
- [102] Zienkiewicz, O. C. and Taylor, R. L., *The Finite Element Method*, 4th ed., McGraw-Hill, London, 1991.

Vita

Yang Dai received the Bachelor degree in Engineering Mechanics in 1982 and the Master degree in Engineering Mechanics in 1986, both from the Northwestern Polytechnic University (NPU), Xi'an, P. R. China.

He joined the faculty of Institute of Acoustic Engineering at the NPU in 1986. He served as Assistant Professor of Acoustic Engineering from 1986 to 1992 and Associate Professor of Acoustic Engineering at NPU from 1992 to 1996. He worked with Vibration and Acoustics Laboratory at Virginia Tech as a visiting scholar from 1993 to 1996. He enrolled Department of Engineering Science and Mechanics at Virginia Tech as a Ph.D. student in 1996. He worked with Aerotek, Inc as an Analysis Engineer on site: General Motors Corporation from 1999 to 2001. He joined Ricardo, Inc. as a Senior Engineer in 2001. His research interests are in noise and vibration CAE analysis and control.
